Spike statistics and coding properties of phase models

From ion channels to neural coding

D I S S E R T A T I O N

zur Erlangung des akademischen Grades

d o c t o r r e r u m n a t u r a l i u m
(Dr. rer. nat.)
im Fach Biophysik

eingereicht an der
Mathematisch-Naturwissenschaftlichen Fakultät I
Humboldt-Universität zu Berlin

von
M.Sc. Jan-Hendrik Schleimer

Präsident der Humboldt-Universität zu Berlin:
Prof. Dr. Jan-Hendrik Obertz

Dekan der Mathematisch-Naturwissenschaftlichen Fakultät I:
Prof. Stefan Hecht, PhD

Gutachter:
1. Prof. Dr. Bernhard Ronacher
2. Prof. Dr. Benjamin Lindner
3. Prof. Dr. Roberto Fernández Galán

eingereicht am: 20.09.2012
Tag der mündlichen Prüfung: 08.04.2013

Zusammenfassung

Sensorische Nervenzellen arbeiten als ein erster Filter für die Wahrnehmung eines Organismus. Sie bilden die unterste Stufe in einer Verarbeitungskette, die relevante Informationen aus dem Lebensraum extrahiert, aufbereitet und an zentrale Schalteinheiten der Nervensysteme weiterleitet. Aus evolutionärer Sicht werden Nervenzellen unter anderem an Hand dieser Filtereigenschaften selektiert, denn sie bestimmen ob überlebensrelevante Information in der Nervenaktivität kodiert wird. Robuste Kodierung und die Filtereigenschaften sind wichtige funktionelle Aspekte des Phänotyps. Sie hängen in komplizierter Art und Weise vom Genotyp und im Speziellen den in der Zellmembran der Nerven exprimierten Ionenkanälen sowie deren Regulation ab. Die Ionenkanäle der Zellmembran sind spezielle Porenproteine, die eine Potenialdifferenz über die Membran erzeugen, und auf Grund ihrer Spannungsabhängigkeit in einer Rückkoplungsschleife Nervenimpulse nach dem Alles-oder-nichts-Prinzip generieren.

Um den Zusammenhang zwischen der zu Grunde liegenden molekularen Maschinerie der Nervenzellmembran und der Funktion eines Neuron zu verstehen benötigt man mathematische Methoden, die diese Betrachtungsebenen verbinden. Dazu möchte die vorliegenden Arbeit beitragen. Hierfür wird eine Brücke zwischen biophysikalisch detaillierter Beschreibung auf der einen Seite und einer makroskopischen Sicht auf das System auf der andern Seite geschlagen. Auf der makroskopischen Ebene stehen die für die Kodierung relevanten Spikezeiten im Vordergrund.

Die Informationsweiterleitung und -verarbeitung in Nervensystemen wird durch Nervenimpulse, den sogenannten Aktionspotentialen oder Spikes getragen. Hierbei ist die genaue Form der Impulse weniger von Bedeutung als ihr zeitliches Muster und ihre Frequenz. Zwei wichtige Aspekte die zum Verständnis der neuronalen Kodierung beitragen sind a) der degradierende Effekt zelleigenen Rauschens auf die Präzision der Nervenimpulse und b) die Filtereigenschaften der Nervenzellen. Diese werden in den zwei Teilen dieser Arbeit beleuchtet.

Die zentrale Methode, die sich diese Arbeit zu Nutze macht ist die Phasenreduktion. Dabei wird das komplette biophysikalische System in Variablen übersetzt, die es direkt ermöglichen das zeitliche Muster der Nervenimpulse vorauszusagen. Diese Phasenvariablen entsprechen im autonomen Neuron ohne den Einfluss von externen Stimuli oder internen Rauschens einfach der Zeit. Wird das System hingegen gestört, so verschiebt sich die Phasenvariable im Vergleich zur normalen Zeit. Ein hierzu wichtiges Konzept ist das der Isochronen. Dies sind Untermengen im Raum der physikalischen Variablen die der gleichen Phase zugeordnet werden. Die Phasenreduktion setzt voraus, dass wir zwischen der deterministischen autonomen Dynamik des Neuron und den Perturbationen unterscheiden können.

Wird einer sensorischen Nervenzelle mehrfach der gleiche Stimulus präsentiert, so zeigt sich in der neuronalen Antwort Variabilität. Die Ursachen dieser Variabilität sind, wenn Netzwerkeffekte ausgeschlossen werden können, zellintrinsische mikroskopische Prozesse. Diese Rauschquellen werden in Kapitel 3 näher beleuchtet. Im Besonderen wird auf Kanalrauschen eingegangen, welches vor allem in der sensorischen Peripherie eine Rolle spielt. Der dem Rauschen zugrunde liegende Prozess ist das statistische Öffnungs- und Schließverhalten einzelner Ionenkanäle. Diese Membranproteine haben disjunkte Konformationen, von denen ein Teil einen Ionenflux durch die Membran erlaubt, andere Konformationen dies verhindern. Die klassische Beschreibung der Konformationsübergänge erfolgt mittels eines Markovschen Sprungprozesses. Der Nachteil dieser Beschreibung ist, dass sich nicht zwischen deterministischer Dynamik und Rauschen unterscheiden lässt, da die gesamte Evolution des Systems durch kleine statistische Sprünge bestimmt wird. Diese Beschreibung ist nicht mit der angestrebten Phasenreduktion kompatibel. Daher wird zuerst der Sprungprozess durch eine stochastische Differenzialgleichung approximiert. Diese Approximation eignet sich für Abschnitte der Zellmembran in de-

nen sich zwar endlich viele aber doch eine große Anzahl an Ionenkanälen befinden. In der stochastischen Differenzialgleichung können die Perturbationen des deterministischen Systems eindeutig bestimmt werden und in Kapitel 4 in eine Störung der Phasengleichung übersetzt werden.

Die Phasenreduktion wird üblicherweise als eine Störungstheorie erster Ordnung betrieben. Die resultierenden Phasengleichungen haben zum Verständnis vieler Phänomene in Nervensystemen beigetragen. Beispielsweise kann das Synchronisationsverhalten in einer Population von Nervenzellen durch einen gemeinsamen Stimulus so beschrieben werden [67]. In der vorliegenden Arbeit wird die Phasenreduktion zur zweiten Ordnung getrieben. Dies ermöglicht statistische Eigenschaften wie die Varianz der Wartezeiten zwischen Aktionspotentialen zu berechnen.

In Kapitel 5 wird der Zusammenhang zwischen einem bekannten Phänomen, der rauschinduzierten Frequenzverschiebung, und der Radialdynamik in einer Phasengleichung zweiter Ordnung hergestellt. Die Radialdynamik wird durch Koeffizienten in einem rotierenden Koordinatensystem dargestellt, welches als der Tangentialraum der Isochronen gewählt ist. Isochronen sind hier Untermannigfaltigkeiten des Zustandsraums mit gleicher aymptotischer Phase. Bei der Analyse stellt man fest, dass die Krümmung der Isochronen eine Auswirkung auf diese Frequenzverschiebung hat, ein Zusammenhang, der so noch nicht herausgestellt wurde. Verdeutlichen lässt sich dieser Effekt an Hand der Normalformgleichung der Hopf-Bifurkation. Dieser Oszillator mit dem Einheitskreis als Grenzzyklus hat logarithmische Spiralen, die so genannte *Spira mirabilis* als Isochronen. Das Modell zeigt je nach Krümmung der Isochronen positive oder negative Frequenzverschiebungen.

Auch die zeitliche Präzision der Aktionspotentiale kann unter zu Zuhilfenahme der Phasenreduktion analysiert werden. Es ist bekannt, dass beispielsweise die Natriumleitfähigkeit einen Einfluss auf die Spannungsfluktuationen hat. Die in dieser Arbeit vorgeschlagene Methode erlaubt es einen Schritt weiter zugehen und die detaillierten mikroskopischen Fluktuationen, in quantitativer Art und Weise, direkt mit den Variationen in den Aktionspotentialzeiten in Verbindung zu setzen. Von besonderer Bedeutung ist, dass unsere Analyse ergibt, dass eine Veränderung der Kanaldichte sowohl die Größe der Fluktuationen auf der einen Seite aber auch die Sensibilität des deterministischen Systems gegenüber diesen Fluktuationen auf der anderen Seite beeinflusst. Nur eine Betrachtung beider Einflüsse erklärt das Gesamtverhalten des Systems. Interessanterweise ergibt sich so, dass eine Veränderung der Natriumkanaldichte einen größeren Einfluss auf den Beitrag des kaliuminduzierten Phasenrauschens haben kann als auf das von Natrium selbst verursachte.

Der Zweite Teil der Arbeit beschäftigt sich mit den Filtereigenschaften von Neuronen, die von einem externen Stimulus über ihre Schwelle getrieben werden, dann einen zeitmodulierten Stimulus erfahren, und daraufhin eine tonische Antwort, in Form eines irregulären Spikeprozesses, zeigen. Wir berechnen in diesem Regime den Filter, der die Eingangssignale in eine zeitabhängige Feuerwahrscheinlichkeit übersetzt, das heißt, man kann für beliebige Eingaben vorhersagen mit welcher Wahrscheinlichkeit ein Neuron zu einem gegebenen Zeitpunkt feuert. Die Stärke der zellintrinsischen Fluktuationen wird im 2. Teil zu einem globalen Systemparameter zusammengefasst, der in die Transferfunktion des Filters eingeht. Die globale Rauschstärke ist somit eine weitere Größe, die die Filtereigenschaften der Nervezelle beeinflusst.

Nahe der Feuerschwelle einer Nervenzelle lässt sich die Membranpotentialdynamik mittels kanonischer Gleichungen beschreiben, die vom Bifurkationstyp des Neurons abhängen, also der Art und Weise, wie die Schwelle überschritten wird. Diese generischen Eigenschaften spiegeln sich auch in den mit den Neuronen assoziierten Filtern wieder, die in Kapitel 6 hergeleitet werden. Das Filterspektrum der Andronov-Hopf-Bifurkationen hat keine Energie im niederfrequenten Bereich, so dass die langsamen Komponenten der Signale ausgefiltert werden. Beginnt ein Neuron durch eine Sattelknoten-Bifurkation auf dem

Grenzzyklus zu feuern, ist es der Nervenzelle auch möglich Signale im niederfrequenten Bereich weiterzuleiten. Andere Nervenzelltypen mit homoklinischen Bifurkationen können wie Bandstoppfilter wirken und spezielle Frequenzbänder im Signal unterdrücken.

Die Filtereigenschaften der Nervenzellen geben Aufschluss über die neuronale Signalverarbeitung. Um eine globale Größe zur Quantifikation der Informationsweiterleitung zu bekommen, zieht man den Shannonschen Informationsbegriff aus der Nachrichtentechnik heran. Für zeitkontinuierliche Systeme wie Nervenzellen stellt sich die Schätzung der Informationübertragungsrate als schwierig heraus, da die zugrunde liegenden Histogramme hochdimensional sind. Wie in Kapitel 7 dargelegt, besteht eine alternative Möglichkeit aus der Berechnung einer unteren Schranke für die Übertragungsrate, welche auf der spektralen Kohärenz zwischen Signal und neuronaler Antwort beruht. Die in Kapitel 6 berechneten Filter bilden die Grundlage zur Herleitung der spektralen Kohärenz. Weitere Komponenten sind das Spektrum des Punktprozess der Aktionspotentiale und das Signalspektrum. Ersteres lässt sich mittels einiger Annahmen über die statistischen Eigenschaften der Nervenzellen approximieren. Das Signalspektrum wählt der Experimentator oder es wird von der Umwelt bestimmt.

Zusammenfassend erlaubt es die hier vorgestellten Methoden beliebige biophysikalische Parameter der Neuronenmodelle zu verändern und ihre Auswirkung auf die Filtereigenschaften und die Varianz der Spikezeiten direkt zu verfolgen. Die verwendeten numerischen Methoden machen eine rechenaufwändige Simulation des Systems unnötig. Durch die vorgeschlagenen numerisch effizienten Methoden können in zukünftigen Studien das statistische Antwortverhalten von Nervenzellen in einem weitläufigen Parameterraum analysiert werden.

Contents

1 Introduction

Nervous systems are inherently complex, underlying the flexible, adaptive behaviour of animals, allowing them to reliably and efficiently manoeuvre through their environments. At the same time, the neural architecture is modular in its construction, and one can discern a set of rules that govern the layout and its electrical activity. For example, the mammalian *cortex* is divided into specialised areas and a homologous organisation has independently evolved in the birds' *hyperstriatum*. Much of the electrical activity in nervous systems relies on specific membrane ion channels. It turns out, that these basic molecular units of the otherwise radically different nervous systems of hydra, housefly and human are remarkably conserved.
That such complex structure can arise out of simple elements and rules has intrinsic aesthetic appeal. Moreover, the ability to precisely define the rules affords us the opportunity to test predictive theories. In particular, the „effective coding hypothesis" [10] has been postulated as a guide for the evolution of the dynamical properties of sensory neurons. The exact nature of „efficiency" has been debated and a multitude of suggestions has emerged over the years, ranging from the maximisation of mutual information between stimulus and the neural response [108], the reduction of redundancy, energy efficient representations [109], robustness to noise and the reduction of free energy [52]. Some of these ideas are interrelated, and most involve looking at the neuron form the functional point of what they are doing, *i.e.*, transmit information.
To understand how the functional level is affected by the underlying molecular machinery, this thesis focuses on developing the link between biophysics and neural coding. The goal is to simplify the relation, based on mathematical principles, which then allows to test theories of optimality.

§1.1 Noise and codes in nervous systems

In his 1880 speech before the Academy of Sciences in Berlin, the physiologist Emil du Bois-Reymond spoke on the limits of our understanding of natural phenomena. On this occasion he named seven „world riddles". The last three of his seven unsolved riddles where neuroscience related. He offered little encouragement, however, exclaiming that „*Ignoramus et ignorabimus*" when it came to problem number 5, „the origin of sensation". On earlier occasions he had already emphasised his firm conviction that no relation can ever be established between microscopic motion of molecules inside the brain and sensory impressions[1].
While such humbleness might be endearing, 130 years of scientific progress have proved the scepticism to have been excessive. We have, in fact, begun to understand how even single odorant molecules cause a moth to respond [97], and what effects the microscopic

[1] *e.g.*: „Welche denkbare Verbindung besteht zwischen bestimmten Bewegungen bestimmter Atome in meinem Gehirn einerseits, andererseits den für mich ursprünglichen, nicht weiter definierbaren, nicht wegzuleugnenden Tatsachen 'Ich fühle Schmerz, fühle Lust; ich schmecke Süßes, rieche Rosenduft, höre Orgelton, sehe Roth ..." [33] and again he concluded with his „Wahrspruch" *Ignorabimus*.

movement of channel proteins within our nervous system have on the electric signalling of nerve networks controlling movement and behaviour [73]. It is not surprising, that books written nowadays on open questions in neuroscience are characterised by far less blanket scepticism, see Ref. [80]. This thesis attempts to add a small contribution to the larger project of relating the microscopic biophysics underlying the dynamics of nerve activity to more macroscopic properties of how stimuli are encoded in nervous systems, without directly taking on the challenge of linking neuronal dynamics to behaviour.

Du Bois-Reymond's question on the causes of sensation, has recently been rephrased into: „What causes a neuron to spike?" [6], which is a somewhat simpler question, perhaps, but also one more amenable to theory and simulation.

The standard equations to describe the electric activity of nerves suggest that neurons are driven excitable systems or oscillators. These nonlinear oscillations take on the form of pulses, known as action potentials (AP), that are suitable for the transmission of information over long distances. Given that neurons are oscillators, it is natural to assume that sensation or motor commands are encoded in the frequency of oscillations, provided that the drive (*e.g.*, synaptic input or currents from sensory transduction) changes slowly. Indeed, frequency coding takes place in many neural systems [2]. More interestingly, however, it has been shown that neurons can also encode quickly varying fluctuations. Firstly, by showing that the pulses can lock to fast time structured stimuli [57], and secondly, by deducing the average stimulus before a spike from the dynamics [37].

This is the first step in determining what causes a neuron to spike. Establishing a tight theoretical link between the biophysical implementation and the statistical and information theoretical properties of neuronal responses is a field with a long history. Certainly, since modern computing techniques have become available, it is now feasible to simulate the biophysical equations and neuronal responses. This process generates input and output ensembles, which can be statistically analysed. The *in silico* system can thus be experimented on in the same way as a biological neuron, *e.g.*, within the frame work of white-noise analysis, which is introduced later in the text. But due to the complexity of the models it is insightful to approximate them with simpler models in order to allow analytic calculations. One of the oldest and simplest models is Lapicque's integrate-and-fire (IF) neuron [107]. Based on this one-dimensional model the input-output relation could be analysed in detail [172], and one can ascertain „what causes the spike" [145, 154]. This is done by calculating the average stimulus preceding an AP, also called the spike-triggered average (STA). In the IF class models some details of the biophysical reality are lost and it is difficult to address Du Bois-Reymond's point about the influence of particular molecules or ion channels on information coding.

The approach taken in this thesis uses a different type of simplified model, the phase oscillator. One of its benefits is that it can be systematically reduced from a complex biophysical model. It should be noted that also IF models have been successfully augmented to incorporate biophysical detail in order to answer particular questions on the relation between biophysical properties and coding, while retaining the possibility for analytic treatment, like investigations on the influence of adaptation currents on spike statistics in Ref. [168]. The difference with the phase oscillator framework is that the general structure of the equation remains unchanged, just the key ingredient, the system's phase response curve (PRC), has to be adapted to account for the different biophysical systems. The PRC is a function that maps perturbations that affect the neuron at different times to shifts in the occurrence of the next nerve impulse.

One important step to understand how neurons code efficiently is to investigate the implications of microscopic noise sources within the nerve cells. To what extend is noise harmful to the workings of a nervous system? Or can fluctuations be exploited to even enhance the acuteness of a sensory system (see Ref. [91] for a review)? Also, in the living, breathing, moving animal neuroscientists are often restricted to recordings from nerve cells extracellularly. Indeed, identifying and correctly assigning spike times to individual neurons is a statistical challenge in multi-electrode recordings. Then conversely, might even observing the list of spike times and their jitter alone allow us to infer the number of ion channels at the microscopic level [168]?
The behaviour of a nonlinear system such as a neuron is hard to grasp in full completeness, yet it can be understood by investigating the properties of local objects in phase space, the attractors, such as equilibria (the resting potentials) or periodic orbits (tonic spikes). Indeed, several of the computational characteristics of a neuron can be understood just by studying these attractors, their stability and the type of bifurcations that occur [92]. Different bifurcations lead to different forms of neuronal excitability and different filtering properties, as we will develop in greater detail later. However, the presence of fluctuations, intrinsic or induced by stimuli, implies that a global picture of the dynamics requires an understanding of how transitions between these attractors occur and how the system behaves in the their surroundings. Stochastic effects can drive the dynamics away from the various stable attractors that would normally determine the dynamics. Yet, for weak noise the system will spend most of its time close to one of the attractors. This supports the idea that one may be able to predict relevant aspects of the global dynamics by modifying the time scales of deterministic motion and combining them with noise induced escape times present in stochastic systems. A well known example is a phenomenon called noise induced frequency shift, in which firing rates in the presents of noise differ from what is expected from the deterministic equations in the continuum limit [177, 76]. There are also further properties of the statistics of spike times that may change, like multimodality in the distribution of inter-spike time intervals (ISI), see [76].
It is therefore beneficial to be able to trace some of these statistics at least approximately, while performing a bifurcation analysis, *i.e.*, sweeping the parameter space of a neuron, tracking its spike orbit or resting potential. This means one needs to calculate ISI mean and variances and other quantities from the information available from a bifurcation analysis. This is attempted in Cpt. 5.

Limitations

While this thesis will study neuronal dynamics, the effects of subcellular compartments will not be taken into account. Instead, we focus on an isopotential membrane patch, representative of the spike-triggering zone, which one would record from with an sharp electrode that just penetrates the membrane. These „point neurons" do not incorporate any spatially extended protuberances that neurons actually possess. We therefore do not discuss intraneuronal computations that can also be addressed within the phase oscillator frame work [150]. Also we focus on tonically spiking neurons above threshold. This excludes subthreshold dynamics and escape processes from the resting potential, as these seem to violate the idea of introducing a phase variable. However, recent publications show that the two worlds may be reconciled through the introduction of a *proto phase* [167].
A further restriction that is inherent to the phase reduction, is that it is only valid for weak fluctuations. Our calculations are of a perturbative nature and therefore, we require that

the perturbation be small. In other words, we always consider large membrane patches with many channels, so that single-channel fluctuations are averaged to some degree. In practice, we can observe that the filters derived for biophysical neurons can accurately predict significant changes in firing rate, so that the small input assumption seems not too restrictive.

§1.2 Structure of the text

The structure of the text is such that chapters are generally build on previous chapters. However, these back-references are made explicit, allowing the inclined reader to skip chapters. Cpt. 2 takes the reader quickly through most of the topics touched upon in this document, reviewing the foundations from the literature that are required in later chapters. Particularly, Cpt. 3, 4 and 5 form a continuous narrative.
Cpt. 3 reviews the biophysical properties of single neurons with particular emphasis on microscopic biophysics of individual voltage-dependent ion channels opening and closing stochastically. Such stochastic gating is a primary source of noise in early sensory systems with negligible network effects. The chapter describes in detail how to coarse-grain the chemical master equations that describe channel opening and closing as a Markovian jump process. This coarse-graining yields an equation that agrees with the classic deterministic formalism in the limit of large channel numbers, but inhabits a larger states space.
The Cpt. 4 introduces the method of phase reduction as a tool to bridge microscopic biophysics and the level of spike time point processes. In addition to the first order phase reduction a conversion into a phase-amplitude coordinate system is discussed. This will allow us to understand how noise shifts the mean firing rate of neurons, which is described in the following chapter.
Cpt. 5, thus, takes the microscopic description of channel noise in neurons and relates it to the induced jitter in spike times, that can be observed in „macroscopic" measurements with sharp or even extracellular electrodes.
In Cpt. 6, we turn from the intrinsic sources of fluctuation to extrinsic stimuli and derive the average stimulus causing a spike from a neuron's PRC. The chapter shows how a filter can be obtained that maps time structured input currents into the instantaneous probability of spike firing. It is also highlighted how the filtering properties are related to the biophysical neurons. The benefit of our approach as compared to previous work is that it explicitly distinguishes stimulus and intrinsic noise. This shows that noise has a frequency-dependent dampening effect on the STA that is stronger for higher frequencies.
The following Cpt. 7 uses the previously derived filter in order to quantify information transmission in single neurons. The lower bound to information transmission rate is rederived and all relevant spectral quantities are calculated from the phase model.
Some of the details on numerics or rederivations of known results that are included to meet the criterion of a self-contained exposure, are packed into appendices.

2 From single neuron biophysics to sensory coding

This chapter sets the conceptual prerequisites for subsequent chapters. It summarises parts of the existing literature on neural coding and dynamical systems relevant to our exposition. And also provides motivation by laying out the general targets for the following chapters.

§2.1 Neural codes

A great many primary or secondary sensory neurons emit patterns of stereotypical pulses in response to stimulation [141], that much became clear ever since the work of Lord Adrian on the toad's optic nerve in 1928[1]. He also observed that it is these spikes that carry the information concerning the environment. How exactly this information is conveyed depends on the specific region of the nervous system one is concerned with. This document will discuss a particular strategy by which sensory pathways can represent information from the outside world: a spike timing code, using the time-resolved firing probability. Specifically, a code word in the spike-timing code's alphabet is a string of spike times $\{\tau_k^{\mathrm{sp}}\}_{k=1}^{N}$. If only one of the spikes occurred at a different time it could mean something else. Suppose that the input percept rearranges spike times, yet keeps the mean firing rate (*i.e.*, the number of spikes in a fixed time interval) unaltered. Then the time averaged quantity of the firing rate does not carry the information, but the spike train does.

Reflections about the nature of the neural code — the way information is represented in nerve cell activity — is central to theoretical neurobiology. At the sensory stage, when external information enters the organism, coding strategies are typically adapted to the physical constraints of the transduction mechanism [141], and the statistics of the natural type of stimuli received in the organism's ecological niche [108, 90, 34, 16]. The codes for the different sensory systems are versatile, yet some share common properties such as Weber's log intensity law found in various olfactory and auditory systems. Along the afferent pathways the representation may change several times to facilitate different computations. For example, comparisons between ipsi- and contra-lateral percept or intensity invariant recognition may favour rates codes with adaptation, while sensory grouping and multi-modal integration could exploit codes based on the synchronisation of neurons [71, 74, 87, 17], and yet at a different stage decisions about appropriate motor responses may benefit from threshold-like on/off-neuron. In efferent nerves the activity reflects also the particular behavioural response and may include phasic or tonic (like CPGs) innervations, depending on how the muscles' kinematic is controlled. Contingently, in the central nervous system there may be the need for a unique, unified and abstract code to allow different areas of the nervous system to communicate and integrate multiple modalities [119]. But at the sensory level one might

[1] Of course, there are also systems like the fly's photo receptors that encode with graded potentials not spikes, and so do passive dendrites [104].

expect *a-priori* multifarious codes, just as rich as the sensory inputs and the anatomical diversity of sense organs themselves.

§2.2 Signals

A classical, ecological theory of sensory organs aims to predict the structural organisation of the peripheral sensory architecture [34, 16], and the coding scheme used to represent information early in the pathway [112], based on the properties of the adequate stimuli occurring in the natural habitat. A related approach is inspired by the engineering task of system identification, in which blackbox (technical) systems are probed to obtain a response which helps uncovering the exact transformation executed by them. In contrast to behavioural experiments that utilise abstractions of the actual stimuli perceived by the animal [125, Cpt. 3], systems identification often relies on unnatural stimuli that, however, possess beneficial statistical properties to facilitate the reverse-engineering scheme. Information theory can be applied within both paradigms as long as there is sufficient data. Examples of such artificial stimuli are a short transient pulse, mathematically idealised by Dirac's δ-function (Green's function method) or „white" unstructured noise (Wiener's kernel method). Both signals have a flat, uniform spectrum that contains all frequencies in an unbiased manner and thus the system's response will not lack structures simply because of missing input complexity. In reality, a uniform spectrum of a physical stimulus can not extend its frequency range to infinity as this would require infinite power. Instead, there will be a reasonable upper bound to the frequency content, $f_c = \sup\{f : P(f) > 0\}$. In addition, artificial stimuli are at times chosen from a Gaussian process, for reasons including the invocation of a central limit theorem, arguments based on maximum entropy, or easement of analytical treatments.

§2.2.1 Bandlimited signal

In contrast to white noise, a band limited signal, with no power above f_c, has only a limited number of $2f_c$ degrees of freedom per second [23]. In accordance with Whittacker-Shannon sampling it can be represented as a finite set of random numbers per unit time. The physical signals that announce themselves on sensory organs can have their power distributed over many octaves. However, signals emitted by other animals, either voluntarily like the communication songs of grasshoppers or involuntary as moth falling prey to a bat, are often constrained to a frequency range that is related to the body size of the sound producing animal (see the next paragraph for three examples of relevant natural stimuli). In such occasions one can identify an upper frequency, f_c, above which no relevant information is expected. Additionally, all primary transduction processes have a time constant restricting the signal frequencies they can follow. This is sufficient reason to consider the stimulus $x(t)$ to fall into the class of bandlimited signals (also called baseband signals).
More precisely according to the sampling theorem a band limit signal with cutoff frequency f_c requires at least a sampling rate of $2f_c$. With the help of the Whittaker-Shannon interpolation formula the signal can be written as [23]

$$x(t) = \sum_n x_n \ \mathrm{sinc}\,(2tf_c - n) \tag{2.1}$$

For an observation interval $[0, T)$ one needs a minimum of $N_T = \lceil 2Tf_c \rceil$ samples to specify the continuous bandlimited process completely.

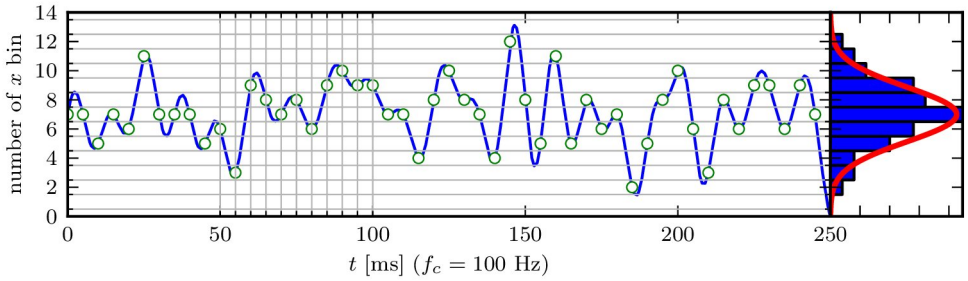

Fig. 2.1: A bandlimited and binomially distributed ($k = 14$, $p_{\mathrm{Bn}} = \frac{1}{2}$) signal as an approximation to a Gaussian process ($\mu = kp_{\mathrm{Bn}}$, $\sigma^2 = kp_{\mathrm{Bn}}(1 - p_{\mathrm{Bn}})$). The cutoff frequency was 100 Hz, implying that the entire stimulus over 250 ms is exactly defined by 50 regularly spaced samples, as according to the Nyquist theorem one needs at least two samples per period to define an oscillation. To check if the binomial amplitude distribution is an adequate approximation to a Gaussian, the Shapiro-Wilk test for normality is used. The Samples are accepted as Gaussian with an α-level of 0.4 (very small α-leves would mean rejection of normality).

In order to compare information theoretic bounds on the information transmitted through continuous channels (physical systems) to histogram based methods for the estimation of mutual information the Whittaker-Shannon sampling has to be augmented by discretisation of the (Gaussian) random variables x_n. The simplest strategy is to start with a discrete set of binomially distributed random variables, $x_n \sim \mathrm{Bn}(k, p_{\mathrm{Bn}})$ with $p_{\mathrm{Bn}} = \frac{1}{2}$, and use the fact that for large k the statistics will be approximately Gaussian. With this there is a correspondence between a time-continuous process on an interval $[0, T)$ and a discrete binomial vector, so that the histogram frequency $p([x_1^1, \ldots, x_1^k, \ldots, x_n^1, \ldots, x_n^k])$ can be estimated. For example the blue time continuous process in Fig. 2.1 between 50 and 100 ms with $f_c = 100$ Hz is described by the 11 samples marked as green circles. The continuous process is statistically similar to a Gaussian process.

§2.2.2 Natural signals

Let us proceed by giving several examples of natural stimuli that can be qualitatively described by baseband signals. The external signals from the natural world relevant to animals can often be categorised into the three broad classes: (*i*) signals relevant to basic body kinematics and movement; (*ii*) signals for predator or prey detection; and (*iii*) communication signals form other (often conspecific) animals. We may pick one example from each category.

Example 1 (Hiving hoverflies)**.** The *dipteran* haltere organ [136] is a biological gyroscope that enables hoverflies to excel in aeronautics. The organ evolved from the second pair of wings. According to behavioural studies halteres measure Coriolis forces during flight.
The white noise analysis of crane fly halteres under direct mechanical stimulation in Ref. [47, Fig. 3] shows that the system is sensitive to stimuli movements on time scales around 10 ms, while very fast stimulus changes are ignored.

Example 2 (Praying paddlefish)**.** The primary afferents in the american paddlefish *Polyodon spathula*'s electrosensory organ show a tonic response to fluctuating stimuli. In their muddy habitat the electrosensory system is used to detect their planctonic prey, like members of the crustacean genus *Daphnia*. The frequency spectrum of the bioelectric profile emitted

by single moving Daphnia shows that most power resides in a baseband below 8 Hz [140, Fig. 4a]. For whole swarms the power is distributed over a larger interval, but still drops at high frequencies. In addition to naturalistic stimuli, the electrosensory system has been investigated with white noise analysis in order to determine the transfer function of the sensory affarents [140]. This has confirmed that information transmission is focused on a passband between 0.5–20 Hz with a steep roll-off.

Example 3 (Greeting grasshoppers)**.** Many gomphocerin grasshoppers like *Chorthippus biguttulus* use acoustic signalling to arrange mating behaviour. The detected signals are amplitude modulations of broad band carrier waves. The important information about the song structure resides in frequency band below 100 Hz, see Refs. [123, Fig. 1b,c] and [163, Fig.1b].

We wish to stress that there often is a separation of time scales between stimulus induced perturbations and those fluctuations that originate from internal biophysical noise in receptor neurons, see Cpt. 3. The three examples clearly fall into this category where the stimulation cutoff renders the stimuli orders of magnitude slower than the intrinsic noise.

§2.3 Information transmission versus -filtering

The reception of information about the outside world is the raison d'être of sensory systems and thus quantifying how well they perform by calculating their transmission rate (in bits/sec) is key to understanding their evolutionary nascence. But, inspecting bit rates may be less enlightening in the parts of a sensory pathways which are processing information rather than just transmitting it to the next level [85, Cpt. 13.2]. This criticism has also been voiced in Refs. [171, 94, 159]. The precise function of such a neuronal construct is to throw some part of the sensory information away, keeping only relevant bits in preparation for decisions and actions of the animalcules. The throwing-away part or filtering-out of irrelevant input „noise" is a crucial task. Instead of the overall bit rate the filtering properties of the pathway or individual neurons are then informative. To this end the filter that maps a time structured, perturbative stimulus into the instantaneous firing rate is derived in §6.2 of Cpt. 6.

§2.4 Trains of spike times

The evolutionary origin of membrane voltage spikes goes back to single celled lifeforms such as members of the genus *Paramecium* [72]. Action potenials (APs) are also found in plants and might have emerged multiple times independently during the cause of evolution. Its hallmark is that by means of an active regenerative process the amplitude of the signal is kept from degrading as it travels along somas and axons or through an active dendrite. The advantage of this active signalling over graded passive potentials is its reliability in terms of signal-to-noise ration (SNR) particularly over long transmission distances, which became more important when animal bodies grew in size. It also implies that the amplitude as such does not code information and instead the spike times (arrival time of AP peaks) is considered important (termed all-or-nothing principle).
In order to focus in on the statistical and information theoretic properties of a timing code one abstracts the voltage trace into a set of spike times $\{\tau_k^{\rm sp}\}_{k=1}^{N_{\rm sp}}$. If we observe the neuron

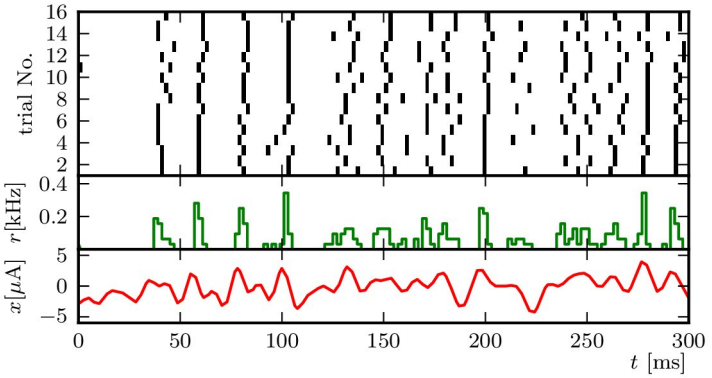

Fig. 2.2: Simulation of the neuron model with Na^+ and K^+ channels. For details on the simulated stochastic differential system see Cpt. 3. The upper panel shows 16 simulations in which the neuron was driven with exactly the same stimulus shown on the lowest panel. Each spike time is depicted as a small black square. The middle panel shows histograms counting spikes through trials over small time bins. This yields the instantaneous probability of spike emittance. One can observe that the increased firing probability is temporally locked to prominent excursions in the stimulus.

continuously for ever we set $N_{\text{sp}} \to \infty$. The all or nothing principle is stated as an idiosyncratic AP wave form $V_{\text{AP}}(t)$, that is shifted and superimposed to compose the AP train[2]

$$V_{\text{rest}} + \sum_k V_{\text{AP}}(t - t_k) = V_{\text{rest}} + (V_{\text{AP}} * y)(t). \tag{2.2}$$

Here, it is found useful to define the delta spike train, deconvolved from the actual AP waveform, as

$$y(t) = \sum_{k=1}^{N_{\text{sp}}} \delta(t - t_k). \tag{2.3}$$

The spike train $y(t)$ is idealised and nonphysical[3], but while the exact wave form V_{AP} in an experimental setup depends in on the placement of electrodes and chosen equipment, the spike times are more robust. So one can conceive $y(t)$ as the underlying platonic ideal of the spike train.

Suppose that the spike train is nearly periodic, say with period T_{p}, but that deviations from perfect periodicity are induced by the input stimulus. Then let us define $\phi(t) \in \mathbb{R}$ as a variable that is almost like time but speeds up and slows down depending on perturbations, *e.g.*, from a stimulus $x(t)$. One can formally write $\phi_t[x]$ indicating that the departure of the phase variable form a linearly increasing time may depend on the stimulus history. With this in mind the spike train can be expressed as

$$y(t) = \sum_{k=1}^{N_{\text{sp}}} \delta(t - t_k) = \sum_{k=1}^{N_{\text{sp}}} |\dot{\phi}(t)| \delta(\phi(t) - kT_{\text{p}}). \tag{2.4}$$

[2]Naturally, the principle is violated somewhere in the nervous system of some species. Graded potential in the visual system of flies as well as the two different AP shapes in an axon of the jellyfish *A. digitale* are counter examples. Indeed, the two wave forms encode two different behavioural responses of the jellyfish, hence amplitude matters in that case.

[3]This will cause some quantities such as the spectral density of y to have slightly unintuitive properties

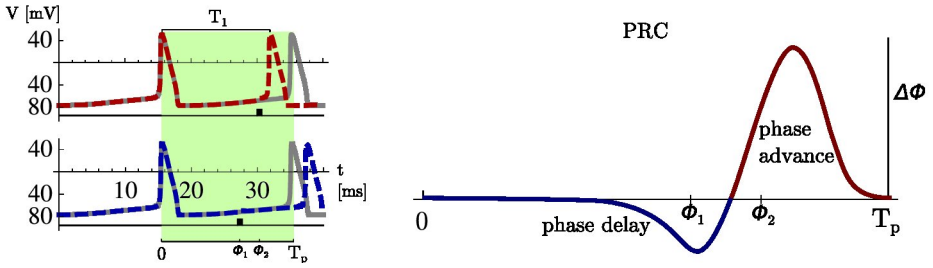

Fig. 2.3: Experimental definition of the phase response curve. Perturbations (■) at two different phases ϕ_1 and ϕ_2 respectively cause phase delay and phase advance. The grey line shows the voltage response with no stimulation, while the overlaid dashed lines show the same neuron with perturbations present. By comparison, the perturbation placed at ϕ_1 causes a delay and the perturbation at ϕ_2 causes and advance in the next spike time. The model is the standard squid axon model (parameters can be found in B).

$\phi(t)$ should be differentiable. The factor $|\dot{\phi}(t)|$ guarantees that time integrals over $y(t)$ (such as spike counts) are not tampered with. For weak stimuli the prefactor is positive and the absolute value can be dropped. The evolution equation for $\dot{\phi}$ will be detailed in Cpt. 4.

§2.5 Phase response curves

Under the assumption that spike times are important, one needs methods to investigate how the timing of spikes changes, conditioned on input perturbation of the neuron. A classical paradigm that is applicable if the neuron is a self-sustained oscillator is the phase response curve (PRC)[4], which was first employed to chronobiological oscillators (*cf.* Ref. [187] for a historical review) and later to spiking neurons in Refs. [39, 36]. See also the recent books [40, 166] for applications in neurobiology. It characterises the phase shifts (or shifts in timing) of a particular event within the limit cycle subject to inputs at particular times within the cycle. To describe a high dimensional nonlinear system such as a biophysical neuron or in chronobiology the whole suprachiasmatic nucleus by just a single one dimensional phase (or time shift) variable amounts to a quite formidable contraction of the biophysical state space.

The PRC can be defined in the following way: It tabulates the persistent change in the inter spike period of a neuron induced by a transient perturbation as a function of the phase at which the perturbation is received, *cf.* Fig. 2.3. Mathematically it is a function from phase (or time) to phase shift (or time shift), $Z : \phi \to \Delta\phi$, where $\phi \in [0, 2\pi)$. In fact, the domain may be scaled to an arbitrary interval, *e.g.*, $[0, 1)$ or $[0, T_\mathrm{p})$ are common choices. We will change between different notations at times. Naturally, $Z(\phi)$ is periodic, but the exact graph of the function is intricately linked to the properties of the dynamical system it describes, see §2.5.2. The definition of the PRC immediately suggests a naive experimental approach with which it can be determined. First, observe the period of the unperturbed system, T_p. Let us use the definition $\phi \in [0, 1)$ for the moment. Then, perturb the system with a short, time-localised pulse of amplitude A, *i.e.*, $A\delta(\phi - \phi_1)$, at a particular time instance $\phi_1 T_\mathrm{p}$ in the inter spike interval and measure the length of the period T_1 as in Fig. 2.3. The phase

[4] In the literature one also finds the terms phase resetting curve, phase sensitivity or phase susceptibility. We can use them interchangeably.

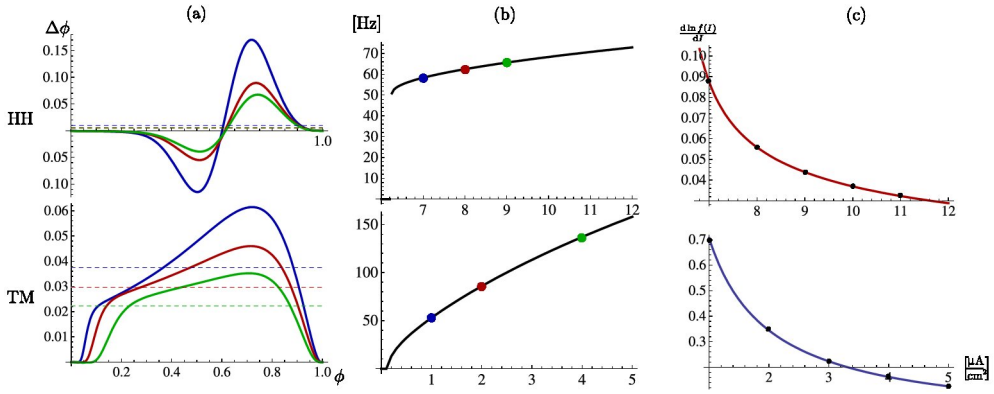

Fig. 2.4: The slope of the f-I curve is related to the average PRC. Two model, the Hodgkin-Huxley (HH) and Traub-Miles (TM), are contrasted. (a) Shows the voltage PRCs the of HH and TM models for different injected DC currents in (b). In (c) the log-slope of the f-I curve is compared with the mean of the PRC (black dots) as predicted from Eq. (2.8).

shift for the phase normalised to $[0, 1)$ is then

$$\Delta\phi(\phi_1; A) = \frac{T_\mathrm{p} - T_1}{T_\mathrm{p}}. \tag{2.5}$$

Repeat this for a sufficiently dense grid of $\phi_i \in [0, 1)$. To first order the strength of the phase shift is linear in the magnitude of the perturbation given, $|\Delta\phi(\phi; A)| \sim A$. It is thus reasonable to normalise the PRC accordingly.

$$Z(\phi) = \lim_{A\to 0} \frac{\Delta(\phi; A)}{A}. \tag{2.6}$$

This is called the infinitesimal PRC and has units of $[\text{stimulus}]^{-1}$ or [rad/stimulus], if we include scaling with 2π. Using the phase $\phi \in [0, 2\pi)$, the unperturbed neuron satisfies $\phi = \omega\, t$. In the presence of phase perturbations at different times t_k

$$\phi(t) = \phi(0) + \omega\, t + \sum_k \int_0^t \mathrm{d}\tilde{t}\, Z(\phi(\tilde{t}))\, A\delta(\tilde{t} - t_k). \tag{2.7}$$

The great utility of PRCs is merited to the fact that it is both an experimental procedure and a well defined mathematical quantity. As will be shown by formal arguments in §4.3, the PRC is a periodic solution to the adjoint of the first variational equation of a limit cycle system. As a consequence, for every system with a stable limit cycle[5] there exists a PRC.
It is important to note that, the above introduced experimental procedure to determine the PRC of the neuron assumes stationary conditions, *i.e.*, the phase sensitivities at various perturbation points do not change while tabulated. A consequence of the PRC being the adjoint to the first variation of the limit cycle (as shall be seen when introducing the PRC mathematically in §4.3), the shape of the PRC is affected by any parameter that affects the flow-field around the limit-cycle or its period. In that sense, the PRC is a local property in the system's parameter space and changes for example with parameters such as the DC input current to a neuron. It is common to characterise tonically spiking neurons, by their

[5] Also termed, Jordan curve, closed or periodic orbit and invariant cycle in various sections of the literature.

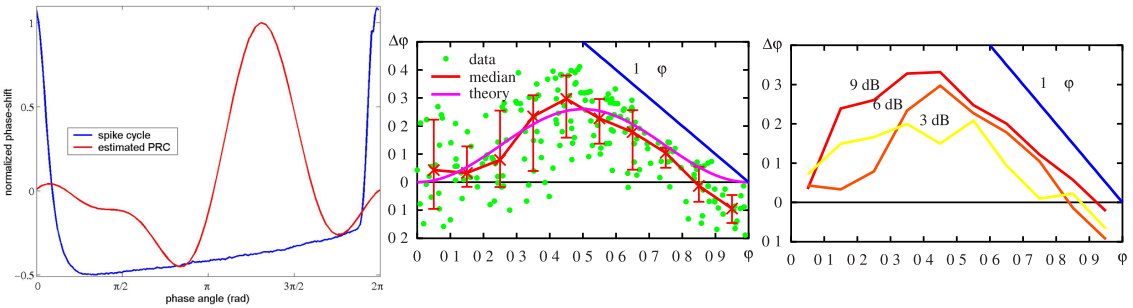

Fig. 2.5: Examples of experimentally measured phase response curves in sensory systems. Left: PRC of a mitral cell in the olfactory bulb from Ref. [60]; Middle: PRC of the auditory receptor in Locusts from Ref. [12]. The median of the measured phase shifts is plotted and for comparison the theoretical PRC of canonical SN on LC bifurcation see §2.5.2. Right: As in the TM model in Fig. 2.4 there is an increase in the PRC mean with the DC stimulus.

f-I curve, which graphs the DC input current *versus* the mean firing rate, see Fig. 2.4b. Some neurons start with a finite firing rate, while others others can spike at arbitrary low frequencies. Two examples of such neurons are the classical Hodgkin-Huxley (HH) equations of the squid axon and the Traub-Miles (TM) equations for the membrane dynamics of a hippocampal pyramidal neuron. The general structure of those biophysical neuron models is introduced in §3.1, with the particular parameters given in App. B.
The intimate connection between the PRC and the *f-I* tuning curve of a neuron can be seen in Fig. 2.4. In a deterministic neuron a simple calculation using the equivalent phase oscillator (which will be introduced in Cpt. 4) shows that the slope of the *f-I* curve is related to the mean of the PRC by

$$\frac{\mathrm{d}\ln f(I)}{\mathrm{d}I} = \frac{1}{T_\mathrm{p}} \int_0^{T_\mathrm{p}} \mathrm{d}\phi \; Z(\phi; I), \tag{2.8}$$

illustrated in Fig. 2.4b.
This highlights the fact that the PRC and the *f-I* curve give complementary information about the neuron. The *f-I* curve characterises the average spike rate to a non-fluctuating constant current over a whole range of DC values, while the PRC describes the changing in individual spikes for fluctuating inputs around one fixed DC value.

§2.5.1 PRCs in experimental systems

The earliest experimentally measured PRCs of biological oscillators are from the circadian system [187]. In a neurobiological context, PRCs have been measured in the *Locust*'s central pattern generators involved in flight [157], and neurons in the central nervous system such as cortical pyramidal neurons [173]. More relevant to our topic, PRC have been measured for some nerve cells of the sensory periphery, like a mitral cell [59]) and the Locust's auditory receptor [12]. Examples are portrayed in Fig. 2.5.
PRC are also used to study the response properties of whole networks. Experimentally, the PRC of carbachol-induced network oscillations in the rat hippocampal CA3 region were determined and modelled with the Wilson-Cowan equations [3].
As can be seen from Fig. 2.5 the data of phase shifts collected may be very noisy, so refined

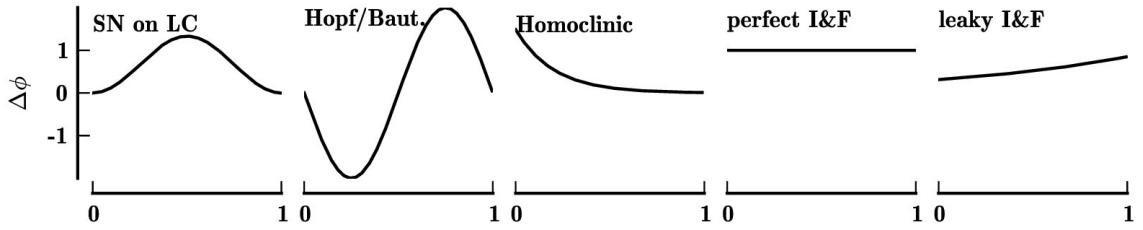

Fig. 2.6: The first three panels show versions of the PRC of normal form models close to The magnitude of the PRC is scaled arbitrarily. The actual scaling depends on how close to the bifurcation the model is. The last two panels are PRC of one dimensional integrate-and-fire models.

estimation techniques only recently developed could improve the situation [59, 38]. This will hopefully lead to estimates of PRC in other sensory systems that use tonically spiking neurons to encode information.

§2.5.2 Canonical PRCs

The PRC of the HH and TM model depicted in Fig. 2.4a show distinct features. While the HH PRC takes positive and negative values, the TM PRC is strictly positive. This matches with the features of their f-I curves. The positive and negative regions in the HH PRC reduces its mean, which according to Eq. (2.8) agrees with the smaller slope of the HH f-I curve. Also the extent of the ISI interval in which perturbations have any effect differs, as the HH models shows longer period of relative phase insensitivity (called dead zone in chronobiology) at the beginning of the ISI. Also the experimentally determined PRC from two exemplary systems show such distinct differences, *cf.* Fig. 2.5.
Mathematical analysis of the normal forms of conductance based models near the onset bifurcations from rest to spiking has revealed that the PRC may be grouped by the bifurcation type [24, 36]. A comprehensive summary of PRCs for many normal forms and one dimensional models is found in Ref. [18] and reprinted in Fig. 2.6. If the neuron enters spiking because the stable resting equilibrium is annihilated by a second unstable equilibrium on a limit cycle (LC), which is called saddle-node (SN) on LC, then the PRC is strictly positive. The normal form of the subcritical Hopf bifurcation is known as the Stuart-Landau (SL) equations. The super- and subcritical Andronov-Hopf bifurcations yield sinusoidal PRCs. The definition for the SL model is included in App. A.3, because we shall use its analytic tractability to exemplify certain noise induced effects in §5.6. The saddle-node on homoclinic orbit bifurcation produces an exponentially decreasing PRC. Note that this canonical PRC is not periodic. In a real biophysical neuron close to a SN on homoclinic orbit bifurcation one would find a steep drop at the spike rendering it periodic.

§2.6 Instantaneous firing rate

In the raster plot of Fig. 2.2 spike trains emitted by a model neuron in response to the time continuous signal $x(t)$ (bottom time series) are shown as small black rectangles. One trial is mathematically represented as the sum of delta functions, $y(t)$, from Eq. (2.3). On closer inspection one notices that repetitive presentation of the same stimulus yields different sets

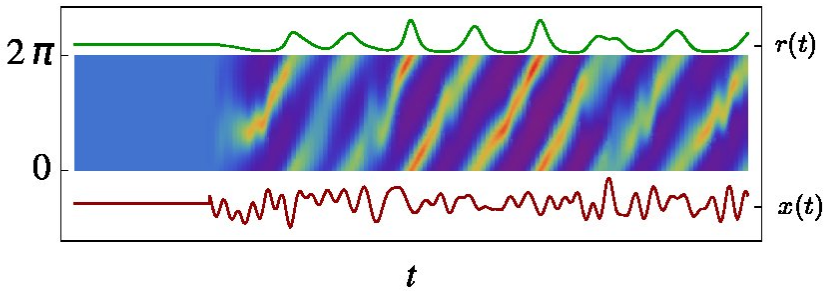

Fig. 2.7: Instantaneous firing rate as the flux of the phase at 2π. The density plot shows the probability distribution over ϕ evolving in time. Initialised with a uniform distribution it stays that way until the stimulus (lower time series) is activated. The time dependent forcing then causes barrelling in the phase distribution, which is reflected in the non-uniform flux.

of $\{\tau_k^{\mathrm{sp}}\}_{k=1}^{N_{\mathrm{sp}}}$. Still locked to strong positive excursions in the stimulus, the different trials are not entirely unrelated to each other, but the individual spike times are distorted. The sources of this jitter are discussed in §3.3 and §3.4.

A reasonable description of the whole ensemble of trial responses is the instantaneous probability of AP triggering, also called instantaneous firing rate, $r(t)$. Experimentally it is estimated via histograms from a finite set of trials (*cf.* histogram beneath the raster plot in Fig. 2.2). Here, a digital representation of the δ-functions is used, with discretisation step Δ_t and a finite impulse hight of Δ_t^{-1}. Mathematically the idealised firing rate is defined as the continuum limit to infinitely many trials, $N_{\mathrm{trials}} \to \infty$

$$r(t) = \langle y(t) \rangle_{y|x}. \tag{2.9}$$

Again the firing rate can also be connected to the variable $\phi(t)$ from the previous paragraph. In the same way as the spike times in Fig. 2.2 vary among trials the evolution of the associated phase variable $\phi(t)$ depends on the noise realisation within each trial. Thus, each trial produces a different path of the phase variable, so that at each time instance produces a histogram of phases, which in the limit of infinite trials produces the phase density $p(\phi, t)$. One can formally introduce the phase density or time dependent histogram of the phase as

$$p(\phi, t) = \langle \delta(\phi - \phi(t)) \rangle_{\phi|x}, \tag{2.10}$$

where the average $\langle \cdot \rangle_{\phi|x}$ indicates trial averaging. One way of interpreting the density $p(\phi, t)$ is to think of it as the number of neurons of an unconnected population being in phase ϕ divided by the population size. More detail on the differential operator, the Fokker-Planck operator, that describes the propagation of this density through time are given in the following chapters and A.2. Postponing the mathematical details Fig. 2.7 shows such a propagation of a phase density for a particular stimulus shown at the bottom. When the stimulus is constant the phase distribution tends to the uniform distribution. But as soon as time dependent forcing begins it creates departure from uniformity in the phase density. Since the phase increases with some average frequency, the peaks in the phase density move in the direction of $\phi = 2\pi$ and pass through the boundary to be reinjected at $\phi = 0$. The directed flux of the probability current through that boundary measures how many oscillators where just about to spike at time t and just had spiked at time $t + \mathrm{d}t$.

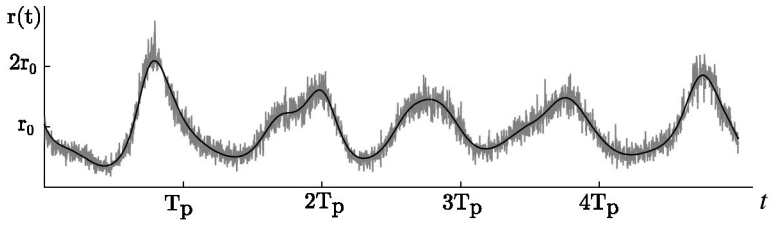

Fig. 2.8: Comparison between the firing rate defined as the flux of the phase density (black line) and by trial averaging (grey) for the two-dimensional Stuart-Landau oscillator (model definition see A.3 with parameter $a = 1$, $b = 2$, $c = -1$, $d = -1$). The model is driven by a Gaussian signal with flat spectrum up to a cutoff frequency $3\omega_0/2\pi$ Hz and standard deviation of 0.15 that is applied to one dimension and intrinsic noise with standard deviation of 0.3 that is applied to the other. Number of simulated trials: 30000.

In the example in Fig. 2.7 the time dependent probability flux is depicted on top of the 2π-barrier. This corresponds exactly to the definition of the instantaneous firing rate. That the probability flux is in good agreement with the trial averaged firing rate can be seen in the numerical example that used the Stuart-Landau equations, the canonical model for Andronov-Hopf bifurcations in Fig. 2.8.

§2.7 Inter-spike interval statistics

Before turning to the encoding of time continuous stimuli, we consider the statistics of spike trains under constant input, that is, when the equations of motion are homogeneous. In particular, the statistics of the waiting time between consecutive spikes—the interspike interval (ISI) is of interest[6]. Calculation of the waiting time density is possible for simplified neuron models. For example, it is long established that the ISI distribution of perfect integrate-and-fire model (IF) driven by uncorrelated Gaussian noise is the inverse Gaussian [183]. More recently, the ISI distribution of the perfect IF model driven by coloured noise was calculated using a weak noise assumption [116, 130]. These expressions are also in approximate agreement with the ISI densities of more complex neurons showing spike-frequency adaptation [168]. The reason is that adaptation processes filter the uncorrelated noise source so the noise in the spike generation process is effectively coloured and the existing theory of Refs. [116, 130] can be applied.

Phase oscillators are similar to IF models, yet instead of the explicit reset they operate on a periodic domain $\phi \in \mathbb{S}([0, 2\pi))$. Specifically, in the differential form of Eq. (2.7) the phase model reads

$$\dot{\phi} = \omega + Z(\phi)x(t), \tag{2.11}$$

where we have replaced the delta stimulus by a noise process $x(t)$.

The spike is defined as a crossing of the periodic boundary, say at $\phi = 2\pi$ with $\phi = 2\pi \mapsto \phi = 0$. However, some caution is necessary with the spike definition, in particular when the system is driven by white noise. To elaborate this, let us denote with N_{cross} the number of level crossings at $\phi = 2\pi$ in the positive direction per unit time. If the noise process is a stationary Gaussian process with covariance $C(\tau)$ and the dynamics resides at the boundary,

[6] Also referred to as first passage time, mean sojourn time or occupancy depending on the context.

then, according to Rice's formula the expected number of crossings is [152, 153]

$$\langle N_{\text{cross}} \rangle = \sqrt{-\frac{\mathrm{d}^2}{\mathrm{d}\tau^2} C(\tau)\bigg|_{\tau=0}} \,. \tag{2.12}$$

For coloured noise this yields a finte number of crossings per unit time. Analysing the white noise, which has $C(\tau) = \delta(\tau)$, as the $(\kappa \to 0)$-limit of process with correlation $C(\tau) = e^{-\tau^2/\kappa^2}/\sqrt{\pi\kappa^2}$, results in an infinite number of zero crossings

$$\lim_{\kappa\to 0} \langle N_{\text{cross}} \rangle = \lim_{\kappa\to 0} \sqrt{\frac{2}{\sqrt{\pi}}} \left(\frac{1}{\kappa}\right)^{\frac{3}{4}} = \infty.$$

This in neurobiological terms non-physiological behaviour is due to counting each crossing of the phase in positive direction irrespective of whether the phase crossed in the negative direction just the infinitesimal time instance before, an event which can happen infinitely often with white noise. While this makes sense in many applications [113], for a neuron, a small jitter at the tip of a spike which causes the phase to jitter around the 2π boundary would not be considered an additional spike. To obtain a complete spike the phase needs to actually traverse all the way trough the up and down stroke of the action potential. In numerical simulations of realistic neuron models, one can ensure that a threshold crossing is counted only once by adding an artificial absolute refractory period during which further threshold crossings are discarded. In phase models, the free running phase may be used and after each crossing the boundary increased by 2π. This is related to the use of reflecting and absorbing boundaries at 0 and 2π, when calculating waiting time distributions, see Cpt. 5; or using periodic boundaries and define an instantaneous spike rate as the net probability flux, not just the unidirectional flux, see Cpt. 6.

In the following we rederive equations for the moments of waiting times as in Ref. [61]. Let $y(t)$ be the process in question, denoting a voltage or a phase variable. The process starts at a particular y_0 that is the initial distribution is $p(y, t_0) = \delta(y - y_0)$ and one is interested in the distribution of times for the process to reach $y = y_1$.

If the process is governed by a differential equation that involves stochastic terms (a stochastic differential equation, SDE), then one can show that the associated density $p(y, t)$ defined in Eq. (2.10) is propagated by a specific evolution operator

$$\dot{p}(y, t) = \mathcal{F}(y)p(y, t). \tag{2.13}$$

This equation is called the Fokker-Planck equation (FPE). An example of its solution was given in Fig. 2.7. The mathematical structure of the Fokker-Planck operator, $\mathcal{F}$, is derived in A.2. We denote the solution of a homogeneous FPE with starting distribution concentrated at one value y_0 by $p(y, t; y_0, t_0)$ such that $p(y, t_0; y_0, t_0) = \delta(y - y_0)$ and write its formal solution as

$$p(y, t; y_0, t_0) = e^{(t-t_0)\mathcal{F}(y)}\delta(y - y_0). \tag{2.14}$$

Our goal is to find a relation between the ISI distribution of the neuron model and the FP operator, which can be determined from stochastic equations such as Eq. (2.11). For that let us assume that the process lives in an interval (y_1, y_2), where y_2 could denote the spike threshold and y_1 the resting potential to which an IF neuron resets, or the two boundaries encapsulating the periodic domain of the phase oscillator interval, $y_1 = 0$ and $y_2 = 2\pi$. At

time t_0, the system is supposed to start inside the interval, $y_1 \leqslant y_0 \leqslant y_2$. The probability at time $t > t_0$ of still being inside the interval (y_1, y_2), and thus no spike occurring, is [61]

$$G(y_0, t) = \Pr(y_1 \leqslant y(t) \leqslant y_2) = \int_{y_1}^{y_2} \mathrm{d}\tilde{y}\; p(\tilde{y}, t; y_0, t_0),$$

with additional condition $G(y_0, t_0) = 1$ because we started with $y_0 \in (y_1, y_2)$. The time derivative of $G(y_0, t)$, *i.e.*, the change in the probability of remaining within (y_1, y_2), at any given t measures the exit probability. This is called the *first-passage time density*, which we denote by

$$q(t, y_0) = \frac{\partial G(y_0, t)}{\partial t}. \tag{2.15}$$

With the help of the formal solution in Eq. (2.14) it can be shown that the inner product of $h(y, t) = G(y, -t)$ and $p(y, t; y_0, t_0)$ is constant

$$\begin{aligned}\langle h, p\rangle = \int \mathrm{d}\tilde{y}\; h(\tilde{y}, t) p(\tilde{y}, t; y_0, t_0) = \iint \mathrm{d}y \mathrm{d}\tilde{y}\, p(y, -t; \tilde{y}, t_0) p(\tilde{y}, t; y_0, t_0) \\ \iint \mathrm{d}y \mathrm{d}\tilde{y}\, e^{-t\mathcal{F}(y)} \delta(y - \tilde{y}) e^{t\mathcal{F}(\tilde{y})} \delta(y_0 - \tilde{y}) = \int \mathrm{d}\tilde{y}\, \delta(y_0 - \tilde{y}) = 1.\end{aligned}$$

Note that the operator $e^{t\mathcal{F}}$ commutes with the identity operator $\delta(y - \tilde{y})$. Taking the time derivative and using $\dot{p} = \mathcal{F}p$ one obtains

$$\partial_t \langle h, p\rangle = \langle \dot{h}, p\rangle + \langle h, \dot{p}\rangle = \langle \dot{h}, p\rangle + \langle \mathcal{F}^\dagger h, p\rangle = 0.$$

Because p may change according to its initial conditions, the last expression implies that $\dot{h} = -\mathcal{F}^\dagger h$, or that $G(y, t)$ is a solution to the *adjoint Fokker-Planck* equation [61]

$$\dot{G}(y, t) = \mathcal{F}^\dagger G(y, t), \quad \text{s.t. } G(y, T_0) = \mathbb{1}_{[y_1, y_2]}(y). \tag{2.16}$$

The adjoint operator $\mathcal{F}^\dagger$ is also called the infinitesimal generator of the stochastic process. In addition to the boundary condition above, trivially stating that if we start in the boundary the initial probability of inside is one, one may include reflecting boundary conditions at the lower end $\partial_y G(y, t)|_{y=y_1} = 0$ and absorbing boundary conditions at the upper end $G(y_2, t) = 0$. This would correspond to an IF model which resets at y_2.

In some cases it is possible to solve for G and obtain expressions for the ISI density $q(t, y_0)$ [183].

Since one of the main objectives in this document is to establish links between the microscopic noise sources such as channel noise and the macroscopic spike jitter one may immediate pose the question: How much information about the underlying diffusion process can we extract from first passage time densities like the ISI distribution? Might there be a unique diffusion process generating it? A sobering answer to the second question was given in Ref. [11]: No—the solution is not unique, there are several possible diffusion processes that may lead to one and the same passage time density.

Yet, not all is lost. If one takes into account constrains from membrane biophysics, then diffusion process derived is not completely arbitrary. In fact, if the model is derived from first principles, then the free parameters in the model can be related to the ISI statistics.

§2.7.1 Moments of the ISI distribution

Instead of attempting to obtain the complete ISI distribution by solving the adjoint Fokker-Planck equation, Eq. (2.16), one may content oneself with the first two moments or the coefficient of variation, which one uses to quantify spike jitter in experiments.

Let us set $t_0 = 0$ and Denote the n^{th} moment of the ISI distribution as [61]

$$T_n(y) = \int_0^\infty \mathrm{d}\tau\ \tau^n q(\tau, y) = -\int_0^\infty \mathrm{d}\tau\ \tau^{n-1} G(y, \tau), \tag{2.17}$$

where the fact was used that for the finite interval (y_1, y_2) exit is guaranteed, *i.e.*, $G(y_0, \infty) = 0$. one may multiply both side of Eq. (2.16) with t^n and integrate to obtain a recursive ordinary differential equation for the moments

$$nT_{n-1} + \mathcal{F}^\dagger T_n = 0, \quad \text{s.t. } T_n'(y_1) = T_n(y_2) = 0 \text{ and } T_0 = 1. \tag{2.18}$$

Here we have imposed reflecting boundary conditions on the lower limit y_1 and absorbing boundary conditions on the upper limit y_2. These conditions are in agreement with an IF model, which once reaching the spike threshold is reset an unable to move inversely through the spike. As we discussed in the beginning of §2.7 they can also be applied as an approximation to the phase oscillator if the noise is weak.

In Cpt. 5 the Eq. (2.18) will be used to calculate ISI moments of conductance based neurons using a phase reduction. Suppose we have an FP operator $\mathcal{F}(\phi)$ for the equivalent phase variable that is accurate to order ε^k in the noise. Then all moment, T_k, up to order the k^{th} can be obtained accurately. For example if one is interested in ISI variance, the method will require finding a suitable SDEs for the phase variable $\phi(t)$ that gives the FP operator to second order.

Renewal equation

In a renewal process, all inter-spike intervals are independent, as though each is separately drawn form the ISI distribution. But slow kinetic processes in the neuronal dynamics or long-term correlations in the external stimulus could make the spike train have negative or positive correlations. A point process with such properties would be called a non-renewal.

The ISI distribution alone does not tell us about the correlation between consecutive inter-spike intervals. Are they independent, negatively or positively correlated? Several types of adaptation currents have time scales spanning orders of magnitude above the spiking period and indeed there contribution to ISI correlations have been analysed [44, 168]. But, for the sake of simplicity, we will ignore the effects on longer times scales and consider a spike train as arising form a renewal process.

In the following we treat the neuron as a threshold device such as an integrate-and-fire neuron or a phase model neuron. We compile here a few known results on renewal processes that we will need in later chapters (*e.g.*, §7.2).

The transition probability $p(\theta, t; y_0, t_0)$ describes probability a spike occurring at time $t = t_0$, when the neuron was in state y_0, is followed by a spike at time t, when the neuron crosses threshold θ. For a stationary renewal process, at any given time after a spike the transition

probability $p(\theta, t)$ in the renewal case can be decomposed into

$$p(y,t;y_0,0) = \int_0^\infty \mathrm{d}\tau\, p(y,t;\theta,\tau) q_\theta(\tau) = \int_0^\infty \mathrm{d}\tau\, q_\theta(\tau) p(y,t-\tau;\theta,0). \tag{2.19}$$

Here $q_\theta(\tau)$ is shorthand for the interspike interval distribution from y_0 at $t_0 = 0$ to threshold θ, corresponding to the transition probability $p(\theta, \tau; x_0, 0)$. The second equality is due to stationarity, which implies a convolution. The spike autocorrelation $C(\tau)$ is the probability that given a spike at t there is an other spike at $t + \tau$. This is equivalent to the transition probability $C(\tau) = p(\theta, \tau; \theta, 0)$ of being back at the spike threshold after τ times has elapsed. By recursively splitting the transition probability in Eq. (2.19) into all consecutive possible spiking events one ends with

$$C(\tau) = p(\theta,\tau;\theta,0) = \sum_{k=0}^{\infty} \underbrace{q_\theta(\tau) * \cdots * q_\theta(\tau)}_{k \text{ times}}. \tag{2.20}$$

The typical approach to isolate the ISI density from Eq. (2.19) is by means of Laplace's transform $\tilde{f}(s) = \int_0^\infty \mathrm{d}t\, e^{-st} f(t)$, with $s \in \mathbb{C}$, then

$$\tilde{q}_\theta(s) = \frac{p(x,s;x_0,0)}{p(x,s;\theta,0)} \tag{2.21}$$

In some cases the result may be transformed back into time domain, if the Mellin-Bromwich integral

$$q_\theta(t) = \frac{1}{2\pi \mathrm{i}} \int_{c-\mathrm{i}\infty}^{c+\mathrm{i}\infty} \mathrm{d}s\, e^{st} \tilde{q}_\theta(s), \tag{2.22}$$

exists, that is. The constant c is to be chosen to the right of the real parts of all the integrand's singularities. In cases where this integral can not be evaluated explicitly one is stuck with an expression in the Laplace domain, which is not all that bad, as at least individual moments of the time domain distribution as well as the spike power spectrum may be evaluated. Moments are given by

$$\langle \tau^n \rangle = (-1)^n \left. \frac{\mathrm{d}^n q_\theta(s)}{\mathrm{d}s^n} \right|_{s=0}. \tag{2.23}$$

The power spectrum of a stationary renewal spike train is the Fourier transform of the spike train autocorrelation Eq. (2.20). First, we can identify $C(\tau)$ again in the infinite series and write

$$C(\tau) = q_\theta(\tau) + \int_0^\infty \mathrm{d}t\, q_\theta(t)\, C(\tau - t). \tag{2.24}$$

Then, the Lapace transform can be applied to this linear Volterra integral equation to solve for the spiketrain spectrum [174, 51]

$$P(\omega) = r \left\{ 1 + \left. \frac{\tilde{q}_\theta(s)}{1 - \tilde{q}_\theta(s)} \right|_{s \to \mathrm{i}\omega} + \left. \frac{\tilde{q}_\theta(s)}{1 - \tilde{q}_\theta(s)} \right|_{s \to -\mathrm{i}\omega} \right\} \tag{2.25}$$

§2.8 Stimulus representation in single neurons

In Cpt. 3 we will summarise the biophysical details of the action potential voltage dynamics in membrane patches, highlighting its key features: (*i*) the nonlinear feedback, provided by voltage gated channels; and (*ii*) the inherent stochasticity. These two combined make for a complex system that shirks being amenable to a complete analytical treatment. Deducing the functional properties of a particular biophysical neuron, for example the answer to the question „Which frequencies in a stimulus is it sensitive to?", can be a challenge without resorting to numerical simulations.
A particular useful strategy has been to derive approximate filters[7] from model equations that are easier to analyse [172]. These models must omit many biophysical details to remain analytically tractable.
One line of research starts with simplified integrate-and-fire (IF) neurons that do not contain the kinetics of a full complement of ion channels as are present in biological neurons, but just retain the feature of a spiking threshold device. Then, for example in Refs. [145, 154] the linear filter that approximates the IF neuron is derived, which helps to understand which stimulus aspects this neuron model encodes. More generally, the idea is to find a simplified model that is input/output (I/O) equivalent to a full biophysical system and that is analytically tractable. This idea has been followed in Refs. [110, 111]. One particular, approximately I/O equivalent system for tonically spiking neurons is the phase oscillator with an appropriately chosen PRC [100]. Its benefit is that the equivalent phase oscillator (*i.e.* the PRC) can be systematically identified from any conductance based model with the help of a numerical procedure that is described in App. C. The key assumption is that once the I/O equivalent phase oscillator is in place one may calculate the spike-triggered average from it and at least for weak stimuli it is similar to the STA of the original neuron. This idea was introduced in Ref. [37], taken up by Ref. [162], and will be explored further in Cpt. 6. It should be noted that the integrate-and-fire class of neuronal models has been diversified and can reproduce a variety of neuronal dynamics including adaptation and resonance. Their response is not restricted to the tonic firing regime but can also be phasic. Within the phase oscillators framework this would require the definition of a proto-phase [167].

§2.8.1 Spike-triggered ensemble

A classic approach to investigate which stimulus characteristics are represented in the activity of sensory neurons is to estimate their receptive field or spike-triggered average [27]. The analysis characterises the components of a complex stimulus that are relevant to elicit a spike response or increased firing rate and could ultimately cause behavioural reactions. It is, therefore, related to the antedating concept of sign stimuli [125, 16]. The method has been applied to recordings from the visual [89] and auditory [35] system.
One can also turn the paradigm around by applying a simple stimulus such as a delta pulse and characterising the nature of the response, which is then called transfer functions or point spread function in the visual system. The term transfer function stems form signal processing and stresses the fact that the neuron is viewed as a linear filter. It is surprising how complete a description of a neuron linear response filter can give, despite the fact that neurons contain so many nonlinear elements. In a sense it parallels the success of linear response theory in complex physical problems [128]. Of course, there is no one linear filter

[7] In fact, the biological literature commonly resorts to engineering vocabulary in order to describe the behaviour of nerve cells.

that describes the whole range of dynamical features of the neuron. But different aspects may be characterised by different filter. In particular, we will linearise around the suprathreshold periodic solution to derive a firing rate filter in §6.2. Linearising the voltage response around the resting potential yields quite a different filter that describes the subthreshold response. So essentially it depends on which output variable one analyses.

Returning to the converse approach, the spike-triggered stimulus, the general guiding question is, how does observing the neuronal spike response affect the conditional statistics of the stimulus? After observing the spike train some external stimuli should have been more likely their cause than others. An immediate idea is to look at the first moments of the conditional ensemble. For example, the mean stimulus before a spike in one trial is

$$\frac{1}{N_{\mathrm{sp}}}\sum_{k=1}^{N_{\mathrm{sp}}} x(t_k-\tau) = \frac{1}{N_{\mathrm{sp}}}\int_{-\infty}^{\infty}\mathrm{d}t\; y(t)x(t-\tau), \tag{2.26}$$

where we used the platonic spike train from Eq. (2.3). To improve the signal to noise ratio, an experimenter might repeat the same stimulus, so that a trial average might smooth out the effect of intrinsic noise. Then, if the number of spikes, N_{sp}, per trial is large and almost constant (modest Fano factor) it may be approximated by

$$\left\langle \frac{1}{N_{\mathrm{sp}}}\int \mathrm{d}t\; y(t)x(t-\tau)\right\rangle_{y|x} \approx \frac{1}{\langle N_{\mathrm{sp}}\rangle}\int \mathrm{d}t\; r(t)x(t-\tau) = \frac{1}{r_0}R_{rx}(-\tau), \tag{2.27}$$

where r_0 is the mean firing rate. This gives rise to the term *reverse-correlation* method, see Ref. [25, Cpt. 1.3] and Ref. [27].

A similar view point is taken in the system identification literature. We know the spike train $y(t)$ (or the firing rate $r(t)$) to be a functional of past stimulus realisations $x(t)$. The notation $y(t) = y_t[x]$ highlights this dependence. We have a functional, $y_t[x]$, for any time parameter t that, in a causal system, depends on prior stimulus values $x(t'), \forall t' \leqslant t$. The idea of the Wiener kernels $g_i(\tau_1, \tau_2, ...)$ generalises the structure of the reverse correlation formula in Eq. (2.27) to higher order correlations by [155]

$$g_0 = \langle y(t)\rangle \tag{2.28a}$$
$$g_1(\tau) = \langle y(t)x(t-\tau)\rangle \tag{2.28b}$$
$$g_2(\tau_1,\tau_2) = \langle y(t)x(t-\tau_1)x(t-\tau_2)\rangle \tag{2.28c}$$
$$\dots$$

We assume that the stimulus statistics are wide sense stationary, *i.e.*, shift invariant in time. Hence, the correlations do not depend on t. Often, we will additionally assume that the system is ergodic, the brackets $\langle\cdot\rangle$ denote trial and ensemble averages. In ergodic systems one is able to replace the ensemble average with the time average $\langle\cdot\rangle = \lim_{T\to\infty} T^{-1}\int_{-T/2}^{T/2}\mathrm{d}t$.

Eqs. (2.28) are the moments of the spike-triggered ensemble $p[x(t)|\{\tau_k^{\mathrm{sp}}\}]$, that is the probability over all possible paths $x(t)$ that lead up to a spike in the spike train $\{\tau_k^{\mathrm{sp}}\}$. We use brackets because it is a distribution over continuous paths not numbers or vectors. But, if the stochastic process that describes the stimulus admits the Karhunen-Loève decomposition, $x(t) = \sum_{k=1}^{\infty} x_k H_k(t)$ within a complete set of basis functions $H_k(t)$, then the path integral

that defines the spike-triggered average can be written as

$$g_1(t) = \sum_{k=1}^{\infty} \int\int \cdots \mathrm{d}x_1 \mathrm{d}x_2 \cdots p(x_1, x_2, \ldots | \{t_k\})\, x_i H_i(t). \tag{2.29}$$

Since the spike train was already expressed in terms of the phase variable ϕ in Eq. (2.4), we can relate the g_i's to a simple phase model based on the PRC, introduced in §2.5. Assume that the phase variable in absence of stimulation is proportional to time and the weak stimulus modulates the rate of phase change through the phase response curve.

$$\dot{\phi} = 1 + Z(\phi)x(t).$$

The phase model spikes whenever ϕ crosses multiples of the deterministic period, kT_p.

Assuming the stimulus is Gaussian with correlation furnction $C(t_1, t_2)$, an application of the Novikov-Furutsu-Donsker (NFD) formula (*cf.* A.1) yields

$$g_1(\tau) = \langle y(t)x(t-\tau)\rangle = \int \mathrm{d}\tilde{t}\, C(t-\tau-\tilde{t}) \left\langle \frac{\delta y_t[x]}{\delta x(\tilde{t})} \right\rangle. \tag{2.30}$$

In order to evaluate the average in the above formula the idea is to use the definition of the spike train from Eq. (2.4) and calculate only the lowest order term in the stimulus x. Inserting the spike train definition yields

$$\begin{aligned} \left\langle \frac{\delta y_t[x]}{\delta x(\tilde{t})} \right\rangle &= \sum_k \left\langle \frac{\delta}{\delta x_{\tilde{t}}}\, \dot{\phi}_t \delta(\phi_t - kT_\mathrm{p}) \right\rangle \\ &= \sum_k \left\langle \frac{\delta}{\delta x_{\tilde{t}}} \left(1 + Z(\phi_t)x(t)\right) \delta(\phi_t - kT_\mathrm{p}) \right\rangle \\ &\approx \sum_k \left\langle \left(\delta'(\phi_t - kT_\mathrm{p}) Z(\phi_{\tilde{t}}) + \delta(\tilde{t}-t) Z(\phi_t) \delta(\phi_t - kT_\mathrm{p})\right) \right\rangle. \end{aligned} \tag{2.31}$$

In the second line we have dropped the terms

$$\sum_k \left\langle x(t) \left[Z(\phi_t) Z(\phi_{\tilde{t}}) \delta'(\phi_t - kT_\mathrm{p}) + Z'(\phi_{\tilde{t}}) Z(\phi_{\tilde{t}}) \delta(\phi_t - kT_\mathrm{p}) \right] \right\rangle,$$

because they are of higher order in the stimulus. To further simplify Eq. (2.31) we replace the ensemble average by time averaging and replace all ϕ_t with t to lowest order. Then, using the fact that $Z(t)$ is periodic with period T_p and integrating the first term by parts results in

$$\left\langle \frac{\delta y_t[x]}{\delta x(\tilde{t})} \right\rangle \approx -r_0 Z'(\tilde{t} - t) + r_0 Z(0) \delta(\tilde{t}).$$

Here we denoted mean firing rate as r_0. This may be plugged back into Eq. (2.30) and in addition without loss of generality one can set $t = 0$ to obtain

$$g_1(\tau) = -r_0 \int \mathrm{d}\tilde{t}\, C(-\tau - \tilde{t})(Z(\tilde{t}) - \delta(\tilde{t}) Z(0)).$$

This is consistent with the result in Ref. [37]. In this article the additional assumption of $Z(0) = 0$, which is true for many neural systems was made so that in the the special case of delta-correlated stimuli one obtains $g_1(\tau) = -Z'(-\tau)$.

If the neuron is not deterministic one can follow Ref. [13] and include the trial average

$$g_1(\tau) = \langle\langle y(t)x(t-\tau)\rangle_{y|x}\rangle_x = \langle r(t)x(t-\tau)\rangle_x = \int_{-\infty}^{\infty} \mathrm{d}\tilde{t}\, C(t-\tau-\tilde{t}) \left\langle \frac{\delta r(t)}{\delta x(\tilde{t})} \right\rangle, \tag{2.32}$$

where the NFD formula was applied again. Tor an uncorrelated stimulus this would simplifty to

$$g_1(\tau) = \left\langle \frac{\delta r(t)}{\delta x(t-\tau)} \right\rangle_x. \tag{2.33}$$

This formulas are going to be used in Cpt. 6, where the instantaneous firing rate is considered as a functional of the stimulus $r_t[x]$. The equations above show us that spike-triggered average is infact related to the linear response function mapping stimulus to instantaneous firing rate.
One may proceed to the second order kernel,

$$g_2(\tau_1,\tau_2) = \langle\langle y(t)x(t-\tau_1)x(t-\tau_2)\rangle_{y|x}\rangle_x = \langle r(t)x(t-\tau_1)x(t-\tau_2)\rangle_x \tag{2.34}$$

where one needs to apply the NFD formula twice [13].
Frist, to obtain

$$\begin{aligned}
\langle r(t)x(t-\tau_1)x(t-\tau_2)\rangle_x &= \int \mathrm{d}\tilde{t}\, C(t-\tau_2-\tilde{t}) \left\langle \frac{\delta r(t)x(t-\tau_1)}{\delta x(\tilde{t})} \right\rangle \\
&= \int \mathrm{d}\tilde{t}\, C(t-\tau_2-\tilde{t}) \left[\langle r(t)\rangle \delta(t-\tau_1-\tilde{t}) + \left\langle \frac{\delta r(t)}{\delta x(\tilde{t})} x(t-\tau_1) \right\rangle \right] \\
&= r_0 C(\tau_1-\tau_2) + \int \mathrm{d}\tilde{t}\, C(t-\tau_2-\tilde{t}) \left\langle \frac{\delta r(t)}{\delta x(\tilde{t})} x(t-\tau_1) \right\rangle.
\end{aligned}$$

To the average in the second term the NFD formulas may be applied again and the final result is expressed as

$$g_2(\tau_1,\tau_2) = r_0 C(\tau_1-\tau_2) + \Delta C(\tau_1,\tau_2), \tag{2.35a}$$

where

$$\Delta C(\tau_1,\tau_2) = \iint \mathrm{d}\tilde{t}\mathrm{d}\check{t}\, C(t-\tau_2-\tilde{t}) \left\langle \frac{\delta^2 r(t)}{\delta x(\tilde{t})\delta x(\check{t})} \right\rangle C(t-\tau_1-\check{t}). \tag{2.35b}$$

With Eqs. (2.35b) and (2.32) one can relate the linear and quadratic transfer functions of a time dependent firing rate model to the first two moments of the spike-triggered ensemble.

§2.9 Summary

In this chapter we summarised some of the basic formulae on point processes, *e.g.*, their power spectra and passage time statistics that are use in the following text. We also introduced the phase response curve as an important quantity in this thesis. The PRC is contrasted to the *f-I* curve of a neuron. While the *f-I* curve characterises the response of the mean firing rate over an interval of DC currents, the PRC characterises the response of individual spike times for one particular DC current. The mean of the PRC is related to the slope of the *f-I* curve. Later, in §6.2, we will also show that the DC component of the filter into the instantaneous firing rate depends on the mean of the PRC.
The relation between the spike-triggered average and the PRC of a phase oscillator was

also established in the absence of noise. This is a known result in the literature [37], yet the derivation presented here uses the NFD formula circumventing a secular perturbation of the spike times. In addition the STA and STC of neurons with intrinsic noise have been connected to the linear response kernel and the second quadratic Volterra kernel of the instantaneous firing rate respectively. This result will be used in Cpt. 6.

3 Biophysical principles of a neuron's membrane

This chapter introduces the biophysical foundations that underlie the dynamics of action potential generation in the neuronal cell membrane. The two aspects that give rise to the richness of neural dynamics are nonlinearity and stochasticity. The biophysical sources of both these elements are detailed in §3.2 and §3.3. During the exposition no particular neuron is assumed, but instead either a generic simple membrane patch with only a subset of the physiological ingredients or some of the classical models are used in simulations. We try to stick to the essential principles, however keeping in mind that single neuron models can — and often have to — be made more detailed [28].

Early on, after Hodgekin & Huxley's description of membrane voltage dynamics with deterministic rate-based kinetic equations [84], real measurements showed greater fluctuations than mere thermal noise ontop of the classic view would suggest [29]. The effects of this noise is two fold. On the one hand, the indeterminacy corrupts the neuron as a reliable communication channel [164, 30, 127], and on the other hand the new phenomena enriches the deterministic dynamics, introduces additional time scales (like escape rates) and selectivity in the signal-to-noise ratio (stochastic resonance [129, 146]), which may be exploited by the nervous system to encode and process information. Progress has been made both, in simulating neurons with microscopic channel noise sources in detailed biophysical models [50, 66] as well as in analytic derivation of the statistical properties from simplified neuron models [116, 117, 56].

The statistics of inter-spike intervals of an autonomous neuron, *i.e.*, in the absence of an external time-varying stimulus, is influenced by the nature and strength of intrinsic noise in conjunction with the geometric arrangement and type of attractors in state space. For example, the presence of subthreshold oscillations or bistability may introduce new time scales and induce multimodal interspike interval distributions when noise fluctuations are present. Many of these properties will also affect neurons with time-varying input.

In the following sections, the basics of membrane biophysics are reviewed with the goal of separating nonlinear dynamics and stochasticity such that the latter can be interpreted as a stochastic perturbation of a deterministic model. This allows a description in terms of a second order phase-amplitude model in the next chapter from which the spike statistics will be derived in Cpt. 5. More detailed on the subject can be found in textbooks such as Refs. [104, 98, 95, 29].

§3.1 Conductance based models

Classically, the voltage dynamics of an active patch of nerve cell membrane is described by a balance equation for the currents as well as deterministic, macroscopic reaction rate equations for the time and voltage dependent change in conductance of the relevant ion channels [84]. In accordance with Kirchoff's law, capacitive, injected and all ionic currents

sum to zero. Thus, membrane potential changes in proportion to

$$C_{\mathrm{m}}\,\dot{V} = I_{\mathrm{inj}} - I_{\mathrm{ions}}(V, \boldsymbol{u}) \tag{3.1a}$$

$$\dot{\boldsymbol{u}} = \boldsymbol{g}(V, \boldsymbol{u}) \tag{3.1b}$$

C_{m} denotes the membrane capacitance per membrane area, often around 1 $\mu\mathrm{F/cm}^2$. The injected current, I_{inj}, is provided by an experimental electrode. It may be composed of, $I_{\mathrm{inj}} = I_{\mathrm{DC}} + x(t)$, where I_{DC} is a constant, DC input current that could elicit periodic spiking in the neuron, as well as a time dependent component, $x(t)$, selected by the experimenter to probe the properties of the system. The fundamental period of the deterministic system is set by I_{DC}. The ionic current, I_{ions}, is a sum of the individual currents carried through various different membrane channels [83]. The symbol $\boldsymbol{u}(t)$ summarises a vector of gating variables that follow first order kinetic equations and are described below.
A plethora of different channels, each with permeability to specific ions, diverse time constants and voltage dependencies[1], has evolved since the establishment of the major channel families during the Cambrian explosion [83]. Hodgkin and Huxley discovered that the generation of a voltage spike can be achieved with only two types of channels, in the case of the squid giant axon, an inactivating Na^+ channel and a delayed rectifying K^+ channel. The succession of sodium channels opening with Na^+-influx, membrane depolarisation, delayed opening of the potassium channels with K^+-efflux and repolarisation to the resting state, followed by refractory time may be traversed periodically time and again, if the ionic batteries that keep the dissipative process alive remain charged. This is maintained by the electrogentic $\mathrm{Na}^+/\mathrm{K}^+$-ATPase, pumping ions against the electrochemical potential at the cost of ATP.

§3.2 Nonlinearity in a membrane patch

Inspection of the current-voltage plots for biological membranes shows that there is no linear relation between membrane current I and holding voltage V as expected from Ohm's law. Instead the slope is voltage dependent[2] $g(V)$. This more complicated nonlinear relation has been explained with the Goldman-Hodgkin-Katz constant field model and Eyring's energy-barrier model [95]. What these models do not describe is the time dependence of the conductance $g(V, t)$, which in turn adds to the complexity of the complete dynamical system. The ionic current of a particular channel flows as a consequence of its conductivity to ions, modelled by the time dependent gating kinetics, and the driving force arising from the difference between membrane voltage and its Nernst's reversal potential, E_{ion}, which in turn depends on the ionic concentrations inside and outside of the cell. So, Hodgkin and Huxley parametrised this by separating out the potential energy that forces ions through the membrane: $V - E_{\mathrm{ion}}$. So for the sodium channel the *specific ionic conductance* is

$$g_{\mathrm{Na}^+}(V, t) = \frac{I_{\mathrm{Na}^+}(t)}{V(t) - E_{\mathrm{Na}}} \qquad [\mathrm{mS/cm}^2]. \tag{3.2}$$

[1] Many adventitiously equipped with different regulatory controls such as sensitivity to neuromodulators and metabotrophic second messenger cascades.

[2] Actually, as the conductance is related to changes between the conformational states of membrane channel proteins it is affected by temperature, pH, voltage, ion concentration, phosphorylation, or ligand binding. Yet, it is common to assume all parameters save the voltage are constant on the time scale in question (milli seconds to seconds).

Furthermore, the Hodgkin-Huxley (HH) model introduces gating particles as part of the transmembrane pore that themselves follow an energy barrier model (like the transmembrane ions in Eyring's model) and determine the conductance state of the model—conducting or non-conducting in the simplest cases. The time dependence of the conductance in then described by first order kinetic equations for the gating particles.
For the case of the giant squid motor axon the HH model formulates

$$I_{\text{ions}}(V,[m,h,n]) = \bar{g}_{\text{Na}} m^3 h (V - E_{\text{Na}}) + \bar{g}_{\text{K}} n^4 (V - E_{\text{K}}) + \bar{g}_{\text{L}} (V - E_{\text{L}}), \tag{3.3}$$

for sodium, potassium and an unspecific leak current carried primarily by Cl^- ions. The conductances are composed of the maximal conductance $\bar{g}$ per cm^2 and time varying gating particles describing the percentage of channels in a conducting state.
To summarise, the major source of nonlinearity in active nerve membranes is the fact that transmembrane proteins alter their conductance for ions in response to a voltage signal and this alteration is supposed to be governed by first order kinetics.

§3.3 Stochasticity in a membrane patch

The presence of non-deterministic components in the membrane voltage dynamic was clear from early on recordings of end-plate potentials in the neuromuscular junction [29], even though the AP was and is commonly described by deterministic rate equations. This spike jitter was also quantified by investigations into the waiting time between spikes [183]. In principle, the noise source can be intrinsic to the neuron or inherited from an already stochastic synaptic input activity, possibly generated by a vast network of presynaptic neurons. Noise causes the timing of spikes to jitter, which is often quantified by the distribution of waiting times between spikes. Which biophysical noise sources contribute most significantly to spike time jitter has been subject to debate. While in the central nervous system network noise does play a mayor role, in the sensory periphery the dominant sources are intrinsic to the receptors and primary sensory neurons [43].
The white noise present in all electrical conductors, also in the cell membrane, is called *Johnson-Nyquist noise*. It is due to the thermal agitation of the charge carrying ions and depends on temperature. It can not be removed, only reduced by narrowing the band width (changing the membrane time constant). Yet, one may often neglect it, as it is of a small magnitude compared to the other noise sources present in neural systems [126, Table 2]. A more prominent source of noise is the stochastic activity of the finite amount membrane channels.
Aside this quantitative arguments about the relative magnitude of the noise sources a further reason to focus on channel noise is because as opposed to thermal noise it can be controlled by cells. The channel densities are under the regulatory control of the cell and, in fact, vary in different membrane areas. It is known that on the order of minutes neurons can actually change their channel densities and researchers have devised current-clamp stimuli to track the number of expressed channels in a cell [42].

§3.4 Channel noise

Channels open and close stochastically. The closed-state and open-state conformation are known individually for several channels [124]. An all-atom molecular dynamics simulation of

the delayed rectifier K^+ channel, has recently provided more insight into the conformational changes between states [93]. Still, most of the evidence for the functioning of ion channels and their detailed kinetics is drawn form indirect experimental settings such as voltage clamp and patch clamp techniques [139, 138]. Direct and indirect insights into channel structure motivate the idea that channels reside in distinct discrete conformations, which are associated with conducting or non-conducting states.

Despite the lack of direct observation of state changes in all channels, mathematical models can help explain measured current noise. In particular, the spectral density of different Markov models with various state configurations (Lorentzian in the two state model, *cf.* [184, Cpt. 8]) can be compared to experimental data, facilitating the deduction of the most appropriate model structure. It turns out that many of the statistical properties of the measurements can be met with Markov channel models [139].

The transitions between these states are statistical in nature and for a finite number of channels the effect of these jumps will be perceivable on a macroscopic level. The simplest assumption one can make is that state transitions are Markov. The Markov assumptions states that once a channel resides in a particular state it is of no consequence through which path it was reached, only the transition rates leaving the state probabilistically dictate what happens next. Even if these assumptions were violated, say that both the path mattered and the transitions show multi-exponential behaviour, equivalent Markov schemes could be found by increasing the state space.

The non-stationary noise variance associated with the channel activity has been derived several times from different perspectives, *e.g.*, by analysing the Bernoulli distribution of individual two-state channels [29] or by simplifying the master equation of a more complicated multi-state Markov channel [50]. Intuitively, one can argue that in regions where the derivative of the steady state activation curve is large one expects the noise to be strong.

We present now the basics of Markov models for ion channels, following roughly the content of Refs. [50, 68]. A comparison between some of the different approaches to model channel noise can be found in Refs. [69, 131].

Both gene sequencing and X-ray crystallography have revealed that many transmembrane channels are constructed of repetition of identical subunits [83, Cpt. 13]. As an example consider the delayed rectifying K^+ channel, which consists of four subunits. The channel is conducting, if all subunits are in the open state[3]. Denote the number of channels with i open subunits as $N_i \in \mathbb{N}$. The number of channels in the actual conducting state is N_4. The Markov chain describing an individual K^+ channel is

$$\boxed{N_0} \underset{\beta_n}{\overset{4\alpha_n}{\rightleftharpoons}} \boxed{N_1} \underset{2\beta_n}{\overset{3\alpha_n}{\rightleftharpoons}} \boxed{N_2} \underset{3\beta_n}{\overset{2\alpha_n}{\rightleftharpoons}} \boxed{N_3} \underset{4\beta_n}{\overset{\alpha_n}{\rightleftharpoons}} \boxed{N_4} \tag{3.4}$$

All opening and closing rates depend on the actual membrane voltage, V, and thus the steady state distribution over the states as well as the first passage probability to the open state depend on V, too.

The assumption underlying these one step schemes is that the probability of two or more subunits changing their conformation simultaneously, *i.e.*, within one small time interval, is negligible. As a consequence, state transition such as the one from N_2 to N_4 directly are excluded, only permitting the route via the intermediate state N_3.

The diagrammatic description in Eq. (3.4), translates to a balance equation, called the master

[3] The view that of channels are composed of interacting subunits that can changing between discrete and finite set of conformational states is classic [95].

equation[4], that describes the dynamics of the transitions between states

$$\dot{\boldsymbol{N}} = \boldsymbol{Q}(V)\boldsymbol{N}, \quad \text{where } \boldsymbol{N} = [N_0, \ldots, N_4]^{\mathsf{T}}. \tag{3.5}$$

The matrix $\boldsymbol{Q}$ is the 5×5 transition matrix. The number of channels in the 5 different states are lumped into the vector $\boldsymbol{N}$, with the coefficients summing up to the total number of K^+ channels in the membrane patch. The one step property translates into a tridiagonal transition matrix for the K^+ channel from Eq. (3.4), where the terms on the diagonal are the rates at which the current state is left

$$\boldsymbol{Q}^{\mathrm{K}} = \begin{pmatrix} -4\alpha_n & \beta_n & 0 & 0 & 0 \\ 4\alpha_n & -(3\alpha_n + \beta_n) & 2\beta_n & 0 & 0 \\ 0 & 3\alpha_n & -2(\alpha_n + \beta_n) & 3\beta_n & 0 \\ 0 & 0 & 2\alpha_n & -(\alpha_n + 3\beta_n) & 4\beta_n \\ 0 & 0 & 0 & \alpha_n & -4\beta_n \end{pmatrix} \tag{3.6}$$

In fact, one only requires a 4×4 submatrix of Eq. (3.6), because the 5^{th} state, say N_0, is uniquely defined by the conservation of the total number of channels $\sum_k N_k = N_{\mathrm{K}^+}$. The entries of the submatrix can be written as

$$Q_{jk} = (1 - k\beta - (4-k)\alpha)\delta_{j,k} + k\beta\delta_{j,k-1} + (4-k)\alpha\delta_{j,k+1}. \tag{3.7}$$

Similarly, the transition matrix for the Na^+ channel can be extracted from Eq. (3.9). It can be found in Ref. [68, Appendix B]. Due to $\sum_{j=0}^{1}\sum_{k=0}^{3} M_{jk} = N_{\mathrm{Na}^+}$ it requires 7 states, so that all together the dimension of the state space of the HH model with detailed channel kinetics is 12.

Defining the relative number of channel in state i as $q_i = N_i/N_{\mathrm{K}^+}$ and considering the tridiagonal structure of $\boldsymbol{Q}$, the state transition dynamics of Eq. (3.5) may be written as

$$\dot{q}_k = \sum_{j=1}^{4} [Q_{kj}q_j - Q_{jk}q_k] = Q_{k,k+1}q_{k+1} + Q_{k,k-1}q_{k-1} - (Q_{k+1,k} + Q_{k-1,k})q_k. \tag{3.8}$$

The sodium channel has an additional inactivation gate compared to the K^+ channel. The state diagram reads

$$\begin{array}{ccccccc} \boxed{M_{00}} & \underset{\beta_m}{\overset{3\alpha_m}{\rightleftharpoons}} & \boxed{M_{01}} & \underset{2\beta_m}{\overset{2\alpha_m}{\rightleftharpoons}} & \boxed{M_{02}} & \underset{3\beta_m}{\overset{\alpha_m}{\rightleftharpoons}} & \boxed{M_{03}} \\ \beta_h \uparrow\downarrow \alpha_h & & \beta_h \uparrow\downarrow \alpha_h & & \beta_h \uparrow\downarrow \alpha_h & & \beta_h \uparrow\downarrow \alpha_h \\ \boxed{M_{10}} & \underset{\beta_m}{\overset{3\alpha_m}{\rightleftharpoons}} & \boxed{M_{11}} & \underset{2\beta_m}{\overset{2\alpha_m}{\rightleftharpoons}} & \boxed{M_{12}} & \underset{3\beta_m}{\overset{\alpha_m}{\rightleftharpoons}} & \boxed{M_{13}} \end{array} \tag{3.9}$$

How do we get from the microscopic description with thousands of channels to a macroscopic model? If the number of channels $N_{\mathrm{Na}^+}, N_{\mathrm{K}^+} \to \infty$ or the membrane patch size $A \to \infty$, a deterministic conductance based model should emerge. With a large but finite number of channels one may employ different expansions to change from the master equation to an approximate Langevin equation, then called the *chemical Langevin equation*, or equivalently a Fokker-Planck equation (see also Ref. [61, Cpt. 7]).

The history of approximating Chapman-Kolmogorov (CK) equations with diffusion equations

[4] It is the differential version of the Chapman-Kolmogorov equation.

like the Fokker-Planck equation goes back to 1905 and Einstein's coarse graining argument. The main focus in later years was on truncation of Kramers-Moyal expansion and van Kampen's system size expansion [186, Cpt. 9]. Although the former seems more ad hoc, this chemical Langevin equation has the benefit of being applicable to systems with multiple stable states [65].
For further discussions on detailed channel models see Refs. [95, Cpt. 10], [104, Cpt. 8] and [78].

§3.5 Large membrane patches

Approximating a channel Markov scheme by stochastic differential equations speeds up simulations and simplifies the implementation of membrane dynamics [115]. Our motivation, however, is to open the door for a different set of analysis methods, in particular, perturbation methods and phase reductions, which rely on a deterministic limit cycle oscillator to be identified. So the reason here, for approximately convert the nonlinear master equation describing the channel dynamics into a Langevin equation is that the latter squares with the phase reduction mechanism.
In a master equation, see Eq. (3.5) or (3.8), there is no distinction between deterministic and stochastic parts of the dynamics. The whole system advances by small jumps occurring statistically according to an exponentially distributed waiting time. The representation in terms of a SDE, however, differentiates the fluctuations from the deterministic dynamics — separated into drift and diffusion terms, which is exactly what we need to proceed with the phase reduction in Cpt. 4. Although the presumption of what in the dynamics is noise and what is deterministic is arguably arbitrary, van Kampen's system size expansion introduces a formal way to separate out noise and at the same time have a macroscopic deterministic law emerge. Interestingly, there are many examples, the HH equations being one of them, where the macroscopic laws where historically discovered first and the microscopic underpinning in terms of jump processes was given later [83]. The system size expansion [186, Cpt. 9] could also be applied to conductance based models separating deterministic and stochastic dynamics. However, concern has been voiced that in the case of systems with multistability this strict divorce of deterministic and stochastic dynamics can produce artefactual results, *i.e.*, the deterministic dynamics converging to one fixed point while in the original system there would be a hopping between the different attractors [65]. As, particularly the HH model of the squid is known to show multistability at onset [76] as well as several other neuron models, one should opt for an approach that waives the segregation of the determinstic dynamics in part. More specifically, in van Kampen's approach drift and diffusion coefficients depend on realisations of a deterministic equation. Once the deterministic equation is converged to a fixpoint it remains there and the stochastic system, though fluctuating, is trapped in the vicinity, while more faithful results for multistable systems are obtained if drift and diffusion depend on the random state variables themselves.
Mathematically, a *jump* Markov process is approximated as a *continuous* Markov process [64, 65]. The biophysical interpretation is that the numbers of channels in particular conformational states are converted in to concentrations of channel-states, and at the same time the discrete transition between conformations is approximated by drift and diffusion between the channel-state concentrations. For completeness we replicate these classical methods [48, 186, 64] that has been applied to channel kinetics in Ref. [50]. There are in fact two important steps taking place, (*i*) the discrete variable is converted into a continuous, and

(*ii*) the non-linear master equation is approximated by a diffusion process.

We take the K^+ channel as an example. The vector $\boldsymbol{N}$, as defined in Eq. (3.5), summarises the number of channels in the states N_i with i gating particles open. According to the Diag. (3.4) the state vector $\boldsymbol{N}$ can change through 8 different reaction channels (the redundant state N_0 is not explicitly included). Each reaction j is accompanied by a stoichiometric *state-change vector* $\boldsymbol{\nu}_j$, which for one reaction step increments and decrements the appropriate elements of the state vector $\boldsymbol{N}$. In our case of simple „monomolecular reactions" they simply are

$$\boldsymbol{\nu}_1 = \begin{pmatrix} 1 \\ 0 \\ 0 \\ 0 \end{pmatrix}, \quad \boldsymbol{\nu}_2 = \begin{pmatrix} -1 \\ 1 \\ 0 \\ 0 \end{pmatrix}, \quad \boldsymbol{\nu}_3 = \begin{pmatrix} 0 \\ -1 \\ 1 \\ 0 \end{pmatrix}, \quad \boldsymbol{\nu}_4 = \begin{pmatrix} 0 \\ 0 \\ -1 \\ 1 \end{pmatrix},$$

and $\boldsymbol{\nu}_{j+4} = -\boldsymbol{\nu}_j$ for $j = 1, \ldots, 4$. Based on the law of total probability and the fact that reaction events are disjunct and exhaustive [81], the evolution of the probability density of states is described by the following balance equation (called the chemical master equation [186, 63])

$$\dot{p}(\boldsymbol{N}) = \sum_{i=1}^{8} W_i(\boldsymbol{N} - \boldsymbol{\nu}_i) p(\boldsymbol{N} - \boldsymbol{\nu}_i) - \sum_i W_i(\boldsymbol{N}) p(\boldsymbol{N}) \tag{3.10}$$

Aside from the state-change vector each reaction i is associated with a propensity functions $W_i(\boldsymbol{N})$ that give the probability $W_i(\boldsymbol{N}(t))\mathrm{d}t$ that the reaction occurs in the small time interval $[t, t + \mathrm{d}t)$. They are related to the entries of transition matrix in Eq. (3.6) by

$$\begin{aligned} W_1(\boldsymbol{N} + \boldsymbol{\nu}_1) &= (N_0 + 1) Q_{10} & W_5(\boldsymbol{N} + \boldsymbol{\nu}_5) &= (N_1 + 1) Q_{01} \\ W_2(\boldsymbol{N} + \boldsymbol{\nu}_2) &= (N_1 + 1) Q_{21} & W_6(\boldsymbol{N} + \boldsymbol{\nu}_6) &= (N_2 + 1) Q_{12} \\ &\vdots & &\vdots \end{aligned} \tag{3.11}$$

and $W_i(\boldsymbol{N}) = N_{i-1} Q_{i,i-1}$ for $i = 1, \ldots, 4$ and $W_i(\boldsymbol{N}) = N_i Q_{i-1,i,}$ for $i = 5, \ldots, 8$. With this definitions one can flesh out the general master equation with the transition probabilities of the K^+ channel

$$\begin{aligned} \dot{q}(\boldsymbol{N}) = \sum_{k=1}^{4} \Big[&(N_{k+1} + 1) W_{k,k+1} q(\boldsymbol{N} + \boldsymbol{\nu}_k) + (N_{k-1} + 1) W_{k,k-1} q(\boldsymbol{N} - \boldsymbol{\nu}_k) \\ &- (N_{k-1} W_{k,k-1} + N_k W_{k-1,k}) q(\boldsymbol{N}) \Big]. \end{aligned} \tag{3.12}$$

Turning back to the general form of the master equation, one notices that the effect of the state-change vector in Eq. (3.10) can be couched in terms of the shift operator on a finite dimensional space vector space, $\mathbb{F} f(\boldsymbol{N}) = f(\boldsymbol{N} + \boldsymbol{e}_i)$. The infinite dimensional counterpart of the shift operator is made use of in the derivation of the NFD formula in A.1 and Refs. [101, 102]. For continuous variables, the shift operator is defined in terms of differential operators. Strictly, this would not apply to $\boldsymbol{N} \in \mathbb{N}^4$, yet we will now approximate the jump Markov process with a continuous Markov process. Observing that the N_i's are extensive variables scaling with the membrane area under consideration, one defines the intensive variable n_i, which is the two dimensional analogue of a chemical concentration, as $N_i = A n_i$. In the limit $n_i = \lim_{A \to \infty} N_i / A$ it will approach a continuous variable $n_i \in \mathbb{R}$ (become dense in $\mathbb{R}$) and the concentration n will follow a deterministic rate equation. But even in large but finite membrane patches n_i can be well approximated as continuous, with

better agreement the larger A. From the definitions of the propensity functions in Eq. (3.11) one concludes that the change to extensive variables yields $W_i(\boldsymbol{N}) = A\tilde{W}_i(\boldsymbol{n})$. Rewriting the master equation in „concentration form" and utilising the shift operator leads to the Kramers-Moyal expansion

$$\dot{p}(\boldsymbol{n}) = A \sum_{k=1}^{8} \left[\exp(-A^{-1}\boldsymbol{\nu}_k \cdot \nabla) - 1\right] \tilde{W}_k(\boldsymbol{n})\, p(\boldsymbol{n}), \tag{3.13}$$

where the change of variables to intensive ones was also applied to the probability density, $A^{-4}p(\boldsymbol{n}) = q(\boldsymbol{N})$. The lowest terms in this expansion are of order A^0 followed by $A^{-1}, A^{-2}, \ldots$.
The membrane area A is the expansion parameter and by assumption A^{-1} is small so that one may truncate the Kramers Moyal expansion at second order ignoring all $\mathcal{O}(A^{-2})$ terms (this is the *linear noise approximation*) one arrives at

$$\dot{p}(\boldsymbol{n}) = -\sum_{k=1}^{8} \boldsymbol{\nu}_k \cdot \nabla \tilde{W}_k(\boldsymbol{n})\, p(\boldsymbol{n}) + \frac{A^{-1}}{2} \sum_{k=1}^{8} (\boldsymbol{\nu}_k \cdot \nabla)^2 \tilde{W}_k(\boldsymbol{n})\, p(\boldsymbol{n}). \tag{3.14}$$

The first term will be connected to the drift and the second to the diffusion part of the FPE. Writing out the terms of the drift part of the equation yields

$$\begin{aligned}\sum_{k=1}^{8} \boldsymbol{\nu}_k \cdot \nabla \tilde{W}_k(\boldsymbol{n}) = {} & \partial_{n_1} Q_{10} n_0 + (-\partial_{n_1} + \partial_{n_2}) Q_{21} n_1 + (-\partial_{n_2} + \partial_{n_3}) Q_{32} n_2 + \ldots \\ & - \partial_{n_1} Q_{01} n_1 + (\partial_{n_1} - \partial_{n_2}) Q_{12} n_2 + (\partial_{n_2} - \partial_{n_3}) Q_{23} n_3 + \ldots .\end{aligned}$$

From this one can identify all the rows of the matrix product $\partial_{n_i}(Q_{i,i-1}n_{i-1} - (Q_{i+1,i} + Q_{i-1,i})n_i + Q_{i,i+1}n_{i+i}$ showing that the drift can actually be written as

$$\sum_{k=1}^{8} \boldsymbol{\nu}_k \cdot \nabla \tilde{W}_k(\boldsymbol{n}) p(\boldsymbol{n}) = \nabla \cdot (\boldsymbol{Q}^{\mathrm{K}} \boldsymbol{n}) p(\boldsymbol{n}).$$

Now, one can rearrange the terms of the diffusion part to obtain a representation in terms of diffusion matrix $\boldsymbol{D}^{\mathrm{K}}$

$$\sum_{k=1}^{8} (\boldsymbol{\nu}_k \cdot \nabla)^2 \tilde{W}_k(\boldsymbol{n}) = \sum_{i,j} = \partial_{n_i} \partial_{n_j} D_{ij}^{\mathrm{K}}. \tag{3.15}$$

The entries of the matrix $\boldsymbol{D}^{\mathrm{K}}$ or $\boldsymbol{D}^{\mathrm{Na}}$ can be found in Ref. [68] and are reproduced in App. B. The corresponding system of Itō SDEs is, as stated in [49, 68, 69]

$$\begin{aligned} C\dot{V} &= I + g_{\mathrm{L}}(E_{\mathrm{L}} - V) + g_{\mathrm{Na}} m_{13} (E_{\mathrm{Na}} - V) + g_{\mathrm{K}} n_4 (E_{\mathrm{K}} - V) \\ \dot{\boldsymbol{n}} &= \boldsymbol{Q}^{\mathrm{K}} \boldsymbol{n} + \sqrt{\boldsymbol{D}^{\mathrm{K}}}\, \boldsymbol{\xi}_t^{\mathrm{K}} \\ \dot{\boldsymbol{m}} &= \boldsymbol{Q}^{\mathrm{Na}} \boldsymbol{m} + \sqrt{\boldsymbol{D}^{\mathrm{Na}}}\, \boldsymbol{\xi}_t^{\mathrm{Na}} \end{aligned} \tag{3.16}$$

The matrix square root operation is denoted by $\sqrt{\boldsymbol{D}}$. The gating SDEs are similar to the multidimensional Ornstein-Uhlenbeck process, with the drift being linear in $\boldsymbol{n}$ and $\boldsymbol{m}$, however, the diffusion matrix is state dependent, too. If the continuum limit $A \to \infty$ is taken the gating states follow a linear ODE system which collapses to the original HH equations, [26, Cpt. 5]. This is due to the particular property of the transition rates in the state

Fig. 3.1: Voltage path of the channel SDE for the squid giant axon. The membrane patch is of size $A = 20\,\mu\text{m}^2$ with $\varrho_{\text{K}^+} = 3 \times 10^8/\text{cm}^2$ and $\varrho_{\text{Na}^+} = 3 \times 10^9/\text{cm}^2$. This leads to an ISI distribution with $\text{CV}_{\text{ISI}} = 0.313$. The phase portrait on the right is a slice view into V-n_4 plane and shows the excursion around the deterministic limit cycle (grey).

diagrams (3.4) and (3.9), where the transition rates are just multiples of the same basic rate functions α and β. Of course, one could envisage more complicated channels in which all transitions rate functions are unrelated to each other and the deterministic ODEs would not simplify so drastically.

In the following and particularly for the phase reduction the Stratonovic's stochastic calculus is more appropriate than Itō's. The conversion induces an additional noise related term to each component i of the drift [61]

$$-\sum_{jk}\left[\sqrt{\boldsymbol{D}^{\text{K}}}\right]_{jk}\left(\frac{\partial}{\partial n_j}\left[\sqrt{\boldsymbol{D}^{\text{K}}}\right]_{ik}\right). \tag{3.17}$$

As this term is proportional to $(A\varrho_{\text{K}^+})^{-1}$ and thus small by assumption it has been suggested in Ref. [49] that one may drop it without significant loss of accuracy. We will follow this suggestion. As the term really vanishes in the $A \to \infty$ limit this amounts to saying that the deterministic system for which we calculate PRCs in later chapters is defined as the continuum limit system not the actual deterministic part of the Stratonovic's channel SDE.

A simulated realisation of the stochastic process for the voltage variable in the HH system is depicted in Fig. 3.1. The noise is visible in the irregularity of the voltage trace, manifests as departure around the deterministic limit cycle of the $(A \to \infty)$-system and induces a waiting time distribution of between spike times with a $\text{CV}_{\text{ISI}} = 0.313$. The voltage trace in the $A \to \infty$ case is equivalent to the one produced by Hodgkin and Huxley's rate based ODEs [26, Cpt. 5].

To conclude the paragraph, the objective of converting the Markov scheme to an approximated SDE, separating the deterministic limit cycle from its noisy perturbations, has been reviewed. The procedure exemplified with the rectifying K^+ channel can be applied to arbitrary complicated Markov schemes in the format of Eqs. (3.4) and (3.9) and always leads to an approximating SDE.

If the whole set of SDEs in Eqs. (3.16) is represented formally as

$$\dot{\boldsymbol{v}} = f(\boldsymbol{v}) + \sqrt{\boldsymbol{D}^{\text{c}}(\boldsymbol{v})}\,\boldsymbol{\xi}_t, \tag{3.18}$$

then the structure of the diffusion matrix $\boldsymbol{D}^{\text{c}}$ is in fact block diagonal with no correlations between different channels, but with indeed correlations within the different states of one

channel type

$$\boldsymbol{D}^{\mathrm{c}} = \begin{pmatrix} \boldsymbol{D}^{\mathrm{K}} & \mathbf{0} \\ \mathbf{0} & \boldsymbol{D}^{\mathrm{Na}} \end{pmatrix}. \tag{3.19}$$

This will lead to the fact that to very first order the phase noise has additive contribution from the individual channel types.
Also note that the matrix square root, $\sqrt{\boldsymbol{D}^{\mathrm{c}}}$, is block diagonal. This follows from the more general fact that for matrix valued functions f that operate on the spectrum of a matrix one has $f(\boldsymbol{A}) = \mathrm{diag}[f(\boldsymbol{A}_1), f(\boldsymbol{A}_2), \ldots]$ for all block diagonal matrices $\boldsymbol{A} = \mathrm{diag}[\boldsymbol{A}_1, \boldsymbol{A}_2, \ldots]$ with $\boldsymbol{A}_j \in \mathbb{C}^{k_j \times k_j}$.

Two state channels and gating noise simplification

In Ref. [50] further simplifications were proposed in order to shrink the state space dimension of the resulting SDE back to the dimensionality of the original HH equations. It was shown in subsequent articles that it these approximations alter some of the statistical behaviour, when compared to the full Markov channel models [131, 115, 68]. However, we may note that if the channel is described by a two state Markov model the approximation in Ref. [50] is valid. This corresponds to the case where the deterministic equations do not raise the gating variables to powers. Such a model is for example the $\mathrm{Na}^+/\mathrm{K}^+$ model in Ref. [92] the SDE describing the channel noise is then

$$\begin{aligned} C\dot{V} &= I - \bar{g}_{\mathrm{Na}} m_\infty(V)(V - E_{\mathrm{Na}}) + \bar{g}_{\mathrm{K}} n (V - E_{\mathrm{K}}) + \bar{g}_{\mathrm{L}}(V - E_{\mathrm{L}}), \\ \dot{n} &= (n_\infty(V) - n)/\tau_n(V) + \sigma_n(V)\,\xi_t, \end{aligned} \tag{3.20}$$

where $m_\infty = a_m/(a_m + b_m)$, $n_\infty = a_n/(a_n + b_n)$, $\tau_n = 1/(a_n + b_n)$ and the noise variance is given by

$$\sigma^2(V) = \frac{a_n b_n}{A \varrho_{\mathrm{K}} (a_n + b_n)}.$$

Here A is the size of the membrane patch and ϱ_{K} the channel density for potassium.
We will use the deterministic limit of this simplified model to exemplify isochrons in 2d, *cf.* §4.1, and as a model for the noise induced frequency shift, whenever the hight dimensional HH and TM models are not feasible.

Unitary conductances

The magnitude of channel noise is related to the membrane area that contributes to spike generation, *e.g.*, the extent of the axon hillock, and the channel density in that area. In general, the channel density can vary greatly, from about one voltage-gated sodium channel per square micrometre in some dendrites, to hundreds of them in the axon hillock and initial segment, or even 1000 sodium channels per square micrometre in the nodes of Ranvier. The densities are closely regulated through mechanisms involving the cytoskeleton.
The conductance of a single ion channel depends on its molecular structure and will dictate how many channels are required to obtain a certain maximal conductance measure by voltage clamps. The unitary conductance of different potassium channels varies from femto siemens to hundreds of piko siemens [151]. Common unitary conductances for the squid axon are $\gamma_{\mathrm{K}} = 12$ pS for K^+ and $\gamma_{\mathrm{Na}} = 4$ pS for Na^+ channels [83], and we will use them throughout this document.

The parameters of a conductance based model are not independent of each other, some can only be varied in conjunction with others. The unitary conductance is partly related to the channel width, which when changed will also have an effect on open and closing kinetics. One would also guess that the selectivity of the channel to a specific ion type is reduced when pore size, and thus unitary conductance, is varied. A parameter that can be altered precisely by the cell without changing kinetic parameter of the individual channel is the channel density in the membrane area. The assumption of course being that channels are independent units, which is challenged by studies of ion channel cooperativity [189]. A further parameter that varies naturally or in experiments is the overall temperature of the system.

§3.6 Summary

For the most part the derivations in this chapter followed the literature on approximating master equations of jump processes with stochastic differential equations. We focused on the fact that separating out the fluctuations from the deterministic flow field paves the way for the formal phase reduction in the next chapter. Although the method reviewed in this chapter was exemplified with the K^+ channel it can be applied to a vast class of channel Markov model, with even more complicated state transition diagrams, than the one for the Na^+ channel in Diag. (3.9).

4 Phase reduction of conductance based limit cycle oscillators

Models for neuron, even single-compartment models, can be complex and depend on many variables. In this chapter, we describe a change of variables that can be applied to any regularly firing neuron, so that the oscillatory dynamics is described by a phase and possibly several radial variables. The structure of the resulting equations are universal and do not depend on the particularities of the original conductance based model. This change of representation has the added benefit that defining the threshold for the spikes and determining the spike times is straightforward and uncomplicated. Hence, simple phase equations are commonly used in neuroscience [188, 176, 166, 88].
As it was stressed in §2.7, the ISI variance is a second order quantity, and so in principal requires a second order phase equation, not to miss any second order effects from the original conductance based model. Higher order phase reductions where formalised by Kuramoto in Ref. [105, Cpt. 4]. In this approach one considers the fluctuation in the SDE Eq. (3.16) as perturbations to the deterministic LC oscillator. We pick up the general form from last chapter, Eq. (3.18), and rewrite it as

$$\dot{\boldsymbol{v}} = \boldsymbol{f}(\boldsymbol{v}) + \boldsymbol{\eta}(\boldsymbol{v}, t), \text{ with for } \boldsymbol{\eta} = \boldsymbol{0} \text{ the stable LC solution } \boldsymbol{v}_0 : \dot{\boldsymbol{v}}_0 = \boldsymbol{f}(\boldsymbol{v}_0). \tag{4.1}$$

In general, the perturbations to the deterministic conductance based equations can be the result of internal (channel) noise, $\boldsymbol{D}(\boldsymbol{v})\boldsymbol{\xi}(t)$, or time dependent external current stimulation, $x(t)$, affecting the voltage dimension. The structure of the perturbation is then

$$\boldsymbol{\eta}(\boldsymbol{v}, t) \overset{e.g.}{=} \boldsymbol{D}^{\mathrm{c}}(\boldsymbol{v})\boldsymbol{\xi}(t) + \begin{pmatrix} x(t) \\ 0 \\ \vdots \end{pmatrix}, \tag{4.2}$$

where $\boldsymbol{D}^{\mathrm{c}}$ follows from the biophysical considerations in Sec. §3.5. In the following $\boldsymbol{\eta}$ is of small magnitude.

§4.1 Isochrons

Before starting on the principled phase reduction it is worth pondering a differential geometric interpretation of the phase variable advocated in Ref. [187], for it also allows a geometric interpretation of the phase response curve, introduced in §2.5.
Isochrons are $(n-1)$-dimensional level sets or fibres of the asymptotic phase that foliate the basin of attraction of a stable limit cycle. The basin of attraction is the n-dimensional stable manifold of the LC, which is a normally hyperbolic invariant manifold. The isochrons can be thought as the starting points, nT_{p} time ago, of a fibre bundle [144] that terminates at a particular phase on the limit cycle, $\boldsymbol{v}_0(\phi_1)$, *cf.* Fig. 4.1a. Each point in the basin of attraction of a limit cycle can be addressed by the phase that it asymptotically reaches if it

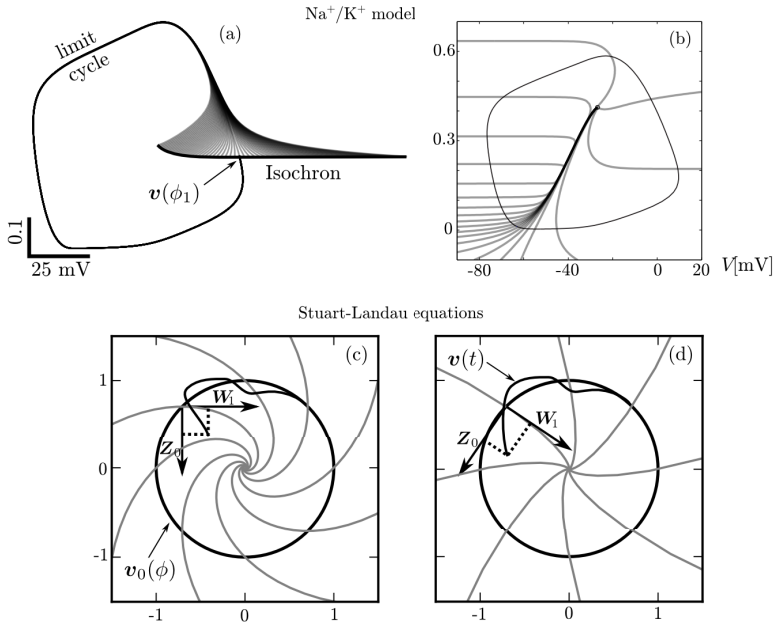

Fig. 4.1: (a) Isochrons can be defined as the set of end point of a fibre bundle with the same asymptotic phase. As the limit cycle is attracting, the dynamics will approach the LC from any one of a number of starting points in phase space. When the dynamics reaches the LC, it attains an asymptotic phase that coincides with a trajectory that starts out on the limit cycle itself. This defines the asymptotic phase. (b) The isochron (grey) is a set of points with the same asymptotic phase. Across phase interval of constant size, the isochron density varies (The model is the two dimensional Na^+/K^+ model defined in Eq. (3.20)). Isochrons are computed with AUTO as described in Ref. [144]. (c,d) The left and right Floquet modes provide a coordinate system that is tangential to the isochron illustrated with the SL model (see A.3 for parametrisation, (c): $[a, b, c, d] = [1, 2, -1, -1]$, (d): $[a, b, c, d] = [1, 1.2, -1, -0.2]$). The isochrons (grey) are the logarithmic spirals. In (c) their curvature is stronger than (d). The coordinate system spanned by the left and right Floquet modes, $\boldsymbol{Z}_0(\phi)$ and $\boldsymbol{W}_1(\phi)$, is rotated accordingly.

had converged back to the limit cycle

$$\phi(\boldsymbol{x}) = \underset{\phi}{\operatorname{argmin}} \left\{ \lim_{t\to\infty} \|\boldsymbol{x}(t) - \boldsymbol{v}_0(t+\phi)\| \right\}. \tag{4.3}$$

In a deterministic system, the final difference for the optimal phase will actually be zero. An orbit that allows for such a phase definition is called *assymptotically orbitally stable with asymptotic phase*.
the $n-1$ dimensional isochron submanifolds are the *level sets* of the asymptotic phase function

$$I(\psi) = \{\boldsymbol{x} : \phi(\boldsymbol{x}) = \psi\}. \tag{4.4}$$

Adding a parametrisation of the isochrons, one finds a new phase/radial-coordinate system that the state variables that are elements of the LC's stable manifold can be uniquely mapped into. State changes along the isochrons do not affect the phase, or formally for $\boldsymbol{x}, \boldsymbol{v_0} \in I(\phi)$: $\phi(\boldsymbol{x}) - \phi(\boldsymbol{v_0}) = 0$. In subsequent chapters this asymptotic phase of the deterministic system is also used to analyse weakly stochastic systems in a perturbative manner.
The isochron coordinate system is an analytical tool that is difficult to define in an experimental system, in particular if they are noisy. Then, even the measurement of the asymptotic phases would be confounded. However, as we have already seen in §2.5 in spiking systems the particular properties of the flow field, around the spike allows one to observe the phase more directly. We will seen in the subsequent paragraphs that a linearisation of the coordinate system provided by the isochrons is related to the experimentally accessible PRC from §2.5. The relation between the PRC and the asymptotic phase is seen from

$$\dot{\phi} = \nabla_{\boldsymbol{x}}\phi(\boldsymbol{x})\dot{\boldsymbol{x}} = \omega + \boldsymbol{Z}(\phi)\boldsymbol{\eta}(\boldsymbol{x}, t),$$

where we used the equation of the simple phase oscillator Eq. (2.11). If one now requires $\langle \boldsymbol{f}(x), \nabla_{\boldsymbol{x}}\phi(\boldsymbol{x})\rangle = \omega$ one can identify the PRC as the gradient of the asymptotic phase $\boldsymbol{Z}(\phi) = \nabla_{\boldsymbol{x}}\phi$.
In addition, the curvature of the isochrons at their intersection with the limit cycle, which may vary with system parameters (see Fig. 4.1c,d), is shown to be related to noise induced shifts in the average inter-spike period or mean firing rate in §5.2.
For realistic neuron models the curvature of the transecting isochron changes constantly along limit cycle. In the canonical Stuart-Landau equations (detailed in A.3), a simplified models of limit cycle oscillations and the normal form of the supercritical Hopf bifurcation, the isochrons are the *Spira mirabilis* (or log-spiral) shown in Fig. 4.1c,d, see also A.3.1. Due to the symmetry of the model the isochron curvature is constant along the limit cycle.

§4.2 Floquet representation

Material for the definition of the asymptotic phase is the stability of the unperturbed stable limit cycle in Eq. (4.1). For periodic dynamical systems stability is analysed using Floquet theory. We provide a short introduction here, and refer the interested reader to Ref. [22]. In the deterministic system, where intrinsic noise is switched off (consider large membrane patches with many channels), the linearised system on the LC, known as the first variational equation, reads

$$\dot{\boldsymbol{W}} = \boldsymbol{J}(t)\boldsymbol{W}(t), \tag{4.5}$$

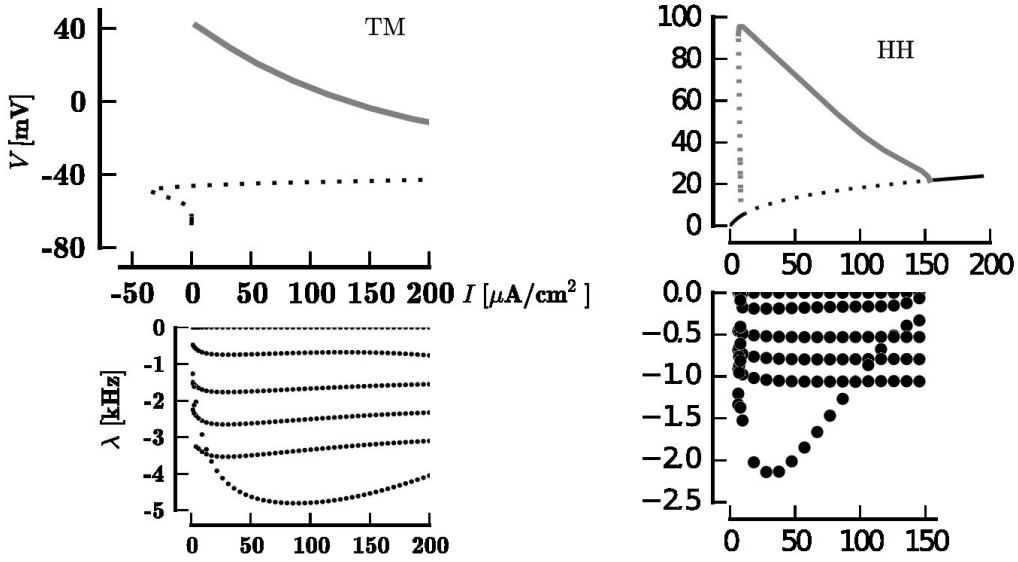

Fig. 4.2: Top: Bifurcation diagram of the 12 dimensional Hodgkin-Huxley and Traub-Miles models (black: fixpoints, solid grey: stable limit cycles, dashed grey: unstable limit cycles). Bottom: 6th lowest magnitude Floquet multipliers indicating limit cycle stability.

with Jacobian $\boldsymbol{J} = \nabla_{\boldsymbol{v}} \boldsymbol{f}(\boldsymbol{v})|_{\boldsymbol{v}=\boldsymbol{v}_0(t)}$, and periodicity $\boldsymbol{J}(t) = \boldsymbol{J}(t + T_\mathrm{p})$. A trivial solution, called the Goldstone mode, is $\boldsymbol{W}(t) = \dot{\boldsymbol{v}} = \boldsymbol{f}(\boldsymbol{v})$, as can be verified by insertion. Eq. (4.5) can also be interpreted as a matrix ODE, with $\boldsymbol{W} \in \mathbb{R}^{n\times n}$. The solution to the initial condition $\boldsymbol{W}(0) = \boldsymbol{I}$ is then termed the *fundamental matrix* solution to Eq. (4.5). The *Floquet normal form* representation decomposes this into a periodic $\boldsymbol{R}(t) = \boldsymbol{R}(t + T_\mathrm{p})$ and an exponential part [106]

$$\boldsymbol{W}(t) = \boldsymbol{R}(t)\, e^{t\boldsymbol{\Lambda}}. \tag{4.6}$$

The matrix $\boldsymbol{\Lambda}$ is a constant, generally nonsymmetric matrix. The condition for which this representation is admissible apply to many physical situations and are detailed as the Floquet theorem [22]. If the original system is a stable limit cycle, one eigenvalue of $\boldsymbol{\Lambda}$ is zero, while the others are negative. In systems of dimension $n > 2$ they may be complex, depending on whether the system rotates while converging back to the LC, but doubling the basic period renders them real. In general, the left and right eigenvalue problems are

$$\boldsymbol{\Lambda}\boldsymbol{w}_k = \lambda_k \boldsymbol{w}_k, \quad \text{and} \qquad \boldsymbol{z}_k\boldsymbol{\Lambda} = \lambda_k \boldsymbol{z}_k. \tag{4.7}$$

One may order the eigenvalues in a decreasing manner, so that $0 = \lambda_0 \geqslant \lambda_1 \geqslant \cdots$, and normalise the eigenvectors to $\boldsymbol{z}_j\boldsymbol{w}_k = \delta_{jk}$. An example of the Floquet spectra of the HH and the TM model are shown in Fig. 4.2. These models are the $d = 12$ dimensional extension of the original equations, including the dimensions for the channel noise, see §3.4 and §3.5. There are d Floquet exponents, with a „trivial" one being zero, $\lambda_0 = 0$. Some of these can be very negative and are not even shown in Fig. 4.2, as their evaluation is subject to numerical inaccuracies. These numerical inaccuracies poses no problem, however, as for such negative Floquet exponents, the attraction along the Floquet vectors is extremely fast, and therefore we can treat the dynamics as „slaved" along these directions and ignore them.

For further use we define the rotated eigenvectors as

$$\boldsymbol{Z}_k(t) = \boldsymbol{z}_k \boldsymbol{R}^{-1}(t) \tag{4.8a}$$
$$\boldsymbol{W}_k(t) = \boldsymbol{R}(t)\boldsymbol{w}_k. \tag{4.8b}$$

If rotated with $\boldsymbol{R}$, the zero right-eigenvector, $\boldsymbol{w}_0$ points tangential to the limit cycle along the flow-field

$$\boldsymbol{W}_0(t) = \boldsymbol{R}(t)\boldsymbol{w}_0 = \frac{\mathrm{d}\boldsymbol{v}_0(t)}{\mathrm{d}t}, \tag{4.9}$$

which is just the Goldstone mode from above. An other useful identity can be obtained by inserting the Floquet Ansatz of Eq. (4.6) into Eq. (4.5)

$$\frac{\mathrm{d}\boldsymbol{R}(t)}{\mathrm{d}t} + \boldsymbol{R}(t)\boldsymbol{\Lambda} = \boldsymbol{J}(t)\boldsymbol{R}(t), \quad \text{and} \quad \frac{\mathrm{d}\boldsymbol{R}^{-1}(t)}{\mathrm{d}t} + \boldsymbol{R}^{-1}(t)\boldsymbol{J}(t) = \boldsymbol{\Lambda}\boldsymbol{R}^{-1}(t). \tag{4.10}$$

Respective right and left multiplication with the eigenvectors yields

$$\frac{\mathrm{d}\boldsymbol{W}_k(t)}{\mathrm{d}t} + \lambda_k \boldsymbol{W}_k(t) = \boldsymbol{J}(t)\boldsymbol{W}_k(t), \quad \text{and} \quad \frac{\mathrm{d}\boldsymbol{Z}_k(t)}{\mathrm{d}t} + \boldsymbol{Z}_k(t)\boldsymbol{J}(t) = \lambda_k \boldsymbol{Z}_k(t). \tag{4.11}$$

Remember that for the stable limit cycle of a HH neuron there is one $\lambda_0 = 0$ and all others are negative *cf.* Fig. 4.2. It turns out that the solution $\boldsymbol{Z}_0(t)$, corresponding to $\lambda_0 = 0$, is exactly the classical phase response curve that was introduced in §2.5.
We will show this more clearly in the next section, in which we formalise the definition of the PRC.
For $k \geqslant 1$, we may term $\boldsymbol{Z}_k(t)$ the amplitude sensitivity (or susceptibility) as projecting onto it maps perturbations of the state variables to the amplitude coordinates. Perturbation along the amplitude directions are not neutrally stable, as they will decay with time. The second order effects of the amplitude sensitivities on the phase will be detailed in §4.4.
Numerically, evaluations of the Z_k and W_k from Eqs. (4.11) is challenging for all but $k = 0$, as only then the equations are stable in either forward or backward time. For all $\lambda_k < 0$ the equations have both a stable and an unstable manifold and can not be evaluated with time integration, but require a Newton-iteration based based approach, see App. C.

§4.3 Formal definition of the PRC

Phase response curves describe how perturbations cause phase shifts in nonlinear oscillators. They are experimentally accessible and easy to interpret (see §2.5), yet at the same time they are mathematically well defined quantities [18, 40]. The idea is simply to replicate the experimental definition of the PRC in mathematical terms. The derivation requires a simple postulate that parallels the experimental definition: *Assume that after a perturbation there remains a fixed time-independent phase shift.* One may take this as an observational fact, but in fact it is a consequence of the existence of a neutral dimension with Floquet exponent $\lambda_0 = 0$. If such a time independent phase shift exists one may term it Z in general it may be a function of the timing and nature of the perturbation. For infinitesimal perturbations, concentrated at a single time instance it is only the time/phase dependence that remains, *i.e.*, $Z(\phi)$.
Again, neuronal spiking is described by Eq. (4.1). The oscillator is experimentally perturbed by some external small amplitude stimulus $\boldsymbol{\eta}$ (*e.g.*, the current from a stimulating sharp

electrode or an induced post synaptic potential with a short time constant). As mentioned, at any given time perturbations in the $\boldsymbol{W}_k(t)$ direction will over the course of one period decay with $e^{\lambda_k t}$, except for the *neutral* direction, *i.e.* perturbations along the Goldstone mode (tangential to the LC). It is these perturbations along the zero modes that will survive and are measurable. As the perturbation $\boldsymbol{\eta}$ is small one can assume that the new solution can be written as a small perturbation of the original LC $\boldsymbol{v}(t) = \boldsymbol{v}_0(t) + \boldsymbol{u}(t)$, where again $\boldsymbol{u}(t)$ is small. With a first order Taylor expansion of the nonlinearities on the r.h.s. of Eq. (4.1)

$$\dot{\boldsymbol{v}} = \dot{\boldsymbol{v}}_0 + \dot{\boldsymbol{u}} = \boldsymbol{f}(\boldsymbol{v}_0) + \boldsymbol{J}(\boldsymbol{v}_0)\boldsymbol{u}(t) + \boldsymbol{\eta}(t).$$

It is necessary to agree on how to geometrically measure phase shifts: Introduce a new time variable $\phi(t) = t + \Delta(t)$ and then monitor the shift Δ in the evolution of $\boldsymbol{v}$

$$\dot{\boldsymbol{v}} = \boldsymbol{v}_0'(\phi)\dot{\phi} + \dot{\boldsymbol{u}} = \boldsymbol{f}(\boldsymbol{v}_0) + \boldsymbol{J}(\boldsymbol{v}_0)\boldsymbol{u}(\phi) + \boldsymbol{\eta}(t)$$

or

$$\boldsymbol{v}_0'(\phi)\dot{\Delta} = \boldsymbol{J}(\phi)\boldsymbol{u}(\phi) - \dot{\boldsymbol{u}} + \boldsymbol{\eta}(t)$$

We write $\boldsymbol{J}(\phi)$, because the LC solution $\boldsymbol{v}_0$ can be one-to-one indexed by ϕ. With the intention of establishing properties of $\boldsymbol{Z}(\phi)$ and with the goal of isolating $\dot{\Delta}$, one left-projects the above equation onto $\boldsymbol{Z}$.

$$\underbrace{\langle \boldsymbol{Z}(\phi), \boldsymbol{v}_0'(\phi) \rangle}_{\stackrel{\text{def.}}{=} 1} \dot{\Delta}(t) = \langle \boldsymbol{Z}(\phi), \boldsymbol{J}(\phi)\boldsymbol{u}(\phi) - \dot{\boldsymbol{u}} \rangle \tag{4.12}$$

The term $\boldsymbol{\eta}(t)$ was dropped by the assumption that the perturbation is delta pulse like, and will not further contribute to the evolution of the phase shift. As required $\dot{\Delta} = 0$, from which it follows as indicated that if $\langle \boldsymbol{Z}(\phi), \boldsymbol{v}_0'(\phi) \rangle = \langle \boldsymbol{Z}, \boldsymbol{f}(\boldsymbol{v}_0) \rangle = 1$ or equals any other nonzero constant, the r.h.s. of Eq. 4.12 must equate to zero for any nonzero $\boldsymbol{u}$ given by the dynamics of $\boldsymbol{v}$

$$\left\langle \underbrace{\left(\boldsymbol{J}^\dagger(\phi) + \frac{\mathrm{d}}{\mathrm{d}\phi} \right) \boldsymbol{Z}(\phi)}_{\stackrel{\text{def.}}{=} 0}, \boldsymbol{u}(\phi) \right\rangle = 0.$$

Unless $\boldsymbol{u}(\phi) = 0$, then it follows that

$$\boldsymbol{J}^\dagger \boldsymbol{Z} + \dot{\boldsymbol{Z}} = 0. \tag{4.13}$$

Hence, $\boldsymbol{Z} = \boldsymbol{Z}_0$, or the PRC is the solution to the second equation in Eq (4.11) for $\lambda_0 = 0$, and thus it is the adjoint to the Goldstone mode. Eq. (4.13) is the adjoint to the first variation of the limit cycle ODE. It can be evaluated numerically through the continuation of boundary value problems, see App. C.

It was mentioned in §2.5 that parameters of the conductance based model that affect the shape of the limit cycle will also alter the phase sensitivity. The normalisation requirement, $\langle \boldsymbol{Z}(\phi), \boldsymbol{u}'(\phi) \rangle = 1$, we read from Eq. (4.12), illustrates this fact. If the limit cycle is altered, and so its derivative, the Goldstone mode, then the PRC needs to also change to enforce the normalisation.

§4.4 Second order phase reduction

In this paragraph we transform the d-dimensional set of biophysical variables in periodic motion to a set of variables that lends itself naturally to the definition of spike times. These are a circular phase variable $\phi \in \mathbb{S}$, which is chosen such that it crosses 0 at a spike, and $d-1$ radial variables α_k. Kuramoto [105] made the general Ansatz for the phase evolution

$$\dot{\phi} = 1 + \Omega(\phi, t) \tag{4.14}$$

With this the dynamical system in Eq. (4.1) can be written as

$$(1 + \Omega(\phi, t))\frac{\partial \boldsymbol{v}}{\partial \phi} + \frac{\partial \boldsymbol{v}}{\partial t} = \boldsymbol{f}(\boldsymbol{v}) + \boldsymbol{\eta}(\boldsymbol{v}, t) \tag{4.15}$$

We know that if $\|\boldsymbol{\eta}\| = 0$ the system has the periodic LC solution, $\boldsymbol{v}_0(t)$. Denote the difference of the perturbed solution to the homogeneous limit cycle solution as $\boldsymbol{u}$. Note that $\boldsymbol{u}$ is the variable containing the information on the stimulus and other fluctuations. On the limit cycle the phase uniquely addresses the state variables. Hence, the dynamics may be decomposed as

$$\boldsymbol{v}(\phi, t) = \boldsymbol{v}_0(\phi) + \boldsymbol{u}(\phi, t). \tag{4.16}$$

Using this Ansatz, Taylor expanding the vector field to second order, and canceling out the LC dynamics, yields the equation

$$\frac{d\boldsymbol{v}_0}{d\phi}\,\Omega + (1 + \Omega)\frac{\partial \boldsymbol{u}}{\partial \phi} + \frac{\partial \boldsymbol{u}}{\partial t} = \boldsymbol{J}(\phi)\boldsymbol{u} + \boldsymbol{H}(\phi)\boldsymbol{u}\boldsymbol{u} + \boldsymbol{\eta}(\boldsymbol{v}_0 + \boldsymbol{u}, t) \tag{4.17}$$

Again, the Jacobian of the vector field evaluated on the limit cycles has been denoted as $\boldsymbol{J}(\phi) = \nabla_{\boldsymbol{v}} \boldsymbol{f}(\boldsymbol{v})|_{\boldsymbol{v}=\boldsymbol{v}_0(\phi)}$ and the Hessian as $\boldsymbol{H}(\phi) = \frac{1}{2}\nabla_{\boldsymbol{v}}\nabla_{\boldsymbol{v}} \boldsymbol{f}(\boldsymbol{v})|_{\boldsymbol{v}=\boldsymbol{v}_0(\phi)}$ respectively (for brevity the tensor $\boldsymbol{H}$ has the factor $\frac{1}{2}$ included).

As a next step, the deviations to the limit cycle are represented in the phase dependent, rotating coordinate system as in Fig. 4.1c. Representing $\boldsymbol{R}^{-1}\boldsymbol{u}$ in coordinates of the right eigenvectors of $\boldsymbol{\Lambda}$ (*cf.* Eq. (4.7)) amounts to

$$\boldsymbol{u}(\phi, t) = \sum_{k \neq 0} \alpha_k(t) \boldsymbol{W}_k(\phi). \tag{4.18}$$

Conversely the coefficients can be obtained by projecting $\boldsymbol{u}$ onto the radial susceptibilities $\alpha_k = \boldsymbol{Z}_k(\phi)\boldsymbol{u}$. Recall that $\boldsymbol{u}(\phi, t)$ is chosen in such a way that it has no contribution from the $\boldsymbol{w}_0$ direction, which renders the coefficient in that direction zero, $\alpha_0 = \boldsymbol{Z}_0(\phi)\boldsymbol{u} = 0$. The coefficients $\alpha_k(t)$ represent the radial deviations in this coordinates and depends on time. The geometric interpretation of the vector is depicted in Fig. 4.1 using the Stuart-Landau equations, for which all modes $\boldsymbol{Z}_k$ and $\boldsymbol{W}_k$ can be calculated analytically, *cf.* App. A.3.

With this representation and Eq. (4.11) we get the identity

$$\boldsymbol{Z}_k \frac{\partial \boldsymbol{u}}{\partial \phi} = -\left(\frac{\partial \boldsymbol{Z}_k}{\partial \phi}\right)\boldsymbol{u} = (\boldsymbol{Z}_k \boldsymbol{J} - \lambda_k \boldsymbol{Z}_k)\,\boldsymbol{u} \tag{4.19}$$

Left-multiplying Eq. (4.17) on both sides with $\boldsymbol{Z}_k(\phi) = \boldsymbol{z}_k \boldsymbol{R}^{-1}$ and using Eqs. (4.9) and

(4.19) yields

$$\delta_{k0}\Omega + \Omega\left(\boldsymbol{Z}_k\boldsymbol{J} - \lambda_k\boldsymbol{Z}_k\right)\boldsymbol{u} + \frac{d\alpha_k}{dt} = \lambda_k\alpha_k + \boldsymbol{Z}_k[\boldsymbol{H}(\phi)\boldsymbol{u}\boldsymbol{u} + \boldsymbol{\eta}(\boldsymbol{v}_0 + \boldsymbol{u}, t)] \tag{4.20}$$

From this equation one can obtain an expression for Ω (and hence for ϕ via Eq. (4.14)) by choosing $k = 0$ and an equation for the radial dynamics by setting $k > 0$.
To obtain a solvable set of equations we systematically expand the phase Eq. (4.14) as in Ref. [105] in orders of $\|\boldsymbol{\eta}\|$

$$\dot{\phi} = 1 + \sum_{j>0} \Omega^{(j)}(\phi, t), \tag{4.21}$$

and accordingly also the quantities

$$\begin{pmatrix} \Omega \\ \alpha_k \\ \boldsymbol{u} \end{pmatrix} = \sum_{j>0} \begin{pmatrix} \Omega^{(j)} \\ \alpha_k^{(j)} \\ \boldsymbol{u}^{(j)} \end{pmatrix}. \tag{4.22}$$

Expressions for Ω to first and second order are obtained with $k = 0$ in Eq. (4.20) and writing $\boldsymbol{\eta}(\phi, t) = \boldsymbol{\eta}(\boldsymbol{v}_0(\phi), t)$

$$\Omega^{(1)} = \boldsymbol{Z}_0(\phi)\boldsymbol{\eta}(\phi, t) \tag{4.23a}$$

$$\Omega^{(2)} = \sum_{j,\ell} h_{j\ell}\, \alpha_j^{(1)}\alpha_\ell^{(1)} - \Omega^{(1)} \sum_j g_j(\phi)\, \alpha_j^{(1)} + \boldsymbol{Z}_0 \nabla\boldsymbol{\eta}\, \boldsymbol{u}^{(1)}, \tag{4.23b}$$

with the abbreviations $h_{j\ell}(\phi) = \boldsymbol{Z}_0\boldsymbol{H}\boldsymbol{W}_j\boldsymbol{W}_\ell$ and $\boldsymbol{g}_j(\phi) = \boldsymbol{J}^D\boldsymbol{W}_j - (\boldsymbol{Z}_0\boldsymbol{J}\boldsymbol{W}_j)\sqrt{\boldsymbol{D}})$. $\boldsymbol{J}^D$ is the Jacobian tensor of the diffusion matrix $\sqrt{\boldsymbol{D}}$. To evaluate these phase contributions we need the first order amplitude dynamics which is obtained with $k \neq 0$ in Eq. (4.20). Together the complete second oder stochastic differential system for phase and amplitude reads

$$\dot{\phi} = \omega + \sum_{j,\ell} h(\phi)_{j\ell}\alpha_j^{(1)}\alpha_\ell^{(1)} + \boldsymbol{Z}_0(\phi)\left(\sqrt{\boldsymbol{D}} + \alpha_j^{(1)}\boldsymbol{g}_j\right)\boldsymbol{\xi}(t) \tag{4.24a}$$

$$\dot{\alpha}_k^{(1)} = \lambda_k\alpha_k^{(1)} + \boldsymbol{Z}_k(\phi)\boldsymbol{N}(\phi)\boldsymbol{\xi}(t). \tag{4.24b}$$

In the following we will drop the explicit mentioning of α being a first order quantity, but keep it in mind!
In Fig. 4.3 we get a first impression of the qualitative improvement in predicting the spike timing of the Na^+/K^+ model, when the phase amplitude model, $\phi^{(2)}$, is used instead of the one dimensional phase equation, $\phi^{(1)}$.

§4.5 Summary

This chapter described a transformation of an n dimensional biophysical system into a time-like phase variable and possibly $n-1$ radial variables Eq. (3.16). Fig. 4.1 shows that a diffeormorphism connects the original dynamics and the phase/amplitude description. As long as one can compute the isochrons the new coordinates can completely replicate the original dynamics in side the domain of attraction of the limit cycle. But for higher dimensions the isochrons are difficult to deduce and the computational load of computing them numerically is large. Hence, the perturbation analysis involving PRCs and the radial sensitivities

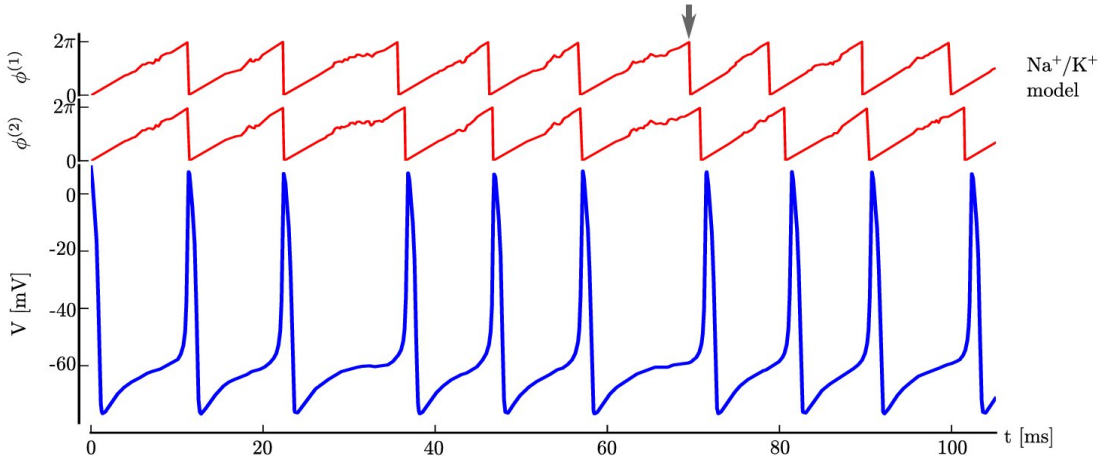

Fig. 4.3: Qualitative improvement of second order phase models in predicting spike times. The difference becomes apparent near the grey arrow. This is quantified statistically in the next chapter. Simulations show the Na^+/K^+ model with parameter from [92]. All three model use the same frozen noise path.

is the natural option as it can applied for high dimensional models.
The transformation discussed in the chapter is related to the more general Hale's transformation. In Ref. [77, Cpt. VI] a general transformation is described that is applicable to limit cycle oscillators. It is a conformal mapping that changes the state variables to phase-amplitude variables.

$$\dot{\phi} = 1 + h_1(\phi, \boldsymbol{\varrho}) \tag{4.25}$$

$$\dot{\boldsymbol{\varrho}} = \boldsymbol{A}(\phi)\boldsymbol{\varrho} + h_2(\phi, \boldsymbol{\varrho}), \tag{4.26}$$

where $\boldsymbol{A}$ is related to the stability of the limit cycle and h_1 and h_2 can in principle be identified from the original system. Our approach is related in the sense that an additional transformation can diagonalise $\boldsymbol{A}$ so that we can recover Eq. (4.24).
It is important to realise that, naturally, the perturbative phase reduction does have its limitations in applicability and will not be able to capture all the phenomena of the original models [114]. In particular, the phase as defined in the following is attributed to each point in the basin of attraction of a limit cycle, which is why LC stability is reviewed in §4.2. If the dynamics shows multistability, in terms of other attractors nearby in state space, separated by a separatrix such as an unstable limit cycle in the HH equations, then the phase description will lose its validity beyond the domain of attraction of the LC. The separatrix forms a phase-less set as discussed in Ref. [187]. In the chapters to follow it can be seen that useful coding properties of neurons can at least be captured by the phase reduction for medium and small stimulus amplitudes [162].

5 Spike statistics

Whilst §3.4 and §3.5 in chapter 3 provided a mesoscopic diffusion approximation to the microscopic intrinsic noise sources in a neuron, this chapter takes the next step and connects the noise in the derived Langevin equations to „macroscopic" quantities that are accessible via recorded spike times such as moments of the inter-spike interval distribution or firing rates. The means to this end are the phase reduction methods introduced in Cpt. 4.
Spike times can be determined from intracellular recordings with sharp electrodes or spike sorted extra-cellular recordings, where both techniques are applicable in *in-vivo* experiments. Intrinsic noise resulting from channel stochasticity can cause shifts in the frequency-current relation resulting in a gain modulating effect.
In particular, the number of ion channels influences the neuron's sensitivity to noise like-perturbations [165]. We will further investigate this, by highlighting that if the noise source is intrinsic channel stochasticity, the phase noise that accumulates within one inter-spike interval to cause the spike jitter is captured by a projection of the high dimensional diffusion matrix of the channel SDEs onto the gating PRCs. If peak conductances are altered they will change the deterministic part of the neuron and thus the PRCs, as well as the channel numbers that scale the diffusion matrix. Both effects conjointly determine the spike jitter.
In the following the spike jitter is quantified by calculating the first passage times statistics [149, 70].

§5.1 First order spike jitter from Markov channels

A hierarchy of differential equations for the moments of the waiting time distribution of a one dimensional threshold crossing model were given in Eq. (2.18), provided the Fokker-Planck operator for the system is known. The equations for phase and radial coefficients from §4.4 do not comply with this technique for one dimensional problems. But if, as a first step, the phase reduction in Cpt. 4 is sought only to first order the result is, as required, a one-dimensional equation that approximately describe the spike times of the biophysical neuron model. We will postpone the inclusion of second order radial terms until §5.2, and first deal with

$$\dot{\phi} = 1 + \boldsymbol{Z}(\phi) \cdot \sqrt{\boldsymbol{D}(\phi)}\, \boldsymbol{\xi}_t. \tag{5.1}$$

The associated FPE operator (*cf.* A.2 or [61]) reads

$$\mathcal{F} = \tfrac{1}{2}\partial_\phi^2 \sigma^2(\phi) - \partial_\phi(1 - \tfrac{1}{2}\sigma(\phi)\sigma'(\phi)), \tag{5.2}$$

where the phase-dependent variance of the phase is given by a quadratic form of the PRCs

$$\sigma^2(\phi) = \boldsymbol{Z}(\phi) \cdot \boldsymbol{D}(\phi)\boldsymbol{Z}(\phi). \tag{5.3}$$

The phase dependent variance will accumulate through one inter-spike interval to determine the overall spike jitter.

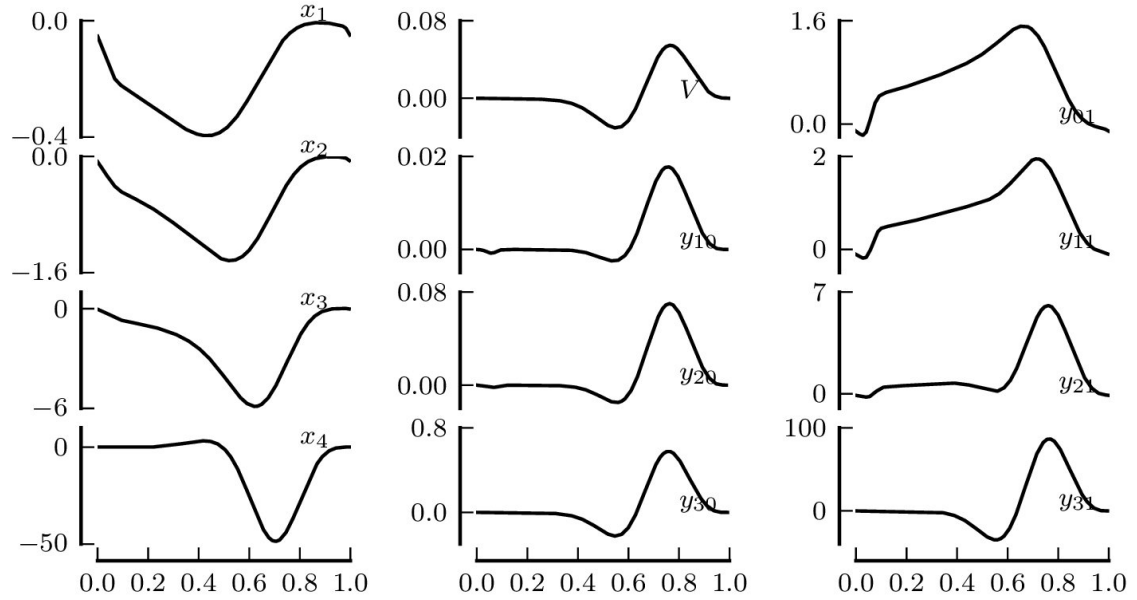

Fig. 5.1: PRCs of in the 12 dimensional HH model, from *cf.* §3.5. The peak of the AP is at 0 (1). $I = 8$ µA so that the neuron fires at 62.12 Hz. The left column depicts the PRCs of the K^+ channel; top graph in the middle column is the known PRC for current stimulations; and the remaining PRC are from the Na^+ channel states.

Fokker-Planck equation, $\partial_t p = \mathcal{F}p$, with operators similar to Eq. (5.2) arise in many synchronisation related problems. For example, the case where the phase-dependent noise strength is a simple trigonometric function, $\sigma(\phi) = \sqrt{2}\sin 2\pi\phi$, has been studied [67].

Spikes in the one dimensional phase SDE in Eq. (5.1) occur at crossings of $\phi = k$ for $k \in \mathbb{Z}$. In principle, this induces periodic boundary conditions for the FPE, $\partial_t p = \mathcal{F}p$, if we take the domain modulo 1 so that $\phi \in [0, 1)$. As the noise is bidirectional, a crossing of the spike in the direction of increasing phase could be followed by a crossing in the opposite direction, see discussion revolving around Eq. (2.12) and Ref. [174, Cpt. 1, Sec. 2]. Spikes in very quick succession (a "burst") could occur, as the dynamical system recrosses the threshold in the positive direction. Chapter 1 of Ref. [174] also offers a strategy on how to calculate the time between such bursts, relating it back to the classical waiting time distribution. The probability of such burst events can also be diminished by the appropriate choice of threshold, *i.e.*, by placing it in a region where the intrinsic dynamics are fast, and the phase response curve and phase noise sensitivities are close to zero. A consequence of the small noise assumption is that changing the boundary conditions from periodic to reflecting at the lower, $\phi = 0$, and absorbing at the upper end, $\phi = 1$, gives comparable results and avoids the burst effect. In fact, in Ref. [174] Stratonovich has arrived at a formula for the inter-burst waiting time, which is the inter-spike time if we do not wish to define each crossing in a burst as a separate spike, that is similar to the normal first passage time with absorbing and reflecting boundaries.

Therefore, one may approximately use Eq. (2.18) with $\mathcal{F}^\dagger$ as the adjoint of Eq. (5.2). The equation for the moments, T_n, of the ISI distribution, Eq. (2.18), can be cast into a set of coupled first order ODEs. With the auxiliary variables $S_n = \mathrm{d}T_n/\mathrm{d}\phi$ the ODE system for

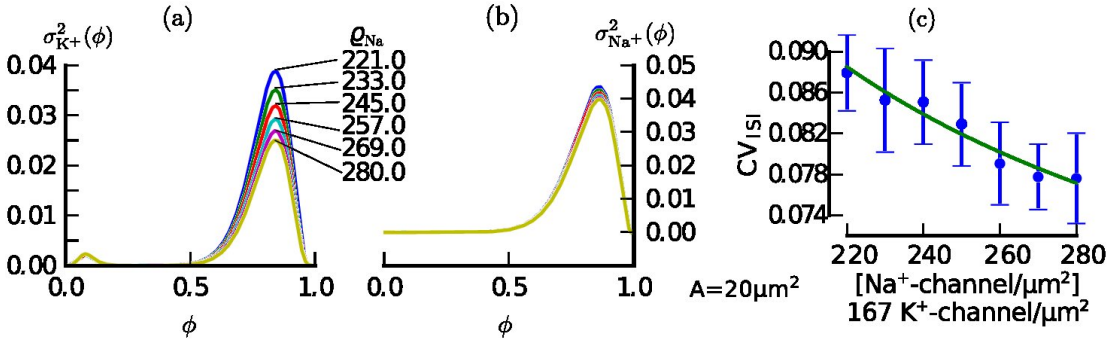

Fig. 5.2: (a) and (b) show the two terms, $\sigma^2_{\mathrm{Na}^+}$ and $\sigma^2_{\mathrm{K}^+}$ of the phase-dependent phase noise variance, $\sigma^2(\phi)$, *cf.* Eq. (5.5), that are associated with the Na^+ (b) and the K^+ (a) part of the channel diffusion matrix. The differently coloured lines depict different Na^+ channel densities. The membrane area was fixed at $A = 20\,\mu\mathrm{m}^2$, DC current is $I = 8\,\mu\mathrm{A}$, unitary conductance Na^+ channel: 4 nS, K^+ channel: 12 nS. Pannel (c) the mean and standard deviation of the CV of simulated spike trains. The green solid line is the CV as predicted by solving the system of equations in Eq. (5.4) plus the equations for the limit cycle and PRCs using continuation software, see appendix C.

the first and second moment are

$$\frac{\mathrm{d}}{\mathrm{d}\phi}T_1 = S_1 \tag{5.4a}$$

$$\frac{\mathrm{d}}{\mathrm{d}\phi}S_1 = -2\,\frac{1+\left[1+\frac{1}{2}\sigma'(\phi)\sigma(\phi)\right]S_1}{\sigma^2(\phi)} \tag{5.4b}$$

$$\frac{\mathrm{d}}{\mathrm{d}\phi}T_2 = S_2 \tag{5.4c}$$

$$\frac{\mathrm{d}}{\mathrm{d}\phi}S_2 = -2\,\frac{2T_1+\left[1+\frac{1}{2}\sigma'(\phi)\sigma(\phi)\right]S_2}{\sigma^2(\phi)} \tag{5.4d}$$

Treating the phase as reflecting at the lower boundary and absorbing at the upper boundary translates to the following set of boundary conditions

$$T_1(T_\mathrm{p}) = 0 \qquad S_1(0) = 0 \qquad T_2(T_\mathrm{p}) = 0 \qquad S_2(0) = 0$$

This ODE system requires a solution of $\boldsymbol{Z}$ and thus also the limit cycle. The complete system for limit cycle, adjoint equation and the moment equations can be implemented as an autonomous system within the framework of numerical continuation, see App. C.2.

Due to the bock diagonal structure of $\boldsymbol{D}(\phi)$, see Eq. (3.19), the first order phase noise splits additively into two separate channels

$$\sigma^2(\phi) = \sigma^2_{\mathrm{Na}}(\phi) + \sigma^2_{\mathrm{K}}(\phi). \tag{5.5}$$

Note, however, that this does not mean that these terms can be independently altered in a physiological system. Even if a biophysical parameters of the conductance model affect only one block in the diffusion matrix it also alters phase sensitivity vector $\boldsymbol{Z}$. This leads to the surprising phenomenon investigated in the next section.

§5.1.1 Changing Channel densities

In a conductance based model one has parameters of very different flavour, ranging from kinetic parameters of the channels to reversal potentials. Some of these parameters such as the kinetic properties are encoded genetically, but can be changed by interaction with G-proteins or phosphorylation. Also reversal potentials can change on the time scales of seconds depending on pump activity. The generally high turnover rate of membrane pores subjects channel densities to a tight regulatory control of the cell's translational and transcriptional machinery. These changes occur on a slower time scale than the membrane dynamics, but it is worth pondering about how changes in channel densities affect spike statistics.
Changes in channel densities will modify both the phase susceptibility to noise-like perturbation of the macroscopic equations (*cf.* §2.5 and §4.3) and the strength of the perturbations itself. The susceptibility of the channel states to noise is described by their PRCs, which for the HH equations are depicted in Fig. 5.1. It can be noted that the PRCs of the K^+ states are mostly negative, meaning that a positive perturbation (increase in channel numbers of all states) delays the timing of the next spike. As the sequence $n_1 \to n_2 \to n_3 \to n_4$ is traversed, the peak of the corresponding PRC shifts. In part the peak is located at the position in the ISI where the proportion of open K^+ channels is low, which is before the AP. Yet, these are entirely properties of the deterministic macroscopic equations.
Surprisingly, in this model, changing the Na^+ channel density has a stronger effect on σ^2_{K} than on σ^2_{Na} itself, as exemplified in Fig. 5.2a,b. The coefficient of variation of the ISI distribution decreases as channel fluctuations are reduced with increasing Na^+ channel density, *cf.* Fig. 5.2c.

§5.2 Radial dynamics and noise induced rate shift

The ISI variance, $\langle(\tau^{\mathrm{sp}} - \langle\tau^{\mathrm{sp}}\rangle)^2\rangle$, being a second order quantity requires inclusion of second order terms in the phase evolution as discussed in §4.4. Relying only on the system's PRC would only strictly be valid when the radial attraction to the limit cycle is almost instantaneous, $\lambda_i \to -\infty$.
When this assumption is violated, deviations from the predicted ISI moments result. A change in mean or average firing rate are referred to as a *noise induced frequency shift* and has been studied in idealised neuronal oscillators.
For one dimensional threshold systems such as integrate-and-fire models, which are but Brownian motion in a potential, the shift in mean rate depend of the shape of the potential [7]. In a single-variable phase model, on the other hand, the lowest order frequency shift is zero if the noise is Gaussian white noise. In Ref. [58] Fernández-Galán showed that coloured noise (instead of white) can cause a frequency shift [58]. More generally, in multi-dimensional nonlinear systems, noise effects are subtly related to the interplay of correlation time of the noise and the return time to the limit cycle (λ_i^{-1}) [177]. If the return time is finite, then white noise, too, can cause frequency shifts [177, 188]. Actually, as the return time is finite, white noise is effectively filtered into a coloured noise process. Particularly, if the radial dynamics is considered along the Floquet modes, see Eq. (4.24b), the equation for the amplitude coefficient is an Ornstein-Uhlenbeck process with diagonal drift matrix and a state-dependent variance

$$\dot{\alpha} = \lambda\alpha + \boldsymbol{Z}(\phi)\sqrt{\boldsymbol{D}(\phi)}\,\boldsymbol{\xi}_t.$$

The application of the iterative equations for the waiting time statistics between spikes,

Eq. (2.18), require a one dimensional equation of motion, *e.g.*, only the phase. Using the full phase amplitude equations as such would require solving a high dimensional exit problem [149], which is more complicated. While this is in principle possible, the boundary in that case is a hyper plane crossing the phase dimension at the defined spike phase and perpendicular to all radial dimensions, one may opt for a simpler approach in which the phase amplitude model is reduced to a single equation that retains the important ramifications of the amplitude dynamics. To this end, the next two sections describes a formal reduction method that explicitly exploits the time separation between return time and spike period.

§5.3 Time evolution of phase and radial density

The evolution of the density of state variables in the phase-radial model in SDE (4.24) is described by a multivariate *Fokker-Planck equation* (see Refs. [156, 61] and App. A.2)

$$\partial_t p(\phi, \boldsymbol{\alpha}) = \mathcal{F}\, p(\phi, \boldsymbol{\alpha}). \tag{5.6a}$$

There are several ways of deriving it, each emphasising different aspects (Kramer-Moyal expansion, kinetic view). The derivation of the one dimensional case has been reproduced in appendix A.2, based on the NFD formula, see appendix A.1 and Refs. [185, 102].
An important simplification results from the fact that in the perturbation analysis the NFD formula increases the order of the diffusion term in the FPE and thus the second order terms in SDE (4.24) that involve the noise process ξ_i can be dropped. This involves all terms involving products of α_i and ξ_j, and consequently the lowest order diffusion term in the FPE depends only on the phase, not on the radial coefficients.
The Fokker-Planck operator to second order reads

$$\begin{aligned}\mathcal{F} = \tfrac{1}{2}\textstyle\sum_{jk}\left[\langle\check{\boldsymbol{Z}}_j, \check{\boldsymbol{Z}}_k\rangle\partial^2_{\alpha_j\alpha_k} - \alpha_j\alpha_k\partial_\phi h_{jk}(\phi)\right] - \partial_\phi(1 + \tfrac{1}{2}\langle\check{\boldsymbol{Z}}_0, \check{\boldsymbol{Z}}_0'\rangle) \\ + \tfrac{1}{2}\partial^2_\phi\|\check{\boldsymbol{Z}}_0\| + \textstyle\sum_j\left[\partial_\phi\langle\check{\boldsymbol{Z}}_0, \check{\boldsymbol{Z}}_j\rangle\partial_{\alpha_j} - \partial_{\alpha_j}(\lambda_j\alpha_j + \tfrac{1}{2}\langle\check{\boldsymbol{Z}}_0, \check{\boldsymbol{Z}}_j'\rangle)\right],\end{aligned} \tag{5.6b}$$

in which we used the redefined sensitivities $\check{\boldsymbol{Z}}(\phi)$, which are weighted with the standard deviation of the respective noise, channel or input related

$$\check{\boldsymbol{Z}}_j(\phi) = \boldsymbol{Z}_j(\phi)\sqrt{\boldsymbol{D}(\phi)}.$$

As Eq. (5.6) neither fulfils the potential conditions nor is in detailed balance, finding solutions is complicated and requires further approximations [61]. If the attraction time scales to the limit cycle, λ_i^{-1}, and period are well separated the following section provides a useful simplification.

§5.4 Quasistatic elimination of the radial dynamics

In a deterministic limit cycle oscillator, the assumption that radial attraction is very strong — so strong, in fact, that perturbations away are instantaneously repositioned back onto the cycle — leads to a complete reduction to a one dimensional phase model [106, Cpt. 3]. A parallel procedure exists for stochastic systems, yet some more care must be taken. The correlation times of the noise and the attraction time scale to the limit cycle play subtle roles

that need to be considered, see Ref. [177]. It is thus convenient to first transform to ϕ, α_i-coordinates, keeping the attraction time finite, and in a second step perform a quasistatic (adiabatic) elimination of the fast radial dynamics. The formal procedure is also referred to as Chapman-Enskog elimination scheme. The complete set of radial coefficients, α_i, can be vanquished, if the relevant time scale of observation is larger than $1/|\lambda_i|$, where λ_i is the Floquet exponent with the smallest magnitude. The time scale of interest here is about one inter-spike interval which is in the order of T_p, hence one requires that all $T_\mathrm{p}|\lambda_i| \gg 1$. Our example of the Na^+/K^+ model fulfils this requirement over a vast interval of bias currents, *cf.* Fig. 5.3.

The goal of the formal elimination procedure is to find a one dimensional "phase only" FPE, valid on the appropriate time scale τ

$$\partial_t \bar{p}(\phi) = \bar{\mathcal{F}}\bar{p}(\phi), \quad \text{suitable for } \tau\,\lambda_i \gg 1. \tag{5.7}$$

It is known from the literature that even in this limit there remains a noise induced frequency shift even if the driving noise is uncorrelated. But so far this has only been studied in detail for the Stuart-Landau equation [176], and there is no general numerical method to evaluate the relevant terms in a conductance based model.

What we expect from the operator $\bar{\mathcal{F}}$ is a modification to the one-dimensional first order phase equation, defined by the operator in Eq. (5.2), that depends on the characteristic exponents of the radial variables, and that will cause a shift in frequency.

The basic idea is to split the Fokker-Planck operator from Eq. (5.6b) into a quickly relaxing (large magnitude) part and the slower dynamics (small magnitude)

$$\mathcal{F} = \underbrace{\mathcal{F}^{(\phi)}}_{\text{small}} + \underbrace{\mathcal{F}^{(\alpha)}}_{\text{large}}, \tag{5.8a}$$

and then apply Bloch's classical operator perturbation theory [20] to calculate the $\mathcal{F}^{(\phi)}$-perturbed eigensystem of $\mathcal{F}^{(\alpha)}$ to gain an approximate understanding of the operation of the complete operator, $\mathcal{F}$. To be more precise, one may quantify the size of the two operator parts in terms of their spectral norm, *e.g.*,

$$\|\mathcal{F}^{(\alpha)}\| = \sup_{\|v\|=1} \left\{ \|\mathcal{F}^{(\alpha)} v\| \right\}.$$

Yet, if the noise is weak this is approximately given by the Floquet exponent with largest amplitude, $\|\mathcal{F}^{(\alpha)}\| \approx \sup_j\{\lambda_j\}$ and the $\|\mathcal{F}^{(\phi)}\| \approx {T_\mathrm{p}}^{-1}$. This leads back to our ad hoc assumption that the radial attraction should be faster than one period.

One must note that there is a certain arbitrariness in the decision on how to group some of the small magnitude terms of $\mathcal{F}$, *e.g.*, the term $\partial_\phi \langle \check{\boldsymbol{Z}}_0, \check{\boldsymbol{Z}}_j \rangle \partial_{\alpha_j}$ may be shoved between $\mathcal{F}^{(\phi)}$ and $\mathcal{F}^{(\alpha)}$. This is due to the fact that adding or substsracting some small terms to a large operator will not blemish the facts that it is large. In our scheme the term $\partial_\phi \langle \check{\boldsymbol{Z}}_0, \check{\boldsymbol{Z}}_j \rangle \partial_{\alpha_j}$ is formally assigned to $\mathcal{F}^{(\alpha)}$ but can be ommited as motivated below.

The strategy is to split the operator in a manner that renders the stationary radial distribu-

tion for fixed ϕ a multivariate Ornstein-Uhlenbeck (OU) process [178, 132]

$$\mathcal{F}^{(\phi)} = \tfrac{1}{2}\partial_\phi^2 \|\check{\boldsymbol{Z}}_0\|^2 - \sum_{jk} \partial_\phi \left[1 + \tfrac{1}{2}(\alpha_j \alpha_k h_{jk}(\phi) + \langle \check{\boldsymbol{Z}}_0, \check{\boldsymbol{Z}}_0' \rangle)\right] \tag{5.8b}$$

$$\mathcal{F}^{(\alpha)} = \tfrac{1}{2}\textstyle\sum_{jk} \langle \check{\boldsymbol{Z}}_j, \check{\boldsymbol{Z}}_k \rangle \partial^2_{\alpha_j \alpha_k} - \sum_j \partial_{\alpha_j} [\lambda_j \alpha_j + \tfrac{1}{2}\langle \check{\boldsymbol{Z}}_0, \check{\boldsymbol{Z}}_j' \rangle]. \tag{5.8c}$$

For $|\lambda_i| T_\mathrm{p} \gg 1$ on the time scale of one period, $\mathcal{F}^{(\alpha)}$ yields fast and $\mathcal{F}^{(\phi)}$ slow dynamics. Due to this assumed difference in time scales a stationary distribution of α_i will equilibrate for every ϕ to $p_0(\boldsymbol{\alpha})$. This means that ϕ is treated as a fixed parameter so that the FPE,

$$\dot{p}(\boldsymbol{\alpha}, t) = \mathcal{F}^{(\alpha)} p(\boldsymbol{\alpha}, t), \tag{5.9}$$

is just the analytically well understood multivariate Ornstein-Uhlenbeck process, which is extensively analysed in Ref. [156, Cpt. 6.5]. Now it is also apparent that for fixed ϕ the term $\partial_\phi \langle \check{\boldsymbol{Z}}_0, \check{\boldsymbol{Z}}_j \rangle \partial_{\alpha_j}$ vanishes.

As the Onsager conditions [61, Cpt. 5.3.6c], which establish the existence of a stationary solution for the general multivariate OU processes, are in our case fulfilled due to the diagonal drift, the equilibrium density for Eq. (5.9), defined by $\mathcal{F}^{(\alpha)} p_\mathrm{eq}(\boldsymbol{\alpha}) = 0$, is just the multivariate Gaussian

$$p_0(\boldsymbol{\alpha}) = (2\pi)^{-(d-1)} |\boldsymbol{C}^{(\alpha)}|^{-\frac{1}{2}} \exp\left(-\tfrac{1}{2}\left\langle (\boldsymbol{\alpha} - \boldsymbol{\mu}^{(\alpha)}), (\boldsymbol{C}^{(\alpha)})^{-1} (\boldsymbol{\alpha} - \boldsymbol{\mu}^{(\alpha)}) \right\rangle\right), \tag{5.10}$$

where mean and covariance are expressions of the scaled sensitivities and the Floquet exponents [178]

$$\boldsymbol{\mu}_i^{(\alpha)} = \frac{\langle \check{\boldsymbol{Z}}_0, \check{\boldsymbol{Z}}_i' \rangle}{2\lambda_i}, \qquad \boldsymbol{C}_{ij}^{(\alpha)} = \frac{\langle \check{\boldsymbol{Z}}_i, \check{\boldsymbol{Z}}_j \rangle}{\lambda_i + \lambda_j}. \tag{5.11}$$

The equilibrium density can be interpreted as the right-eigenfunction of $\mathcal{F}^{(\alpha)}$ corresponding to the zero eigenvalue (the ground state). The left-eigenfunction of the ground state is $q_0(\boldsymbol{\alpha}) = 1$. The complete biorthogonal set of left/right-eigenfunctions and corresponding eigenvalues can be expressed in the basis of Hermitian polynomials, but only the lowest order is retained here. Due to a correspondence between the Chapman-Enskog elimination scheme and Bloch's classical perturbation theory of operators as highlighted in Ref. [179], the perturbation of the ground state energy also yields the „phase only" Fokker-Planck operator, *i.e.*,

$$\bar{\mathcal{F}}(\phi) = \textstyle\int \mathrm{d}^{d-1}\boldsymbol{\alpha}\; q_0(\boldsymbol{\alpha}) \mathcal{F}^{(\phi)}(\phi, \boldsymbol{\alpha}) p_0(\boldsymbol{\alpha}). \tag{5.12}$$

The higher order adiabatic elimination process follows Bloch's scheme too and involves the complete set of eigenfunction q_k, p_k, but these terms are not used in this document. Since $q_0(\boldsymbol{\alpha}) = 1$, the lowest nonzero order of $\bar{\mathcal{F}}$, Eq. (5.12), just requires averaging the operator $\mathcal{F}^{(\phi)}$ over the stationary distribution of the radial variables at every ϕ to obtain

$$\begin{aligned}\bar{\mathcal{F}} = \tfrac{1}{2}\partial_\phi^2 \|\check{\boldsymbol{Z}}_0(\phi)\|^2 - \partial_\phi \Big[& 1 + \tfrac{1}{2}\langle \check{\boldsymbol{Z}}_0(\phi), \check{\boldsymbol{Z}}_0'(\phi) \rangle \\ & + \tfrac{1}{2}\sum_{ij} h_{ij}(\phi) \left(\frac{\langle \check{\boldsymbol{Z}}_i, \check{\boldsymbol{Z}}_j \rangle}{\lambda_i + \lambda_j} + \frac{\langle \check{\boldsymbol{Z}}_0, \check{\boldsymbol{Z}}_i' \rangle \langle \check{\boldsymbol{Z}}_0, \check{\boldsymbol{Z}}_j' \rangle}{4\lambda_i \lambda_j} \right) \Big].\end{aligned} \tag{5.13}$$

One may observe that phase dependent variance is the same as for the first order phase

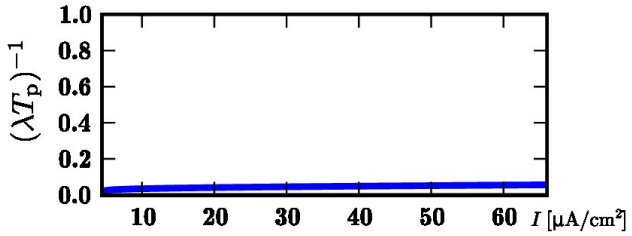

Fig. 5.3: Ratio of characteristic time scale of limit cycle attraction, λ^{-1}, and period of the deterministic system, T_p, for the Na^+/K^+ neuron. One can observe that the attraction to the limit cycle for this model is significantly fast than one period. Such models are suitable for the quasi-static elimination of radial variables.

equation in Eq. (5.3), so the general structure of the phase Fokker-Planck operator with quasistatic eliminated radial dynamics is

$$\bar{\mathcal{F}} = \tfrac{1}{2}\partial_\phi^2 \sigma^2(\phi) - \partial_\phi[1 + \bar{h}(\phi)] \tag{5.14}$$

From the corresponding „phase only" FPE with operator as in Eq. (5.13) one writes the associated Stratonovic SDE as

$$\dot{\phi} = 1 + \tfrac{1}{2}\sum_{ij} h_{ij}(\phi)\left(\frac{\langle \check{\boldsymbol{Z}}_i, \check{\boldsymbol{Z}}_j\rangle}{\lambda_i+\lambda_j} + \frac{\langle \check{\boldsymbol{Z}}_0, \check{\boldsymbol{Z}}'_i\rangle\langle \check{\boldsymbol{Z}}_0, \check{\boldsymbol{Z}}'_j\rangle}{4\lambda_i\lambda_j}\right) + \|\check{\boldsymbol{Z}}_0(\phi)\|\,\eta_t. \tag{5.15}$$

Note that while whenever the Langevin Eq. (4.24) is driven with the same white noise realisation as the original biophysical model the obtained spike times will actually be similar (*cf.* Fig. 4.3), yet this is not true for Eq. (5.15). Here, the equivalence is only true on the level ISI statistics. This is because the phase susceptibilities, *cf.* Fig. 5.1, change sign so do the original standard deviations $\boldsymbol{Z}\cdot\sqrt{\boldsymbol{D}}$, and this information is lost when taking the square to obtain variances in the FPE description. We can not expect particular spike train for Eq. (5.15) to correspond to the full system even if one uses the same noise realisation.

§5.5 Stationary phase density

For periodic boundary conditions the equilibrium solution, $\bar{\mathcal{F}}(\phi)p_0(\phi) = 0$, to the above equation must have a time independent flux

$$J = \left(1 + \bar{h}(\phi) - \tfrac{1}{2}\partial_\phi\sigma^2(\phi)\right)p_0(\phi), \qquad \text{with } J(0) = J(T_\mathrm{p}), \tag{5.16}$$

as opposed to the natural boundary case, where the flux at the boundary vanishes. This flux is the firing rate as motivated in §2.6. For one dimensional problems it is convenient to express solutions in terms of the *generalised potential*

$$\Phi(\phi) = 2\int_0^\phi \frac{1+\bar{h}(\psi)}{\sigma^2(\psi)}\,\mathrm{d}\psi. \tag{5.17}$$

Now, we nilly-willy wrote down the potential without ensuring that the integral actually exists. The main concern is the existence of a finite number of isolated poles, whenever the phase dependent variance $\sigma^2(\phi) = 0$ (*e.g.* the PRC changes sign) at some special ϕ'.

This causes both analytic and numerical challenges. Analytically, chopping the integral in to segments between poles and applying variable transformations that move them to infinity can provide solutions. The case for $\sigma^2(\phi) = \sqrt{2}\sin 2\pi\phi$ has been studied [67]. Numerically, chopping in combination with special integration methods can lead to success. Other robust numerical technique is the use of homotopy parameters in a numerical solution using AUTO's collocation method [31].
Real poles are likely to appear whenever noise is present only in a single dimension (degenerated diffusion), because the PRC of that dimension may cross zero. In such a case the integrability depends on how the PRC approaches zero and one may need to resort to residual integration of the complex augmented integrand. If however several or all dimensions of the biophysical model contribute to the phase noise, which is likely in a neuron where typically several channels species with different kinetics are at work as well as Johnson-Nykquist noise (*cf.* §3.3), then it is unlikely that the PRCs of all dimensions cross zero at the same phase. In fact, if the flow field of the r.h.s. of the conductance based model, which also is the Goldstone mode, is well behaved (differentiable and bounded), then the norm of the PRC can not be zero and thus not all components of the PRC can be zero an the same time. More precisely, if there is a real finite positive number M such that the norm of the flow field is bounded $\|\dot{\boldsymbol{v}}(\phi)\| \leqslant M < \infty$, $\forall\phi$, then form our chosen normalisation, $\omega = \langle \boldsymbol{Z}, \dot{\boldsymbol{v}}\rangle$ and the Cauchy-Schwarz inequality it follows $0 < \frac{\omega}{M} \leqslant \|\boldsymbol{Z}\|$.
If the potential exists, then aside from a normalisation, the stationary density can be expressed as [156]

$$p_0(\phi) \propto \int_0^\phi \mathrm{d}\theta\, e^{\Phi(\phi)-\Phi(\theta)-\Phi(T_\mathrm{p})} + \int_\phi^{T_\mathrm{p}} \mathrm{d}\theta\, e^{\Phi(\phi)-\Phi(\theta)-\Phi(0)}. \tag{5.18}$$

Also one may check by insertion that

$$p_0(\phi) \propto \Big(c - 2J\int_0^\phi \mathrm{d}\varphi\; e^{-U(\varphi)}\Big)e^{U(\phi)}/\sigma^2(\phi), \tag{5.19}$$

satisfies Eq. (5.16). The constant can be fixed to $c = p_0(0)B(0)$ by evaluating the equation above at $\phi = 0$, where $p_0(0)$ itself has to be chosen to meet with the normalisation condition $\int \mathrm{d}\phi\, p_0(\phi) = 1$. But prior to that let the flux J be brought to agree with the periodic BC, $p_0(0) = p_0(T_\mathrm{p})$, which results in [61, 156]

$$J = p_0(0)B(0)\,\frac{1 - e^{-U(T_\mathrm{p})}}{2\int_0^{T_\mathrm{p}} \mathrm{d}\varphi\; e^{-U(\varphi)}} \tag{5.20}$$

All relevant quantities are integrals over one period of the limit cycle oscillator and can be determined numerically within the continuation of BVPs frame work, *cf.* App. C. This allows us to easily determine both the firing rate J as well as the stationary phase density $p_0(\phi)$.

§5.6 Period change in the Stuart-Landau model with isotropic noise

To illustrate the relation between the noise induced second order frequency or mean period shift and the curvature of the isochrons one may consult a simple pair of equations, which

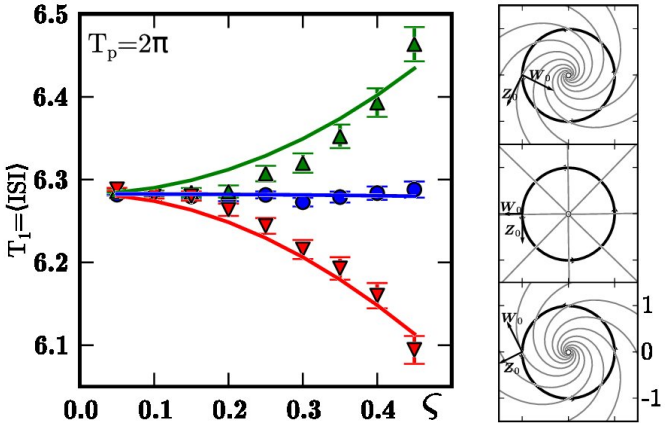

Fig. 5.4: Simulation of the Stuart-Landau model with isotropic noise in the Cartesian coordinates. The model with linear radial isochrons shows no shifts in the mean ISI for increasing noise (○,$[a,b,c,d] = [1, 1.01, -1, -0.01]$). Positive curvature of the isochron in the W_1, Z_0 coordinates leads to an increase in spike period with noise strength (△,$[a,b,c,d] = [1,3,-1,-2]$), while negative curvature reduces the spike period (▽,$[a,b,c,d] = [1,-1,-1,2]$).

exhibit a limit cycle oscillation, yet allow analytic treatment. These are the Stuart-Landau equations, the normal form of a supercritical Andronov-Hopf bifurcation [92]. Augmented with intrinsic noise the two dimensional mode reads

$$\frac{\mathrm{d}}{\mathrm{d}t}\begin{pmatrix} x \\ y \end{pmatrix} = \begin{pmatrix} ax - by + (cx - dy)\,(x^2+y^2) \\ ay + bx + (cy + dx)\,(x^2+y^2) \end{pmatrix} + \boldsymbol{D}\begin{pmatrix} \xi_1(t) \\ \xi_2(t) \end{pmatrix}, \tag{5.21}$$

where $\boldsymbol{D}$ is a 2×2 diffusion matrix. A more detailed analysis can be found in many textbooks on nonlinear dynamics and is summarised for reference in App. A.3. The supercritical Hopf bifurcation is typical for the excitation block that terminates repetitive spiking in neurons. The onset bifurcation for spiking if a Hopf bifurcation is usually subcritical yielding an unstable LC, tailed by a fold of limit cycles which results in a stable spiking orbit.

Assuming the noise has a constant, isotropic variance in the Euclidean coordinates, $\boldsymbol{D} = \varsigma^2 \boldsymbol{I}$, one only requires the following quantities to calculate the stationary phase density, firing rate and ISI statistics. Phase noise, Floquet exponent and curvature related term are

$$\sigma^2(\phi) = \langle \boldsymbol{Z}_0 | \boldsymbol{D} | \boldsymbol{Z}_0 \rangle = -\varsigma^2 \frac{c(c^2+d^2)}{a(bc-ad)^2}, \qquad \lambda = -2a, \qquad h = \frac{4d(c^2+d^2)}{c(bc-ad)}.$$

The norm and dot products between Floquet modes are

$$\|\boldsymbol{Z}_1\|^2 = \varsigma^2, \qquad \langle \boldsymbol{Z}_0, \boldsymbol{Z}_0' \rangle = 0, \qquad \langle \boldsymbol{Z}_0, \boldsymbol{Z}_1' \rangle = \varsigma^2 \sqrt{-\frac{c}{a}},$$

which renders the quasistatic phase FPE to have a constant drift and diffusion

$$\dot{p} = -\frac{c^2+d^2}{ac}\partial_\phi^2 p - \left[1 - \frac{2}{c}(c^2+d^2)\left(\frac{d}{2ac} + \frac{d(bc-ad)^2}{4a^3c^2}\right)\right]\partial_\phi p. \tag{5.22}$$

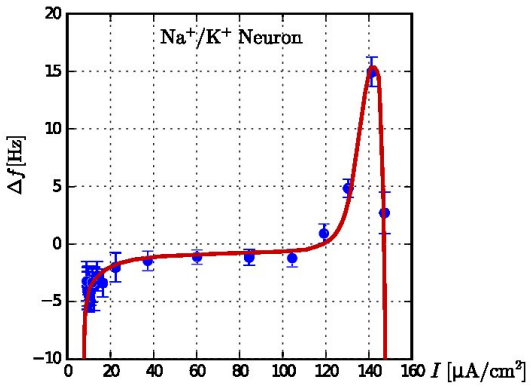

Fig. 5.5: Noise induced frequency shift in the Na^+/K^+ neuron. The figure shows the difference between the *f-I* curve of the simulated stochastic model and the deterministic neuron, where $f = N_{\text{spikes}}/T_{\text{sim}}$ and Eq. (5.27).

The generalised potential is linear

$$\Phi(\psi) = \left(2\frac{d}{c} + \frac{d(bc-ad)^2}{(ac)^2}\right)\psi$$

and the period can be calculated as $T_{\text{p}} = \frac{2\pi}{(b-ad/c)}$.

As a consequence the stationary phase density is uniform, $p_0(\phi) = 1/T_{\text{p}}$. The firing rate, Eq. (5.16), simplifies to

$$r_0 = J = \frac{1+\tilde{h}}{T_{\text{p}}}, \tag{5.23}$$

which tells us that the shift is actually given by the sign and magnitude of the term

$$\bar{h} = \tfrac{1}{2}h\left(\frac{\varsigma^2}{2\lambda} + \frac{\varsigma^4 A^2}{4\lambda^2}\right),$$

where $A = \sqrt{-a/c}$ is the amplitude of the LC.

Anisotropic noise leads to a sinusoidal modulation of the noise variance in the phase dynamics as well as a nonuniform phase density.

§5.7 Noise induced frequency shifts and *f-I* curves

Ref. [177] calculated the phase shift in a limit cycle oscillator induced by stochasticity. The actual calculation of the term was however restricted to the Stuart-Landau equations. This section expresses this term through the Floquet-models which can be obtained numerically via an efficient procedure (*cf.* App. C).

The average frequency of a noisy oscillator can be defined by the following ensemble average over different realisation paths [9, Cpt. 7.7]

$$r_0 = \langle\dot{\phi}(t)\rangle = \frac{1}{T_{\text{p}}}\lim_{\tau\to\infty}\frac{1}{\tau}\int_0^\tau \mathrm{d}t\;\dot{\phi} = \frac{1}{T_{\text{p}}}\int_0^{T_{\text{p}}}\mathrm{d}\phi\,\dot{\phi}\,p_0(\phi) \tag{5.24}$$

In principle, we have an expression for the steady state phase density in Eq. (5.18), but a more intelligible expression firing rate shift can be found if we content ourselves with a lowest order approximation following Ref. [177]. One can take a power series Ansatz in orders of the noise variance σ^2, $p = p_0^{(0)} + p_0^{(2)} + \cdots$. Insertion into $\bar{\mathcal{F}}p = 0$ leads to

$$\begin{aligned} \mathcal{O}(\sigma^0): &\qquad p_0^{(0)}(\phi) = c_0 \\ \mathcal{O}(\sigma^2): &\qquad p_0^{(2)}(\phi) = \frac{c_0}{2}\left(\partial_\phi \|\check{\boldsymbol{Z}}_0\|^2 - \langle \check{\boldsymbol{Z}}_0, \check{\boldsymbol{Z}}_0' \rangle - h_{ij}\frac{\langle \check{\boldsymbol{Z}}_i, \check{\boldsymbol{Z}}_j \rangle}{(\lambda_i + \lambda_j)}\right) + c_2. \end{aligned}$$

The integration constants can be determined by the normalisation condition, enforced at each cumulative order. We denote the phase density up to order $\mathcal{O}(\sigma^2)$ as $p_0^{(\sigma^2)} = p_0^{(0)} + p_0^{(2)}$, it then reads

$$p_{\mathrm{eq}}^{(\sigma^2)}(\phi) = \tfrac{1}{T_\mathrm{p}}\left(1 + \tfrac{1}{2}\langle \check{\boldsymbol{Z}}_0, \check{\boldsymbol{Z}}_0' \rangle - \tfrac{1}{2}\textstyle\sum_{ij} h_{ij}(\phi)\left(\frac{\langle \check{\boldsymbol{Z}}_i, \check{\boldsymbol{Z}}_j \rangle}{(\lambda_i + \lambda_j)}\right) + \Omega_2\right), \tag{5.25}$$

where the normalisation integral is

$$\Omega_2 = \frac{1}{T_\mathrm{p}} \int_0^{T_\mathrm{p}} \mathrm{d}\phi \sum_{ij} h_{ij}(\phi)\left(\frac{\langle \check{\boldsymbol{Z}}_i, \check{\boldsymbol{Z}}_j \rangle}{(\lambda_i + \lambda_j)}\right). \tag{5.26}$$

Using this and $p_0 = p_0^{(\sigma^2)}$, from Eq. (5.25), the lowest order noise effect is captured by [177]

$$\bar{r}^{(\sigma^2)} = \frac{1}{T_\mathrm{p}} + \Omega_2, \tag{5.27}$$

where the noise induced frequency shift is given by Eq. (5.26).
The effect of the noise on the Na^+/K^+ model neuron can be inspected in Fig. 5.5. At the onset of spiking theory and simulation predict a decrease in firing rate. Yet, near the excitation block at high DC input currents there is a region where noise increases the firing rate.

§5.7.1 ISI moments for stiff limit cycles

In biophysical models of neurons and certainly when operating away from the regime where normal form reductions are valid, the second order term term $\bar{h}$ and the noise variance will be phase dependent and not have simple sinusoidal form, which also leads to nonlinear potentials in Eq. (5.17). In many of these cases the ingredients for the above ISI statics have to be determined numerically. Because this is cumbersome for a high dimensional system such as the 12 dimensional HH equations the simplified Na^+/K^+ model chosen as exemplary neuron.
In Fig. 5.6 a comparison between the spike times of the original Na^+/K^+-model, the first order phase model and the second order model with quasi-stationary elimination of the radial dynamics is displayed. The quasi-static elimination procedure relies on the fact that the characteristic time scale of attraction to the limit cycle is smaller than the period or $(\lambda T_\mathrm{p})^{-1} \ll 1$, which can be verified over a broad range of DC inputs in Fig. 5.3. The numerical recipes for the evaluation of Floquet modes are described in App. C.
The mean ISI shift in Fig. 5.6c compared to the deterministic period is strong at the onset of spiking (66% reduction in mean due to noise). Comparing the CV of the noisy phase mode

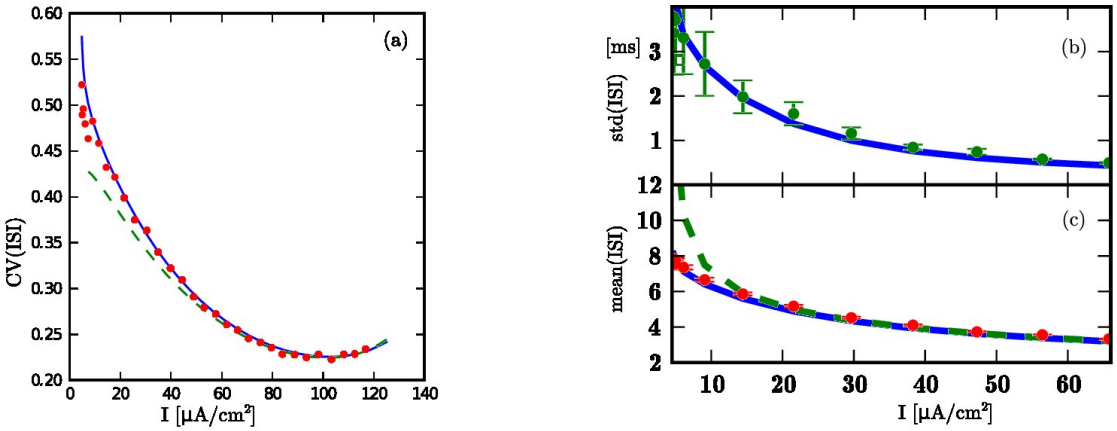

Fig. 5.6: Comparison of spike statistics for the Na^+/K^+ model. (a) Coefficient of variation of the ISI distribution. Floquet exponent and modes were calculated numerically using AUTO. Theoretical predictions were obtained by using the FP operator Eq. (5.13), including the radial term in the iterative equations for the moments Eq. (2.18). The dashed line shows the prediction without radial term. (b) Standard deviation of the inter-spike interval and theoretical prediction including shift induced by radial dynamics. (c) Mean ISI as predicted by the moment equations including radial term. Dashed line shows the same prediction without radial term. (errorbars: standard error).

with and without radial term in Fig. 5.6b shows that the radial term helps explaining the increase in CV at low firing rates (approximately 80% increase in CV, see Fig. 5.6a).

§5.8 Summary

This chapter started by showing that the first order phase reduction is applicable to a high dimensional channel SDE, which captures detailed channel kinetics. The different channels contribute additively to the phase-dependent phase noise, which integrated over one interval predicts the ISI variance of the spike train. In order to study the effects of radial dynamics for stiff limit cycles a quasi-static approximation was used to collapse the phase/amplitude equations to a single phase equation. For the Na^+/K^+ model this procedure is able to predict the noise induced frequency shift. The effect was further investigated in the Stuart-Landau equation where one can control the analytically known isochrons by changing the system parameters. It can be seen that the curvature of the isochron is important to determine the frequency shift.

6 Temporal filters from phase response curves

Linear and nonlinear system identification are commonly applied to neuronal input-output mappings. One of the techniques is the calculation of spike-triggered ensembles [155], that can be related to kernels in the Wiener series, see §2.8.1. This chapter illustrates how these can be calculated from the phase response curves of an underlying neuronal oscillator. In other words we assume that the black box is filled with a concrete biophysical model and identify an equivalent transfer function[1] mapping input to output.
Experimentally there are different paradigms concerning the choice of input stimuli. One emphasises naturalistic stimuli, possibly recorded in the natural habitat and corrupted with realistic environment noise, another works with stimuli designed to represent an idealised "sign stimulus", while a third strategy uses artificial white-noise stimuli, which provide an unbiased estimation of the system's transfer function. The latter does assume that the system's transfer characteristics is as such independent of the stimulation itself. Since it is possible to select statistically simple stimuli, it is often the method of choice for approaches involving analytical treatments.
In this chapter we will investigate the mapping of a time structured stimulus $x(t)$ into the instantaneous firing rate $r(t)$. Note again, that this rate $r(t)$ is an idealised quantity used by an experimental observer. It is defined as the trial average, $r(t) = \langle y(t) \rangle_{y|x}$, over a "frozen path" of a stimulus (illustrated in Fig. 2.2 and discussed in §2.8). In the nervous system such stop-and-rewind experiments do not occur. Yet, the trial average may be implemented as an ensemble average over a large (but finite) population of noisy realisations of otherwise identical neurons. Using these parallel channels seems a possible way for real-time nervous systems to achieve the noise reduction that experimentalists reach by trial averaging. Yet, even for large population sizes the population averaged instantaneous firing rate is a time resolved histogram, not a deterministic differentiable function as we have defined it through the probability flux in a FPE in §2.6. Second order statistics around the instantaneous firing rate [181] is not available in this FPE based approach. Though, they could possibly be included by some self-consistent argument adding noise to the FPE drift as in [19].

§6.1 Averaging intrinsic noise strength

In the following we include the external stimulus $x(t)$ and assume it perturbs the voltage dimension of the conductance based model like in Eq. (4.2). This would represent the condition, where a stimulating current is injected into a neuron with a sharp electrode. More complex stimulation via synapses or transduction processes may be better modelled as perturbations to special conductances. In this chapter the analysis uses a phase model with an averaged, phase independent noise strength, $\bar{\sigma}$, summarising the channel noise effects of

[1] Also termed susceptibility in the physics literature [5].

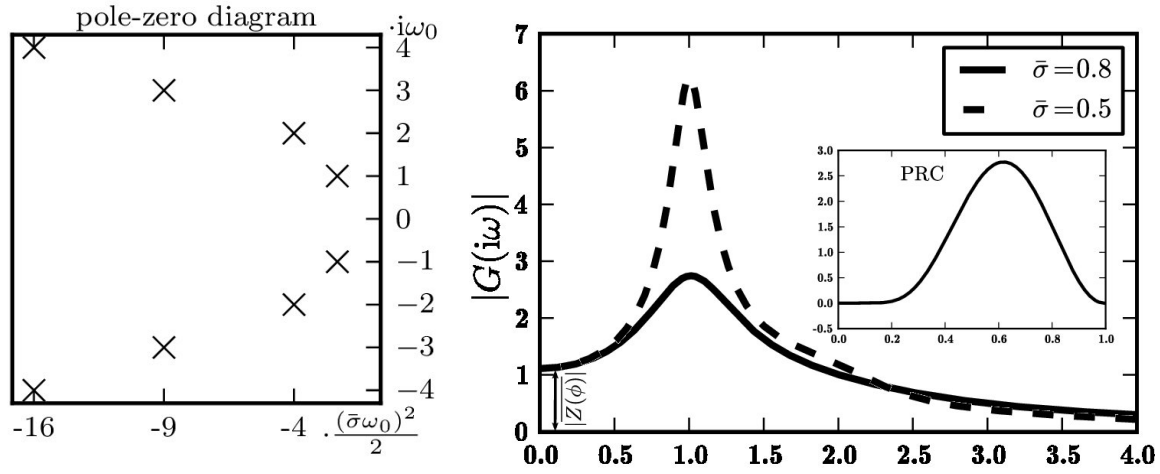

Fig. 6.1: Left: The pole-zero diagram shows the location of poles ν_k ($\times$) and zeros ($\circ$) in the complex plane, as given in the text; Right: Associated power spectral density resulting from the location and properties of the poles.

all contributing membrane pores, averaged over one inter-spike interval

$$\dot{\phi} = \omega + Z(\phi)x(t) + \bar{\sigma}\,\xi(t). \tag{6.1}$$

This simplification glosses over the phase dependence of the noise highlighted in Cpts. 3 and 4. On the other hand, there are now two sources the system in Eq. (6.1): the stimulus, $x(t)$, and intrinsic (*e.g.*, channel related) noise, $\xi(t)$, and we are interested in computing the stimulus's influence on the neuron's firing rate, so the influence of the intrinsic noise is simplified. There are additional arguments for this choice, which are postponed until the discussion in §8.2.

The input $x(t)$ is band-limited and Gaussian, as motivated in §2.2.1. The external signal is assumed to vary on a longer time scale than the intrinsic fluctuations; hence the upper cutoff frequency of $x(t)$ is limited. In some cases, this assumption is warranted. The examples in §2.2.2 show that the behaviourally relevant time scales of natural signals are at least several milliseconds long, much longer than the microsecond scale of conformational changes in ion channels.

Once again, the analysis assumes the signal is small enough so that the ISI's can be treated as a perturbation of the basic period T_p. Both the signal and the inter-spike time scale must be longer than the correlation time of the intrinsic noise, T_p and $\tau_x \gg \tau_\xi$.

In experiments, one will often repeat the same time-varying stimulus $x(t)$ many times. Such a stimulus can be called "frozen noise". Intrinsic noise, on the other hand, will not repeat from trial to trial: on each trial, the internal channel fluctuations will be different. This implies that the stimulus only affects the deterministic drift part of the FPE or SDE describing the neuron. Including the first order stimulus perturbation in to the Fokker-Planck operator derived in Eq. (5.14) yields

$$\bar{\mathcal{F}}(\phi) = \partial_\phi^2\sigma^2(\phi) - \partial_\phi[\omega + \bar{h}(\phi) + x(t)Z(\phi)]$$

To formalise the argument above we note $x(t)$ is fixed deterministic function and will only

later be interpreted as originating from a stochastic process. This allows us to transform into a stimulus dependent reference frame [135, 162]

$$\psi = \phi - \theta, \qquad \text{where } \dot{\theta} = \omega + Z(\theta)x(t). \tag{6.2}$$

This change of variables [156, Cpt. 3] results in the Fokker-Planck operator for $q(\psi)$

$$\mathcal{F}(\psi) = \partial_\psi^2 \sigma^2(\psi+\theta) - \partial_\psi[\bar{h}(\psi+\theta)]$$

If the intrinsic noise is weak we find ourselves again in the situation where the deviation ψ evolves on a slower time scale than θ and we may average θ over one period. Both σ and $\bar{h}$ are periodic functions such that the average is independent of ψ

$$\Delta = {T_\mathrm{p}}^{-1} \int_0^{T_\mathrm{p}} \mathrm{d}\theta\, \bar{h}(\theta), \qquad\qquad \bar{\sigma}^2 = {T_\mathrm{p}}^{-1} \int_0^{T_\mathrm{p}} \mathrm{d}\theta\, \sigma^2(\theta).$$

The constant Δ changes the frequency to $\bar{\omega} = \omega + \Delta$. Inverting the transformation in Eq. (6.2), one obtains the homogenised FP operator

$$\mathcal{F}(\phi, t) = \tfrac{1}{2}\bar{\sigma}^2 \partial_\phi^2 - \partial_\phi[\bar{\omega} + x(t)Z(\phi)] \tag{6.3}$$

This transformation effectively changed the problem from one of multiplicative noise to additive noise and is known to be a great simplification.

§6.2 Phase resetting and the transfer characteristic

The calculation of response filters for neuronal models is a long standing exercise in theoretical biology, see Ref. [172] for an early reference. An overview of the literature on this topic was given in §2.8.1. We expand the FP operator, flux and the probability density function in orders of the stimulus.

$$\begin{pmatrix} \mathcal{F} \\ p \\ J \end{pmatrix} = \sum_i \begin{pmatrix} \mathcal{F}^{(i)} \\ p^{(i)} \\ J^{(i)} \end{pmatrix}$$

The zero order corresponds to the stimulus switched off. In this case diffusion in the neutral phase direction is uncompensated and leads to a uniform steady state distribution $p^{(0)} = \frac{1}{2\pi}$. The first order FPE in the magnitude of the external stimulus is

$$\frac{\partial p^{(1)}}{\partial t} = \mathcal{F}^{(0)} p^{(1)} + \mathcal{F}^{(1)} p^{(0)} = \Big(\frac{\bar{\sigma}^2}{2}\partial_\phi^2 - \bar{\omega}\partial_\phi\Big)p^{(1)} - \frac{x(t)}{2\pi}\partial_\phi Z(\phi).$$

After Fourier- and Laplace transforming in $\phi \mapsto \chi$ and $t \mapsto s$ respectively the equation reads

$$s\tilde{p}^{(1)}(\chi, s) + \left(\frac{(\chi\bar{\sigma})^2}{2} + \mathrm{i}\bar{\omega}\chi\right)\tilde{p}^{(1)}(\chi, s) + \mathrm{i}\chi\frac{X(s)}{T_\mathrm{p}}\tilde{Z}(\chi) = 0, \tag{6.4}$$

where we assumed the system starts in a uniform phase density at $t = -\infty$. The Fourier transform of the periodic PRC, $Z(\phi) = \bar{\omega}\sum_{k=-\infty}^{\infty} c_k e^{\mathrm{i}k\phi}$, has a discrete spectrum expressed as a weighted Dirac's comb

$$\tilde{Z}(\chi) = \bar{\omega} \sum_{k=-\infty}^{\infty} c_k \delta(\chi - k),$$

the factor $\bar{\omega}$ is included for convenience and could be absorbed into the coefficients of the Fourier series c_k. Inserting this into Eq. (6.4) one can solve for $\tilde{p}^{(1)}(\chi, s)$. Denoting the poles of the expression as $\nu(\chi) = -\frac{1}{2}(\chi\bar{\sigma})^2 - \mathrm{i}\bar{\omega}\chi$ one finds

$$\tilde{p}^{(1)}(\chi, s) = -\frac{1}{2\pi}\frac{\mathrm{i}\chi\tilde{Z}(\chi)}{s-\nu(\chi)}X(s). \tag{6.5}$$

The Fourier and Laplace transformed flux can be rearranged as

$$\begin{aligned}\tilde{J}^{(1)}(\chi, s) &= \left(\bar{\omega} - \mathrm{i}\chi\frac{\sigma^2}{2}\right)\tilde{p}^{(1)} + \frac{1}{2\pi}\tilde{Z}(\chi)X(s) \\ &= \frac{1}{2\pi}\left(1 + \frac{\nu(\chi)}{s-\nu(\chi)}\right)\tilde{Z}(\chi)X(s) = \frac{1}{2\pi}\left(\frac{s\tilde{Z}(\chi)}{s-\nu(\chi)}\right)X(s).\end{aligned}$$

The inverse Fourier operator $\int_{-\infty}^{\infty}\mathrm{d}\chi e^{\mathrm{i}\chi\phi}$ transforms $\chi \mapsto \phi$ followed by evaluation at $\phi = 0$ yields the Laplace transformed instantaneous firing rate, $r \mapsto R$, in accordance with §2.6

$$R(s) = \tilde{J}^{(1)}(\phi, s)|_{\phi=0} = \frac{1}{2\pi}\int_{-\infty}^{\infty}\mathrm{d}\chi\left(\frac{s\tilde{Z}(\chi)}{s-\nu(\chi)}\right)X(s).$$

From the last expression one may identify the system's linear transfer function induced by its PRC as

$$G(s) = \frac{1}{2\pi}\int_{-\infty}^{\infty}\frac{s\tilde{Z}(\chi)}{s-\nu(\chi)}\,\mathrm{d}\chi = \frac{1}{T_\mathrm{p}}\sum_{k=-\infty}^{\infty}\frac{sc_k}{s-\nu(k)}. \tag{6.6}$$

This is also called the complex susceptibility of the system. In this last equation one can observe how the discrete spectrum of the periodic PRC is changed into a continuous spectrum of the linear response filter. The filter's poles are located in the left half plane at $\nu_k = -\frac{1}{2}(k\bar{\sigma})^2 - \mathrm{i}\bar{\omega}k$, implying stability for $0 < \bar{\sigma} \in \mathbb{R}$, this can be spotted in the pole-zero diagram in Fig. 6.1. The location of the poles of $G(u + iv)$ in the complex u-v plane is determined by the parameters $\bar{\omega}$ and $\bar{\sigma}^2$. While the location of the poles along the imaginary axis, does not change with the frequency content of the PRC, their number and the exact behaviour of the meromorphic function G near the poles does. The distance of the poles to the imaginary axis drops quadratically in multiples of the fundamental frequency.

The complex valued susceptibility $G(\mathrm{i}\omega)$ can be split in to the frequency gain $|G(\mathrm{i}2\pi f)|$ and the phase shift $\Psi(f) = \arg G(\mathrm{i}2\pi f)$. Note that the gain is given by the magnitude of the transfer function along the imaginary axis, and characterises the frequency mask the filter applies to its input signals. Examples for the HH and TM model are shown in Fig. 6.2 for frequencies up to 250 Hz, because natural stimuli are typically restricted to the lower Hz rage, see §2.2.2. The peaks of the spectrum are at multiples of the fundamental frequency, $\bar{\omega}$. The number of peaks depends on how many higher order harmonics are present in the PRC. But even for a PRC with high frequency content, as the poles move away from the imaginary line, the peaks in the spectrum get smeared out, which is visible in HH example of Fig. 6.2.

One may proceed by investigating several limiting cases. In the limit of low frequencies near the DC component all but the a_0 term vanish, while the high frequency behaviour is

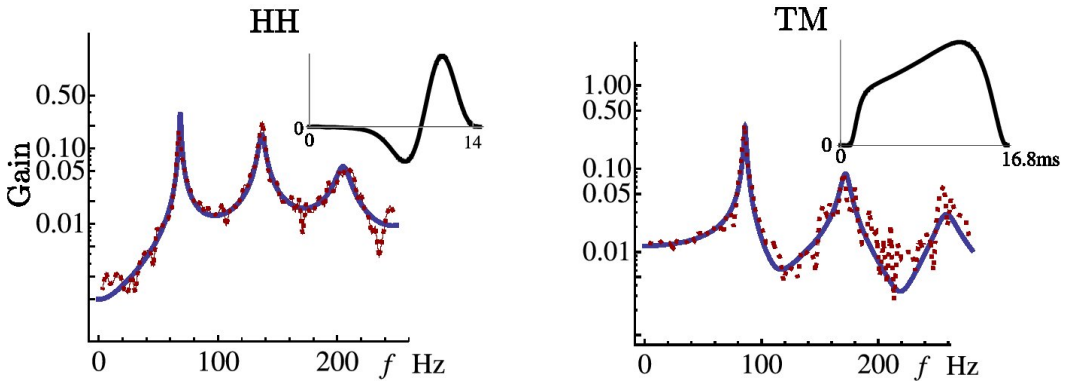

Fig. 6.2: Comparison between the filter properties obtained from LRT and trial averaged simulations of the original conductance based models. Shown are the power spectral densities of the transfer function from current to instantaneous firing rate for the type II Hodgkin-Huxley (HH) and the type I Traub-Miles (TM) models (solid blue line is LRT, dotted line are simulations). The corresponding PRCs from which the filter were obtained are shown as insets. In both cases the perturbing stimulus was band limited white noise with a variance of 0.4 μA/cm^2 and a cutoff of $f_c = 400$ Hz. For both models, the level of intrinsic channel noise, simulated with the approximate method from [50], was adjusted to meet a phase noise level of $\bar{\sigma} = 0.2$. For the other model parameters of HH and TM model see appendix B.

determined the sum of all cosine terms

$$\lim_{\omega\to 0} G(\mathrm{i}\omega) = \frac{\bar{\omega} c_0}{2\pi} = \frac{1}{2\pi}\int_0^{2\pi} \mathrm{d}\phi\, Z(\phi) = \overline{Z(\phi)}. \tag{6.7}$$

The DC component of the susceptibility is the DC or average of the PRC. Recall that the mean of the RPC is also connected to the slope of the FI curve, *cf.* Eq. (2.8). Equation (6.7) immediately implies that the transfer function of the $\sin\phi$-PRC of the Hopf bifurcation will have zero gain at DC component, while the canonical $(1-\cos\phi)$-PRC of the SN on LC bifurcation includes DC component. In a sense, this complements the picture of integrator and resonator properties of neurons that are derived from their sub-threshold dynamics. Filtering properties in subthreshold dynamics are analysed by the linear response of the resting state. It is interesting to note that the filtering property is carried through the bifurcation to the subthreshold regime. It can also be noted that the DC susceptibility is not affected by the intrinsic noise strength $\bar{\sigma}$.

Although the relevant information of sensory stimuly rarely resides at extremely high frequencies this limit can be be studied in models. The high frequency limit is also related to the PRC by

$$\lim_{\omega\to\infty} G(\mathrm{i}\omega) = \frac{\bar{\omega}}{2\pi}\sum_{k=0}^{\infty} a_k = \frac{Z(0)}{2\pi}, \tag{6.8}$$

where a_k is the real part of $c_k = a_k + \mathrm{i}b_k$. Thus, the high frequency susceptibility to signals in Eq. (6.1) is given by the PRC at the spike point, $Z(0)$. In typical neurons the PRC of the voltage dimension is very small at $\phi = 0 = 2\pi$, which is the peak of the action potential. This is because in spiking neurons the voltage dimension in particular has very fast dynamics during the spike, causing the phase at that moment to be less susceptible to any perturbations as can be seen in Fig. 5.1. Consequently, the filter gain of typical spiking neurons, perturbed in the voltage dimension, will drop to zero at very high frequencies. The

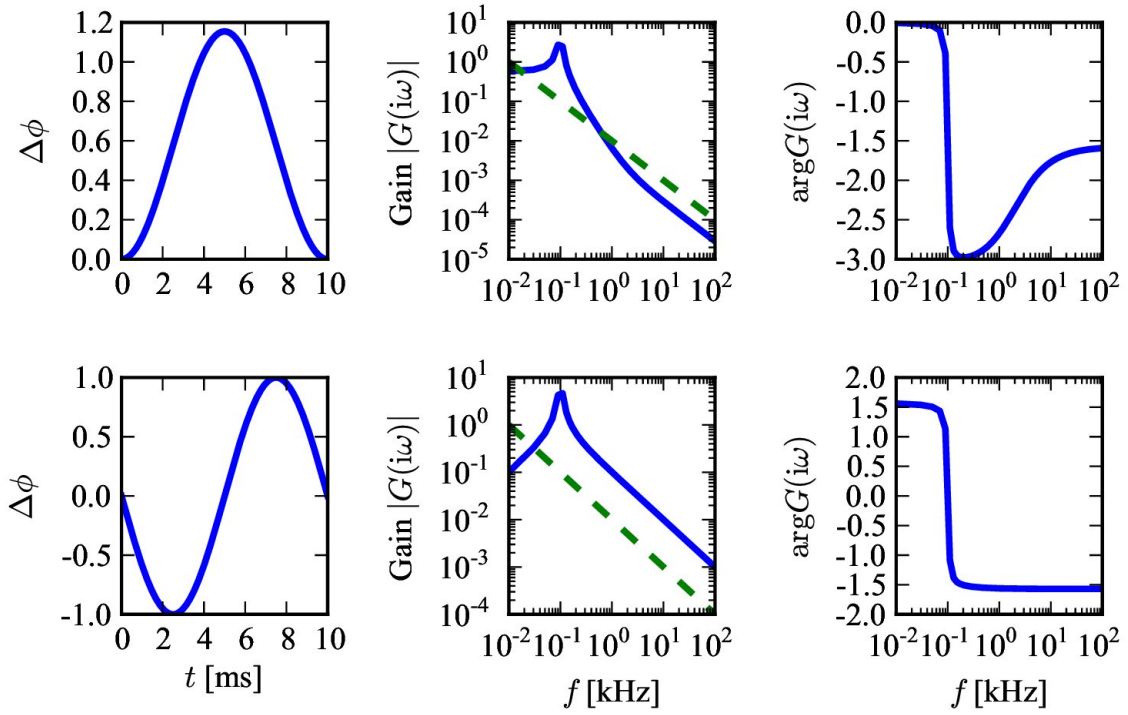

Fig. 6.3: Asymptotic behaviour of the transfer function from Eq. (6.6), for the canonical type I phase oscillator (top row) and canonical type II phase oscillator (bottom row). The green dotted line in the middle column shows a f^{-1} decay for comparison.

intuitive explanation is that if there is a "dead zone" of no phase sensitivity near the spike, then high frequency stimuli, with time scales on the order of the dead zone are not able to uniquely modify the spike time of the system. Of course, high frequency stimuli can affect the spike time during other parts of the ISI. Yet, for zero mean high frequency stimuli this will average out, with only the perturbations near the spike time being effectively translated into the spikes. As a consequence the gain for $f \to \infty$ decays to zero.

The asymptotics of the decay in magnitude gain can be seen in Fig. 6.3, middle column, shows a f^{-1}-behaviour. This is consistent with the numerical findings for conductance based models from which the phase equations are derived. In Ref. [46, Figure 12], the Wang-Buzaki model were simulated and the estimated filters showed the same f^{-1} decay. The asymptotic limit of the phase spectrum is 90° irrespective of the excitation type as seen in the last column of Fig. 6.3. This too concurs with the simulation results from [46, Figure 5B]. The asymptotic behaviour of the type I phase oscillator also agrees with the one of the quadratic integrate-and-fire (IF) model, the canonical model for type I neurons, which was analysed in Ref. [137]. The difference between two excitability classes is that type I systems jump to an even larger phase delay of 180° around the cutoff frequency and then approach the limit from below, while the type II neurons jumped directly to 90°. The Wang-Buzaki model studied in Ref. [46] being a type I neuron shows the undershoot to a more pronounced phase delay as well. The cutoff frequency after which the asymptotic decay starts is determined by the highest significant Fourier coefficient of the model's PRC as can be seen by comparing Fig. 6.2 and Fig. 6.3.

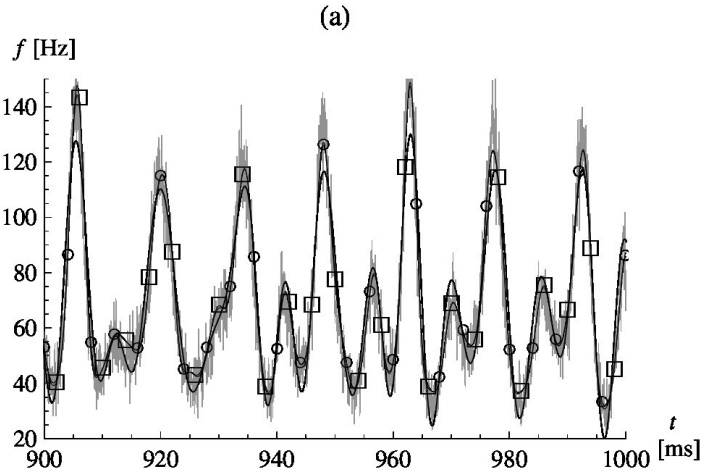

Fig. 6.4: Comparison of trial estimated instantaneous firing rate (grey) and theoretical prediction (black). The trial averaged histogram (grey) was obtained from simulating the stochastic HH equations for 100000 trials with the same parameters as in Fig. 6.2 and a single stimulus path. The theoretical prediction is obtained by convolving the input signal with the linear response filter obtained from the PRC of the model by Eq. (6.9) (black-circled line). Also plotted is the numerical solution of the flux from the simulated phase FPE (black-boxed line).

§6.2.1 Impulse response

The impulse response in the time domain is the inverse Laplace transformation of Eq. (6.6) (defined by the Mellin-Bromwich integral in Eq. (2.22)). It can be evaluated term by term

$$\forall t \geqslant 0: \qquad g(t) = \frac{\bar{\omega}}{2\pi} \sum_k c_k \left(\nu_k \, e^{\nu_k \, t} + \delta(t) \right). \tag{6.9}$$

Convolving this kernel with a realisation of the stimulus gives a prediction of the instantaneous firing rate, which is illustrated in Fig. 6.4 for the HH equations.
Here, we can also investigate the limit $\bar{\sigma} \to 0$, which

$$\lim_{\bar{\sigma}\to 0} g(t) = -\frac{1}{2\pi}[Z'(-t) - Z(0)\delta(t)] \tag{6.10}$$

This system would be critically stable and is equivalent to the result in Ref. [37].

§6.2.2 Spike-triggered average

As introduced in §2.8, a common strategy in experimental sensory physiology is to sample the spike triggered stimulus ensemble and characterise it by its statistical moments. If the stimulation was executed with white noise, the result would be proportional to the filter in Eq. (6.9).
Otherwise, when correlations in the stimulus are present as in the Ornstein-Uhlenbeck SDE approximation to balanced inhibitory and excitatory synaptic input (Stein's model, *cf.* [183]), then according to Eq. (2.32) the STA is the convolution of stimulus covariance function and linear response filter $\mathrm{STA}(t) = (C_x * g)(-t)$. We stick with the example of a bandlimited signal with sharp cut-off frequency ω_c, as they provide unbiased estimates of the STA. Then

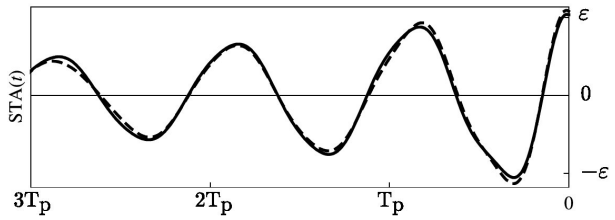

Fig. 6.5: Spike-triggered averages from the PRC of the Stuart-Landau equations as obtained when stimulating with a band-limited stimulus (dashed line). The theoretical results used Eq. (6.11).

the convolution with the filter kernel from Eq. (6.9) can be obtained in terms of elementary functions

$$\mathrm{STA}(t) = \sum_k c_k \left[\mathrm{sinc}(\omega_c t) - \frac{\nu_k}{2\omega_c} \left[\Gamma_0((\nu_k + \mathrm{i}\omega_c)t) - \Gamma_0((\nu_k - \mathrm{i}\omega_c)t) + \mathrm{i}2\pi \right] \right], \tag{6.11}$$

where Γ_0 is the Gamma function. In Fig. 6.5 this is compared with the STA from simulations of the Stuart-Landau model. Also shown is the instantaneous firing rate and its prediction from the LRT kernel.

§6.3 Filter design

Analogue filters are often designed by placing the poles into the Laplace domain and choosing their properties such that the desired spectral mask results and the stability criteria are met. The location of the poles of the neuronal firing rate filter along the imaginary axis is determined by the neuron mean firing rate. On the one hand, the mean rate may be controlled by the neuron through changes in threshold, spike frequency adaptation, or by additional network inputs. On the other hand, it may be set by the mean input signal. The location on the real axis is related to the intrinsic noise level of the neuron. This in turn can be controlled by the neuron through the incorporation of more or less of channels into the membrane patch.

Asides the position of a pole, μ_k, the exact shape of the spectral peak is related to the characteristics of the meromorphic function $G(s)$ around the pole, which is determined by the particular Fourier coefficients of the PRC, c_k. The PRC, again, depends in subtle ways on biophysical parameter of the neuron. To make progress in this complicated parameter dependence, it is useful to investigate neurons near their firing onset bifurcations, where dynamical properties pigeon-hole into canonical forms (the dynamics in the centre manifold see [75]). Near the onset, the PRCs from neurons with the same dynamical type share features and so do their input to rate filter. The canonical PRCs as derived in Ref. [18] were reviewed in §2.5.2. Here, in Fig. 6.6 we can see the gain of the associated transfer functions. Particularly in primary sensory neurons which receive input of distinctly relevant frequency content the type of dynamical system best suited for its transmission may be chosen from the list of canonical models. The two integrate-and-fire models were added because they are discussed in Ref. [18]. Note, however, that these are not real limit-cycle oscillator in the sense we defined in Cpt. 4. A phase equation, even in the small perturbation limit and with the same PRC as an IF model, is not equivalent to it, due to differences in boundary conditions. In particular, with a constant PRC only the DC component, which does not

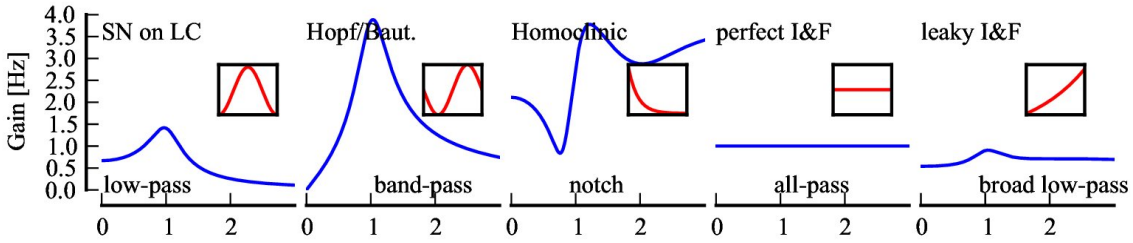

Fig. 6.6: Filters mapping time dependent input currents to instantaneous firing rate for various canonical neuron models. They can be categorised into different classes of filters. The category names where chosen to highlight their dominant feature. The filter power of the high-pass filter of the Hopf bifurcation does actually drop to zero for high frequencies, but the filter is suited to transmit information above the mean firing rate of the neuron.

depend on noise variance, remains in Eq. (6.6). Therefore the spectrum does not decay even for $f \to \infty$ and is the same in the noiseless perfect IF model [172]. The leaky IF model analysed in Ref. [118] does not share the f^{-1} gain asymptotics of conductance based models but decays with $f^{-1/2}$.

§6.4 Stimulus perturbation of the second-order phase model

For simplicity we just consider a two dimensional phase-amplitude model, the generalisation to higher dimensions is possible

$$\dot{\phi} = \omega + h(\phi)\alpha^2 + Z_0(\phi)(x_t + \xi_t) \tag{6.12a}$$
$$\dot{\alpha} = \lambda\alpha + Z_1(\phi)(x_t + \xi_t) \tag{6.12b}$$

Formally, we can split the radial dynamics into deviations due to stimulus and noise related perturbations

$$\alpha(t) = \beta(t) + \eta(t) = \int_{-\infty}^{t} \mathrm{d}\tau Z_1(\phi_\tau)x(\tau)e^{\lambda(t-\tau)} + \int_{-\infty}^{t} \mathrm{d}\tau Z_1(\phi_\tau)\xi(\tau)e^{\lambda(t-\tau)},$$

where λ is the Floquet exponent. The corresponding Fokker-Planck operator may be split into

$$\mathcal{F}^{(\phi)} = \partial_\phi^2\|Z_0\|^2 - \partial_\phi[\omega + h(\phi)(\beta+\eta)^2 + Z_0(\phi)x(t) + \langle Z_0, Z_0'\rangle]$$
$$\mathcal{F}^{(\eta)} = \partial_\eta^2\|Z_1\| - \partial_\eta[\lambda\eta + \langle Z_0, Z_1'\rangle]$$

According to §5.4 and the citations therein, mean and variance of the stationary solution of $\mathcal{F}^{(\eta)}p(\eta|\phi) = 0$ at a fixed ϕ are

$$\mu = \frac{\langle Z_0, Z_1'\rangle}{2\lambda}, \qquad c_{11} = \frac{\|Z_1\|^2}{4\lambda}.$$

which is used to average the operator $\mathcal{F}^{(\phi)}$ to obtain an operator only for the phase. The part of the drift that is affected by the averaging procedure is

$$\int \mathrm{d}\eta\, p(\eta|\phi)(\beta+\eta)^2 = \beta^2 + \beta\,\lambda^{-1}\langle Z_0, Z_1'\rangle + \frac{\|Z_1\|^2}{4\lambda} + \frac{|\langle Z_0, Z_1'\rangle|^2}{4\lambda^2} \tag{6.13}$$

An additional averaging step absorbs all terms that do not depend on the stimulus into a shifted mean firing rate $\bar{\omega}$ and noise variance $\bar{\sigma}^2$. The result is the following phase only FPE, that still depends on the integrated stimulus past

$$\begin{aligned}\bar{\mathcal{F}}^{(\phi)} = \bar{\sigma}^2/2\partial_\phi^2\|Z_0\|^2 - \partial_\phi[\bar{\omega}+ \\ h(\phi)\left(\beta^2 + \beta\,\lambda^{-1}\langle Z_0, Z_1'\rangle + \frac{\|Z_1\|^2}{4\lambda}\right) + Z_0(\phi)x(t) + \langle Z_0, Z_0'\rangle],\end{aligned} \tag{6.14}$$

where we have already omitted the term $\frac{|\langle Z_0, Z_1'\rangle|^2}{4\lambda^2}$ which is of fourth order in the stimulus strength.

§6.5 Volterra expansion

The purpose of the following calculation is to obtain an expansion of the firing rate $r(t) = J(0,t)$ in orders of the signal strength. The firing rate at any time has a functional relation to the stimulus time series, $r_t[x]$, which can expanded as Volterra integral series

$$r(t) = r_0 + \int_{-\infty}^{\infty} g_1(\tau)x(t-\tau)\,\mathrm{d}\tau \; + \iint_{-\infty}^{\infty} g_2(\tau_1,\tau_2)x(t-\tau_1)x(t-\tau_2)\,\mathrm{d}\tau_1\mathrm{d}\tau_2 + \dots. \tag{6.15}$$

Remember that this is essentially a polynomial expansion in orders of the stimulus. Its usefulness as an approximation depends on the type of nonlinearity involved in the mapping into firing rate and the smallness of the stimulus magnitude[2]. As in many cases this is a saturating nonlinearity, polynomial approximations covering the saturation require many terms to provide accuracy. Nonetheless, each additional term can provide new insight into the nonlinear problem [148].

To apply a principled perturbation analysis we rewrite the FPE in Eq. (6.14) in operator form and isolate the terms of a certain order in the stimulus

$$\partial_t\rho(\phi,t) = \left(\bar{\mathcal{F}}^{(0)} + \sum_{j=1}^{\infty}\mathcal{F}^{(j)}\right)\rho(\phi,t). \tag{6.16}$$

The expanded operator $\mathcal{F}$ is also called the forward operator [143], and is the adjoint of the

[2]Note that if the stimulus ensemble is a Gaussian process, then even for a low variance there is no guaranty that $x(t)$ is small at all time instances.

generator associated with the stationary stochastic process. The first three terms are

$$\bar{\mathcal{F}}^{(0)}(\phi) = -\bar{\omega}\frac{\partial}{\partial\phi} + \frac{\bar{\sigma}^2}{2}\frac{\partial^2}{\partial\phi^2}, \tag{6.17a}$$

$$\bar{\mathcal{F}}^{(1)}(\phi,t) = -x(t)\frac{\partial}{\partial\phi}Z(\phi), \tag{6.17b}$$

$$\bar{\mathcal{F}}^{(2)}(\phi,t) = -\frac{\partial}{\partial\phi}h(\phi)\beta^2(t). \tag{6.17c}$$

The higher order operators $\mathcal{F}^{(n)}$ describe perturbations to the homogeneous equation caused by the time dependent stimulus, $\mathcal{F}^{(n)}(\phi,t)$.
The time dependent solution of the FPE may be expanded accordingly in orders of the stimulus strength

$$\rho(\phi,t) = \rho^{(0)}(\phi) + \sum_{j=1}^{\infty}\rho^{(j)}(\phi,t) \tag{6.18}$$

The normalisation condition for probability densities, requires that $\forall t : \int \mathrm{d}\phi\rho_j(\phi,t) = \delta_{j0}$. With the expansion we can write a set of equations as the solution to Eq. (6.16), one for each stimulus order

$$\mathcal{O}(n): \quad (\partial_t - \bar{\mathcal{F}}^{(0)})\rho_n = \sum_{j=1}\mathcal{F}^{(j)}\rho_{n-j} \tag{6.19}$$

These can be iteratively solved for the phase density at any order starting with the stationary solution to the homogeneous equation without stimulus, $\rho^{(0)} = \frac{1}{2\pi}$. Assuming that $\rho^{(n)}(\phi,-\infty) = 0, \forall n \geqslant 1$ the formal solution to this equation is (we basically switched on the stimulus at some point in the distant past $t = -\infty$)

$$\rho^{(n)}(\phi,t) = \sum_{j=1}^{n}\int_{-\infty}^{t} e^{(t-t_1)\bar{\mathcal{F}}^{(0)}}\mathcal{F}^{(j)}(\phi,r)\rho^{(n-j)}(\phi,r)\,\mathrm{d}t_1. \tag{6.20}$$

The operator exponential can be evaluated if we choose to represent the $\mathcal{F}^{(j)}\rho^{(n-j)}$ in terms of the eigenfunctions of the homogeneous operator $\bar{\mathcal{F}}^{(0)}$. With periodic boundary conditions the spectrum, μ_k, of the non-Hermitian operator $\bar{\mathcal{F}}^{(0)}$ is complex and discrete and has the Fourier basis as eigenfunctions

$$q_k(\phi) = e^{\mathrm{i}k\phi}, \text{ with } \mu_k = -\tfrac{1}{2}(k\bar{\sigma})^2 - \mathrm{i}k\bar{\omega}. \tag{6.21}$$

Thus, the operator exponential can be evaluated as $e^{(t-t')\bar{L}^{(0)}} = \sum_k e^{\mathrm{i}k\phi}e^{\mu_k(t-t')}e^{-\mathrm{i}k\phi}$. The expansion of the probability density consequently leads to an expansion of the flux

$$J^{(n)}(\phi,t) = -\sum_{j=0}^{n}\int_0^{\phi}\mathrm{d}\psi\ \mathcal{F}^{(j)}(\psi,t)\rho^{(n-j)}(\psi,t) \tag{6.22}$$

In order to compute the first and second Volterra kernel we need to compute $J^{(n)}$ and thus $\rho^{(n)}$ up to $n = 2$ by solving first Eq. (6.20) and then (6.22).

§6.5.1 First order Volterra kernel

The solution for the first order density ($n = 1$ in Eq. (6.20)) requires the expression of $L^{(1)}\rho_0 = -x(t)Z'(\phi)/2\pi$ in terms of its eigenfunctions $q_k(\phi)$. Hence, we denote with c_k the

coefficients of $Z(\phi)$ expressed in the eigenbasis of $\bar{L}^{(0)}$

$$Z(\phi) = \sum_k c_k q_k(\phi). \tag{6.23}$$

Then, the solution for the first order density reads

$$\rho^{(1)}(\phi, t) = -\frac{\mathrm{i}}{2\pi} \sum_k k c_k \, e^{\mathrm{i}k\phi} \int_{-\infty}^{t} e^{\mu_k (t-t')} x(t') \, dt'. \tag{6.24}$$

The equation for the flux, Eq. (6.22), has two contributing terms

$$J^{(1)} = (\bar{\omega} + \bar{\sigma}^2/2\partial_\phi)\rho^{(1)} + x(t) Z(\phi) \rho^{(0)}.$$

In Fourier representation one has $(\omega - \sigma^2/2\partial_\phi) \to (\omega - \mathrm{i}k\sigma^2/2)$. This gives us the flux as

$$J^{(1)} = \frac{1}{2\pi} \sum_k c_k \, e^{\mathrm{i}k\phi} \int_{-\infty}^{t} \Big(\mu_k \, e^{\mu_k (t-t')} + \delta(t-t') \Big) \, x(t') \, dt',$$

where the definition of the eigenvalues, μ_k, from Eq. (6.21) was applied. We recall that the flux at the periodic boundary measures the instantaneous firing rate

$$r_1(t) = J^{(1)}(\phi, t)|_{\phi=0} = \int \mathrm{d}\tau \; g_1(t-\tau) x(\tau).$$

Here from, we can immediately identify the first order causal Volterra kernel

$$g_1(t) = \frac{1}{2\pi} \sum_k c_k \Big(\mu_k \, e^{\mu_k \, t} + \delta(t) \Big) \, \Theta(t). \tag{6.25}$$

Heaviside's step function is denoted as $\Theta(t)$. This is in agreement with the already derived result in Eq. (6.9) obtained via Laplace transformation. But now we can belabour the next term in the hierarchy.

§6.5.2 Second order Volterra kernel

What is now calculated is the quadratic term of a nonlinear response theory, describing how second order interactions in the stimulus influence the system's output. We will split $J^{(2)}$ into terms that only involve first order phase dynamics related to the PRC and those terms that originate from the second order phase dynamics and involving radial dynamics, *i.e.*, $J^{(2)} = J_\mathrm{p}^{(2)} + J_\mathrm{a}^{(2)}$. In the limit of strong attraction to the limit cycle the latter are less important. To sort these terms one also needs to split the second order contribution to the phase density, $\rho^{(2)} = \rho_\mathrm{p}^{(2)} + \rho_\mathrm{a}^{(2)}$.

Starting with the part without radial dynamics

$$J_\mathrm{p}^{(2)} = \int^{\phi} \mathrm{d}\psi \left[\mathcal{F}^{(1)}(\psi, t) \rho^{(1)}(\psi, t) + \mathcal{F}^{(0)}(\psi) \rho_\mathrm{p}^{(2)} \right], \tag{6.26}$$

one calculates the part of the phase density as

$$\begin{aligned}\rho_{\mathrm{p}}^{(2)} &= \int_{-\infty}^{t} e^{(t-t_1)\bar{\mathcal{F}}^{(0)}}\mathcal{F}^{(1)}(\phi,t_1)\rho^{(1)}(\phi,t_1)\,\mathrm{d}t_1 \\ &= -\sum_{k=-m}^{m}\sum_{\ell=k-m}^{k+m}\frac{k\ell c_{\ell-k}c_k}{2\pi}e^{\mathrm{i}\ell\phi}\int^{t}\mathrm{d}\tau_2\int^{\tau_2}\mathrm{d}\tau_1 x(\tau_2)x(\tau_1)e^{\mu_\ell(t-\tau_2)+\mu_k(\tau_2-\tau_1)}.\end{aligned}$$

To obtain the expression one writes

$$\begin{aligned}\partial_\phi\sum_{j=-m}^{m}c_j e^{\mathrm{i}j\phi}\sum_{k=-m}^{m}\mathrm{i}kc_k e^{\mathrm{i}k\phi} &= -\sum_{j=-m}^{m}\sum_{k=-m}^{m}c_j c_k(jk+k^2)e^{\mathrm{i}(k+j)\phi} \\ &= -\sum_{k=-m}^{m}\sum_{\ell=k-m}^{k+m}c_{\ell-k}c_k c_k k\ell e^{\mathrm{i}\ell\phi}.\end{aligned}$$

Hence, the second term in Eq. (6.26) is

$$-\sum_{k=-m}^{m}\sum_{\ell=k-m}^{k+m}\frac{\mathrm{i}k\mu_\ell c_{\ell-k}c_k}{2\pi}e^{\mathrm{i}\ell\phi}\int^{t}\mathrm{d}\tau_2\int^{\tau_2}\mathrm{d}\tau_1 x(\tau_2)x(\tau_1)e^{\mu_\ell(t-\tau_2)+\mu_k(\tau_2-\tau_1)},$$

while the first is

$$-\sum_{k=-m}^{m}\sum_{\ell=k-m}^{k+m}\frac{\mathrm{i}k\mu_\ell c_{\ell-k}c_k}{2\pi}e^{\mathrm{i}\ell\phi}x(t)\int^{t}\mathrm{d}\tau_1 x(\tau_1)e^{\mu_\ell(t-\tau_1)}.$$

Combining these together one finds the expression for the flux contribution

$$J_{\mathrm{p}}^{(2)} = -\sum_{k=-m}^{m}\sum_{\ell=k-m}^{k+m}\frac{\mathrm{i}kc_{\ell-k}c_k}{2\pi}e^{\mathrm{i}\ell\phi}\int_{-\infty}^{t}\mathrm{d}t_1\left(\mu_\ell e^{\mu_\ell(t-t_1)}+\delta(t-t_1)\right)\int_{-\infty}^{t'}\mathrm{d}t_1 e^{\mu_k(t_1-t_2)}x(t_2).$$

Not otherwise than with the first order filter, the flux at $\phi=0$ yields the instantaneous firing rate and one can identify the part of the second order kernel that neglects radial dynamics

$$g_{\mathrm{p}}^{(2)}(t_1,t_2) = \frac{\Theta(t_1)\Theta(t_2-t_1)}{\mathrm{i}2\pi}\sum_{k=-m}^{m}\sum_{\ell=k-m}^{k+m}kc_{\ell-k}c_k\left(\mu_\ell e^{\mu_\ell t_1}+\delta(t_1)\right)e^{\mu(t_2-t_1)}. \tag{6.27}$$

The first two Volterra kernel can be inserted into to Eqs. (2.32) and (2.35b) yielding the STA and ΔC. The spike triggered covariance ΔC has one term that is proportional to

$$\Delta C_{\mathrm{p}}(t_1,t_2) = \iint \mathrm{d}\tau_1\mathrm{d}\tau_2\; C(t_1,\tau_1)[g_{\mathrm{p}}^{(2)}(\tau_1,\tau_2)+g_{\mathrm{p}}^{(2)}(\tau_2,\tau_1)]C(\tau_2,\tau_1). \tag{6.28}$$

This is a sufficient description if the attraction to the limit cycle is strong enough to justify a first order phase model.

For comparison we choose again the Stuart-Landau equations,see App. A.3, because we can control the Floquet exponent directly. By comparing this to the STC estimated from simulations one may observe that the main features are captured, *cf.* Fig. 6.7. Yet if the attraction to the limit cycle is weaker, *e.g.* $\lambda=-1$ in Fig. 6.7, some structure seen in the difference is unaccounted for, particularly close to the spike, $\Delta C(0,0)$. In Fig. 6.8 the difference between the Estimated ΔC and the prediction obtained from the first oder phase equation, Eq. (6.28), is shown. One can see that for a model with the strong attraction to the limit cycle (a stiff LC), the error is small as compared to the overall order in Fig. 6.7. If

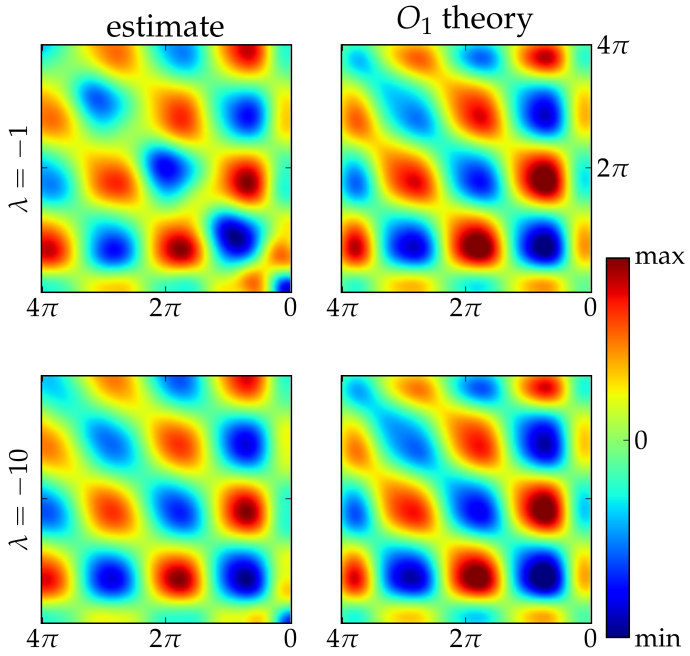

Fig. 6.7: Comparison of the STC, estimated from simulations of the Stuart-Landau model with the predictions not involving radial contributions. Left column shows the estimates from simulations. The right column shows predictions from Eq. (6.28). In the bottom row the system has a strong attraction to the limit cycle ($\lambda = -10$). In such a case, the first order phase equation is a valid approximation. The top row shows a system with a slower return time to the limit cycle ($\lambda = -1$). The spike occurs at $\Delta C(0,0)$ (lower right corner). Here the deviation between theory and simulation are most evident.

the attraction to the limit cycle is weaker (Fig. 6.8, top row), the error gets more significant and has more structure. It contains a twice as high frequency than the main structure of the ΔC in Fig. 6.7. One can account for that higher frequency structure by including the radial terms from $\bar{\mathcal{F}}^{(2)}$ in Eq. (6.17c). The calculations are separated into App. A.4, for they are more bulky.

§6.6 Relation to subthreshold dynamics

Both from the dynamical system perspective and physiologically, one distinguishes between neurons in two dynamical regimes, (*i*) in the subthreshold or excitable regime APs are brought about by special temporal waveforms in the stimulus, while the neuron is otherwise close to its resting state, or (*ii*) in the suprathreshold regime the cell is tonically firing, *e.g.*, due to mean activation and the stimulus waveforms only delay and advance spiking. In both cases STAs are used to analyse encoding. In the first case the overall spike statistics tends to be closer to an inhomogeneous Poisson process, while in the second the neuron is closer to periodic spiking. It is interesting to note that while this chapter treated case (*ii*), also for case (*i*) the STA has been calculated from a linearisation around the fixed point in Ref. [120].

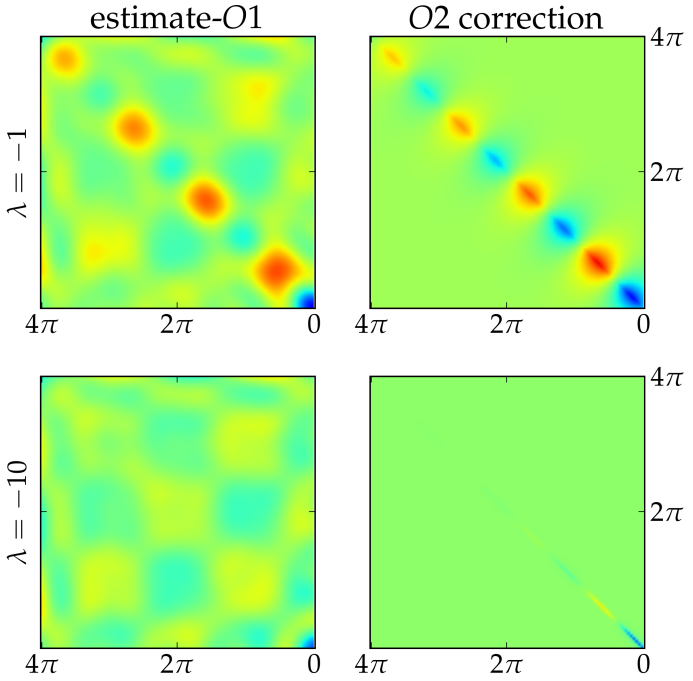

Fig. 6.8: The difference in the STC between first-order theory (Eq. (6.28)) and numerical simulations of the Stuart-Landau model, compared to a second-order correction. Note that the radial dynamics introduce a second harmonic in the STC. The left column subtracts the numerical estimate from the covariance predicted from the first order phase equation Eq. (6.28). The colour scale is the same as indicated in the colour bar in Fig. 6.7.

§6.7 Summary

In this section we discussed the linear and nonlinear response of a system that transforms a stimulus into the instantaneous firing rate. It was shown that applying linear response theory to the first order phase reduced system yields a filter that adequately describes the response of nonlinear conductance based neuron, see Fig. 6.2. With the help of this filter one can predict the instantaneous firing rate of the system. It was highlighted that neurons with different bifurcation types yield filter with distinct properties. Within the frame work of perturbation theory one can also compute that first nonlinear response kernel of the phase oscillator. It was shown that in the case where radial attraction to the limit cycle is not sufficiently strong the radial terms in the phase reduction have to be considered.

7 Information transmission

Information theory has long been used to quantify the performance of sensory processing [8]. This led Joseph Atick, Horace Barlow and others to postulate to use this theory to study how nervous systems adapt to the environment. The goal is to make quantitative predictions about what the connectivity in the nervous system and the structure of receptive fields should look like, for instance. In this sense, information theory becomes the basis for an ecological theory of adaptation to environmental statistics [8, 10].
We seek to do the same here for phase dynamics and ask what PRC would maximise the information. But first, one needs to develop how the PRC predicts a lower bound on the mutual information rate. We begin with a short review of the basic tenets of information theory. Within information theory, a neural pathway is treated as a noisy communication channel in which inputs are transformed to neuronal responses and sent on:

$$\text{input signal } x(t) \rightarrow \boxed{\text{neural pathway}} \rightarrow \text{response } y(t)$$

The mutual information rate measures the amount of information a neural pathway transmits about an input signal $x(t)$ is the mutual information rate,

$$\mathcal{M}[x,y] = \mathcal{H}[y] - \underbrace{\mathcal{H}[y|x]}_{\text{encoding}} = \mathcal{H}[x] - \underbrace{\mathcal{H}[x|y]}_{\text{decoding}}, \tag{7.1}$$

between the stochastic process, $x(t)$, and the stochastic response process, $y(t)$. The entropy rate $\mathcal{H}$ measures the number of discriminable input or output states, either by themselves, or conditioned on other variables. The mutual information rates, which is the difference between unconditional and conditional entropy rates, characterises the number of input states that can be distinguished upon observing the output. The response entropy rates $\mathcal{H}[y]$, for instance, quantifies the number of typical responses per unit time, while $\mathcal{H}[x|y]$ is a measure of the decoding noise in the model. If this noise is zero, then the mutual information rate is simply $\mathcal{H}[x]$, provided that this is finite.
The conditional entropy rates $\mathcal{H}[y|x]$ and $\mathcal{H}[x|y]$, characterising the noise in the encoding and decoding model respectively, are each greater than zero. In information theory, these quantities are also called equivocation. Hence, both the stimulus and response entropy rates, $\mathcal{H}[x]$ and $\mathcal{H}[y]$, are upper bounds for the transmitted information. The mutual information is a „global" quantity, as it compares two entire statistical distributions — an input ensemble $p(x,t)$ with an output ensemble $p(y,t)$. In contrast, Fisher's information, $J(\theta)$, specifies a particular parameter, θ, and is „local" in the sense that it reveals how discriminable nearby θ's are. Information theory is a general tool and can be applied whenever there is a statistical model of the communication channel.
The nature of the ensembles $p(x,t)$ and $p(y,t)$ can be quite varied. The input might be discrete quanta with a particular statistics or it might be a continuous variable that changes continuously in time. Likewise, the output may be discrete, *e.g.*, the number of spikes in a fixed time window, or continuous as the instantaneous firing rate or a phase shift relative to

a continuous oscillation [87, 17, 133].

§7.1 Linear stimulus reconstruction and a lower bound on the information

In many cases, the mutual information cannot be calculated directly. At least two strategies to estimate it exist, though: Either, create a statistical ensemble of inputs and outputs by stimulation, followed by (histogram based) estimation techniques for the mutual information; or, find bounds on the information that can be evaluated more easily. In general, the estimation of mutual information from empirical data is difficult, as the sample size should be much larger than the size of the alphabet. Indeed, each element of the alphabet should be sampled multiple times so that the underlying statistical distribution can, in principle, be accurately estimated. But this prerequisite is often violated, so many techniques of estimating the information from data directly rely on extrapolation [175]. The problem becomes particularly hairy when the alphabet is continuous or a temporal processes had to be discretised, resulting in large alphabets.

Another approach, which will allow us to perform a theoretical analysis of phase dynamics, relies on a comparison of the neuronal "channel" to the continuous Gaussian channel [85, Cpt. 13], which has been extensively studied and is analytically solvable [23]. Richard Stein, Andrew French and Arun Holden used this approach to estimate the information transmission of neuronal models [172] and recorded data from the spider's stretch receptor [96]. More recent applications include the electric sense of weakly electric fish [21] and paddle fish [140], as well as the posterior canal afferents in the turtle [158]. Rob de Ruyter van Steveninck and William Bialek proved in Ref. [14] that this method leads to a guaranteed lower bound of the actual information transmitted. These results will be recapitulated in the remainder of this section.

As we often have experimental control of the stimulus ensemble we can choose this to be a Gaussian process with a flat spectrum up to a cutoff. The mutual information between stimulus $x(t)$ and response $y(t)$ can be bound from below as

$$\mathcal{M}[x,y] = \mathcal{H}[x] - \mathcal{H}[x|y] \geqslant \mathcal{H}[x] - \mathcal{H}_{\text{gauss}}[x|y], \tag{7.2}$$

by using the decoding perspective and invoking the property that a Gaussian process has the maximum entropy of all processes with a given variance. Here, $\mathcal{H}_{\text{gauss}}[x|y]$ is the equivocation of a process with the same mean and covariance structure as the original decoding noise, but with Gaussian statistics. In the Gaussian case all higher order moments are completely determined by the first two moments. The conditional entropy of the stimulus given the response is also called reconstruction noise entropy. It reflects the uncertainty remaining about the stimulus when particular responses have been observed.

In general, the entropy rate of an ergodic process can also be defined as the the entropy of the process at a given time conditioned on its past realisations in the limit of large time

$$\lim_{t\to\infty} \mathcal{H}[x_t|x_\tau : \tau < t].$$

If the process is Gaussian, then the conditional distribution is a univariate Gaussian with variance σ^2_∞. Hence, the entropy rate of a wide-sense stationary Gaussian process is $\sigma^2_\infty = e^{2\mathcal{H}_{\text{gauss}}[x]}$, see Ref. [23, Cpt 12.5]. This also holds if the process is conditioned on side

information y. Thus

$$\sigma_\infty^2 = e^{2\mathcal{H}_{\text{gauss}}[x|y]}.$$

The conditional variance σ_∞^2 provides a lower bound on any estimator, $\hat{x}(t)$ that uses information about the infinite past of the process to predict the present value. Only an optimal estimator would achieve σ_∞^2. Therefore

$$\begin{aligned}\langle (x(t) - \hat{x}(t))^2 \rangle_{x|y} &\geqslant \inf_{\hat{x}} \langle (x(t) - \hat{x}(t))^2 \rangle_{x|y} \\ &= \langle (x(t) - \langle x(t) \rangle_{x|y})^2 \rangle_{x|y} = \sigma_\infty^2 = e^{2\mathcal{H}_{\text{gauss}}[x|y]}.\end{aligned}$$

The second line uses the fact that in this case the optimal estimator is given by the conditional mean. We have the following bound on the equivocation

$$\mathcal{H}[x|y] \leqslant \mathcal{H}_{\text{gauss}}[x|y] \leqslant \tfrac{1}{2} \ln \langle (x(t) - \hat{x}(t))^2 \rangle. \tag{7.3}$$

In order to obtain a tight bound the estimator $\hat{x}(t)$ should be as close to optimal as possible. For the case of additional information given by the response of the neural system $y(t)$ to the process $x(t)$, the estimator should make use of it, $\hat{x}_t[y]$. The process $\hat{x}(t)$ is an appropriate repatriation of the response $y(t)$ back to stimulus space. For simplicity one can assume it is carried out by a filtering operation, $\hat{x}(t) = (f * y)(t)$ specified later [56]. The deviation between stimulus and its estimate, $n(t) = x(t) - \hat{x}(t)$, is treated as the noise process. Like the whole system the noise process is stationary, and its power spectral density, $P_{nn}(\omega)$, is well defined. Then, an additional usage of Jensen's inequality yields the same result as in Ref. [54]

$$\mathcal{H}_{\text{gauss}}[x|y] \leqslant \tfrac{1}{2} \ln \langle n^2(t) \rangle = \tfrac{1}{2} \ln \int_{-\infty}^{\infty} \frac{\mathrm{d}\omega}{2\pi} P_{nn}(\omega) \leqslant \tfrac{1}{2} \int_{-\infty}^{\infty} \frac{\mathrm{d}\omega}{2\pi} \ln P_{nn}(\omega). \tag{7.4}$$

Recall that the input ensemble is a Gaussian process, so that according to Kolmogorov's famous result, $\mathcal{H}[x] = \frac{1}{2} \int \frac{\mathrm{d}\omega}{2\pi} \ln P_{xx}(\omega)$. Inserting Eq. (7.4) into Eq. (7.2), one notes that the last expression is the difference between the entropies of two Gaussian processes, which is

$$\mathcal{M}[x, y] \geqslant \frac{1}{2} \int_{-\infty}^{\infty} \frac{\mathrm{d}\omega}{2\pi} \ln \left(\frac{P_{xx}(\omega)}{P_{nn}(\omega)} \right) \tag{7.5}$$

So as to render the inequality in Eq. (7.3) as tight a bound as possible one should use the optimal reconstruction filter from y to $\hat{x}$. In other words, it is necessary to extract as much information about x from the spike train y as possible.

The next step should be to find an expression for the noise spectrum, $P_{nn}(\omega)$, based on the idea of ideal reconstruction of the stimulus. As opposed to the forward filter, the reconstruction filter depends on the stimulus statistics (even without effects such as adaptation). We seek the filter h that minimises the variance of the mean square error

$$\langle n^2(t) \rangle = \langle (x(t) - \hat{x}(t))^2 \rangle, \quad \text{with } \hat{x}(t) = \int \mathrm{d}\tau \, h(\tau) y(t - \tau). \tag{7.6}$$

Taking the variational derivative [101] of the error w.r.t. the filter (coefficients) $h(\tau)$ and equating this to zero one obtains the orthogonality condition for the optimal Wiener filter [79]

$$\langle n(t) y(t - \tau) \rangle = 0, \qquad \forall \tau. \tag{7.7}$$

Inserting the definition of the error, $n(t) = x(t) - \hat{x}(t)$, into Eq. (7.7) yields

$$\langle x(t)y(t-\tau)\rangle - \int \mathrm{d}\tau_1\, h(l)\langle r(t-\tau_1)r(t-\tau)\rangle = R_{xy}(\tau) - (h * R_{yy})(\tau) = 0$$

In order to obtain h we need to deconvolve the equation, which amounts to a division in the Fourier domain

$$P_{xy}(\omega) = H(\omega)P_{yy}(\omega) \Longrightarrow H^{\mathrm{opt}}(\omega) = \frac{P_{xy}(\omega)}{P_{yy}(\omega)}. \tag{7.8}$$

To compute the mutual information rate, we now calculate the full auto-correlation of the noise when the filter is given by Eq. (7.8). For an arbitrary filter $h(t)$, we have

$$R_{nn}(\tau) = \langle n(t)n(t+\tau)\rangle = \langle n(t)x(t+\tau)\rangle - \int \mathrm{d}\tau_1\, h(\tau_1)\langle n(t)y(t+\tau-\tau_1)\rangle.$$

When the orthogonality condition of Eq. (7.7) holds, the right-most term vanishes. Proceeding by expanding the first term algebraically leads to an expression for the noise correlations

$$R_{nn}(\tau) = \langle n(t)x(t+\tau)\rangle = R_{xx}(\tau) - \int \mathrm{d}\tau_1\, h(\tau_1)R_{xy}(\tau-\tau_1).$$

This expression can be Fourier transformed in order to obtain the required noise spectrum

$$P_{nn}(\omega) = P_{xx}(\omega) - H(\omega)P_{xy}(\omega) = P_{xx}(\omega) - \frac{|P_{xy}(\omega)|^2}{P_{yy}(\omega)}, \tag{7.9}$$

where the definition of the optimal filter, Eq. (7.8), was utilised. This result can then be inserted into Eq. (7.5) to obtain the following well known bound on the information rate [15, 117, 85, 172]

$$\mathcal{M}[x,y] \geqslant -\frac{1}{2}\int_{-\omega_c}^{\omega_c} \frac{\mathrm{d}\omega}{2\pi} \ln\left(1 - \frac{|P_{xy}(\omega)|^2}{P_{xx}(\omega)P_{yy}(\omega)}\right). \tag{7.10}$$

This information bound involves only spectra and cross-spectra of the communication channel's input and output processes which are experimentally measurable in macroscopic recordings [96, 21, 140, 158]. The channel, in this case the neuron, can remain a black box. But since we can bridge the divide between microscopic, biophysical models and their filtering properties, we will, in the following section, derive the mutual information rates.
The following expression in Eq. (7.10) is termed the squared signal response coherence

$$\mathrm{coh}^2(\omega) = \frac{|P_{xy}(\omega)|^2}{P_{xx}(\omega)P_{yy}(\omega)}. \tag{7.11}$$

It quantifies the linearity of the relation between x and y in a way that it equals 1 if there is no noise and a linear filter transforms input to output. Both nonlinearities and noise reduce the coherence.
The stimulus spectral density is given by the environment or controlled by the experimental setup, while cross- and output spectra need to be measured or calculated from the model in question. In what follows we characterise cross-spectral and spike train spectral densities by describing the neuron as a phase oscillator, defined by its PRC, *cf.* Cpt. 4. This means we do not treat the channel as a blackbox but assume a particular model.
The cross-spectrum can be obtained by averaging the Fourier transformed quantities over trials (*i.e.*, intrinsic noise $\langle\cdot\rangle_{y|x}$) as well as the input statistics ($\langle\cdot\rangle_x$), *cf.* [117]. It is related to the transfer function of the encoding filter, $G(s)$, which we determined through linear

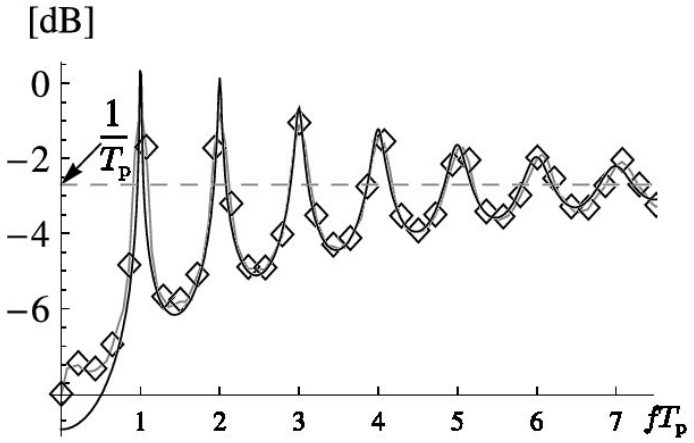

Fig. 7.1: Spike spectrum of the noisy Na^+/K^+ model without external stimulus, compared to the spectrum obtained from the inverse Gaussian first passage time density in Eq. (7.16).

response theory in Eq. (6.6) from §6.2, by

$$P_{yx}(\omega) = \langle\langle \tilde{y}(\omega)\tilde{x}^*(\omega)\rangle_{y|x}\rangle_x = \langle\langle \tilde{y}(\omega)\rangle_{y|x}\tilde{x}^*(\omega)\rangle_x = G(\mathrm{i}\omega)P_{xx}(\omega). \tag{7.12}$$

This shows us that although we are computing the cross-spectrum of stimulus and spike train the response filter $G(\mathrm{i}\omega)$ for the instantaneous firing rate suffices. This simple relation reminds us of the fact that the cross-spectrum is not really a second order quantity, but can be exactly determined by linear response theory. The spike train spectrum $P_{yy}(\omega)$, on the other hand, is truly a second order quantity, *viz.*, the Fourier transform of the auto covariance, and can not be related to the linear response filter without further approximations.

§7.2 Spike train spectra

Spike train spectra are used to characterise neuronal background noise (*cf.* Refs [55, Cpt. 18] and [62, Cpt. 5]). A simple approximation is the use of the spectral addition rule, using the term coined in Ref. [182]

$$P_{yy}(\omega) = P_{y_0y_0}(\omega) + |G(\mathrm{i}\omega)|^2 P_{xx}(\omega). \tag{7.13}$$

The rule is trivially legitimate if the system behaves linearly, $Y(\omega) = G(\omega)(N(\omega)+X(\omega)) = Y_0(\omega)+G(\omega)X(\omega)$, and the noise N is independent of the stimulus. But for nonlinear systems its applicability is less clear. The rule has be established for more complicated systems such, as certain metabolic system in molecular biology [182, 170] and genetic networks [147, 82]. In Ref. [56] it is argued that in neural systems the rule may hold if spike correlations are dominantly induced by correlations in the stimulus, which is perfectly true for the inhomogeneous Poisson spiker.

An important counter example has been put forward by Benjamin Lindner in Ref. [117]. Through the analysis of IF neurons with random threshold, it was shown that the spike spectrum under stimulation is not the result of straightforward addition to $P_{y_0y_0}$. Instead

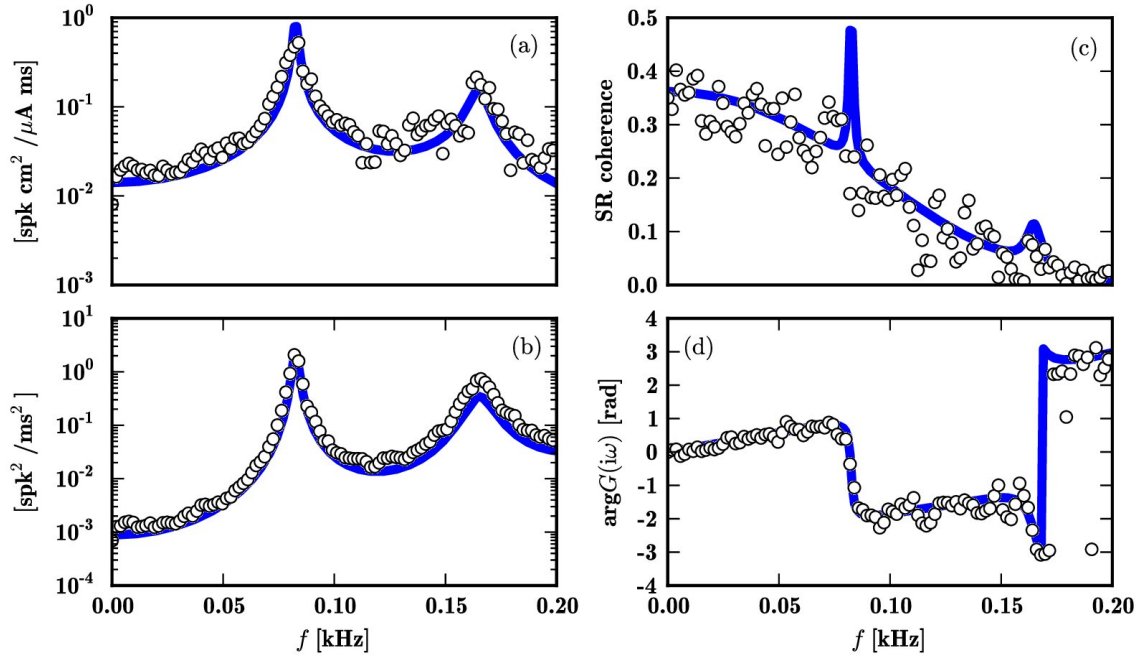

Fig. 7.2: (a) shows the response filter of Na^+/K^+ model estimated from simulations ($\circ$) and obtained from linear response theory (solid line). Both stimulus and noise where additive currents to the voltage dimension with amplitudes 80 nA/cm^2 and 30 nA/cm^2 respectively. (b) shows the spike spectrum in the presence of stimuli. In panel (c) one can see the stimulus response coherence (Eq. (7.11)). The peaks in the theoretical prediction are due to the fact that the spectral addition rule is violated. The information lower bound is 0.795 bits/spike at a rate of 82.5 Hz. The phase spectrum (d) does not influence the coherence based information bound.

a convolution formula was derived to account for the structure of the spectrum obtained in simulations.

For the sake of simplicity we will still follow the spectral addition rule, but note that additional research into the spike spectrum of driven phase oscillators is necessary. The first task is to calculate the noise spectrum of a regularly and tonically firing neuron that is kept at a certain mean firing rate by a constant bias current, but has no additional time varying inputs.

Assuming a renewal neuron, the power spectrum of emitted spike trains can be calculated with the help of Eq. (2.25). The condition is certainly violated if the neuron is driven with a time correlated input process, but without input it might just hold, because of the strong time separation between intrinsic noise and the ISI time scale on which we observe the process (so that δ-correlation in time is the appropriate description, *cf.* [102, Cpt. 7.1]). The basic ingredient is the Laplace transformed ISI density. The phase reduction of limit cyle oscillators allows one to calculate the ISI distribution of the phase equation as an approximation to the biophysical model. Using the averaged phase equation with a constant noise term and switching off the input yields a simple Brownian motion with drift

$$\dot{\phi} = 1 + \bar{\sigma}\,\xi(t)$$

It is well established [183] that in this case the ISI distribution is the inverse Gaussian

$$p(\tau) = \frac{T_\mathrm{p}\, e^{-\frac{(\tau - T_\mathrm{p})^2}{2\bar{\sigma}^2\tau}}}{\bar{\sigma}\sqrt{2\pi\tau^3}}. \tag{7.14}$$

The inverse Gaussian distribution is the inverse Laplace transform of

$$p(s) = \exp\left\{\frac{T_\mathrm{p}}{\bar{\sigma}^2}\left(1 - \sqrt{1 + 2\sigma^2 s}\right)\right\}. \tag{7.15}$$

Eq. (2.25) requires to take $s \to \pm\mathrm{i}\omega$, so that the principal root in the exponent for $\omega > 0$ evaluates to $\sqrt{1 \pm 2\sigma^2\mathrm{i}\omega} = (\frac{1}{2}(\sqrt{1 - 4(\sigma^2\omega)^2} + 1)^{1/2} \pm \mathrm{i}(\frac{1}{2}(\sqrt{1 - 4(\sigma^2\omega)^2} - 1)^{1/2}$. With the notation

$$\alpha(\omega) = \frac{T_\mathrm{p}}{\bar{\sigma}^2}\left(1 - \sqrt{\gamma(\omega) + \tfrac{1}{2}}\right), \qquad \beta(\omega) = -\frac{T_\mathrm{p}}{\bar{\sigma}^2}\sqrt{\gamma(\omega) - \tfrac{1}{2}}, \qquad \gamma(\omega) = \sqrt{(\omega\bar{\sigma}^2)^2 + \tfrac{1}{4}},$$

one may split the exponent in Eq. (7.15) into its real and complex part $p(\pm\mathrm{i}\omega) = \exp(\alpha \pm \beta), \forall\omega > 0$ and identify hyperbolic trigonometric functions

$$P_{y_0y_0}(\omega) = \frac{\sinh(\alpha(\omega))}{\cos(\beta(\omega)) - \cosh(\alpha(\omega))} \tag{7.16}$$

A comparison between the estimated noise spectra and Eq. (7.16) is seen in Fig. 7.1. The pronounced peaks at the mean firing rate and its higher order harmonics are visible. In addition one recognises the saturation of the spectrum to a nonfinite value at high frequencies, that is a feature of the Fourier transformation of Dirac delta spike trains. This noise spectrum does not incorporate phenomena such as missing spikes, where the dynamics of the system leaves the attraction of the limit cycle oscillator.

Finally, inserting both the cross-spectrum, Eq. (7.12), and the spectral addition rule from Eq. (7.13), into the coherence based expression for the mutual information rate, Eq. (7.10), yields

$$\begin{aligned}\mathcal{M} &= -\int_{-w_\mathrm{c}}^{w_\mathrm{c}} \frac{\mathrm{d}\omega}{2\pi} \ln\left(1 - \frac{|G(\mathrm{i}\omega)|^2 P_{xx}^2(\omega)}{P_{xx}(\omega)(P_{y_0y_0}(\omega) + |G(\mathrm{i}\omega)|^2 P_{xx}(\omega))}\right) \\ &= \int_{-w_\mathrm{c}}^{w_\mathrm{c}} \frac{\mathrm{d}\omega}{2\pi} \ln\left(1 + |G(\mathrm{i}\omega)|^2 \frac{P_{xx}(\omega)}{P_{y_0y_0}(\omega)}\right),\end{aligned} \tag{7.17}$$

where $|G(\mathrm{i}\omega)|^2 P_{xx}(\omega)/P_{y_0y_0}(\omega)$ plays the role of a signal to noise ratio. The squared signal response coherence is $|G(\mathrm{i}\omega)|^2 P_{xx}(\omega)/(P_{y_0y_0}(\omega) + |G(\mathrm{i}\omega)|^2 P_{xx}(\omega))$. In Fig. 7.2 the estimated signal response coherence is compared to the theoretical predictions. The simplicity of Eq. (7.17) which is largely due to the spectral addition rule also allows us to define the optimal input spectrum given fixed power constraint by taking the variational derivative of $\mathcal{M} + \lambda \int \frac{\mathrm{d}\omega}{2\pi} P_{xx}(\omega)$ w.r.t. P_{xx}. The optimal stimulus spectrum, yielding the highest information rate, is

$$P_{xx}^\mathrm{opt}(\omega) = 1 + \lambda \frac{P_{y_0y_0}(\omega)}{|G(\mathrm{i}\omega)|^2},$$

where λ is chosen to meet the power constraint.

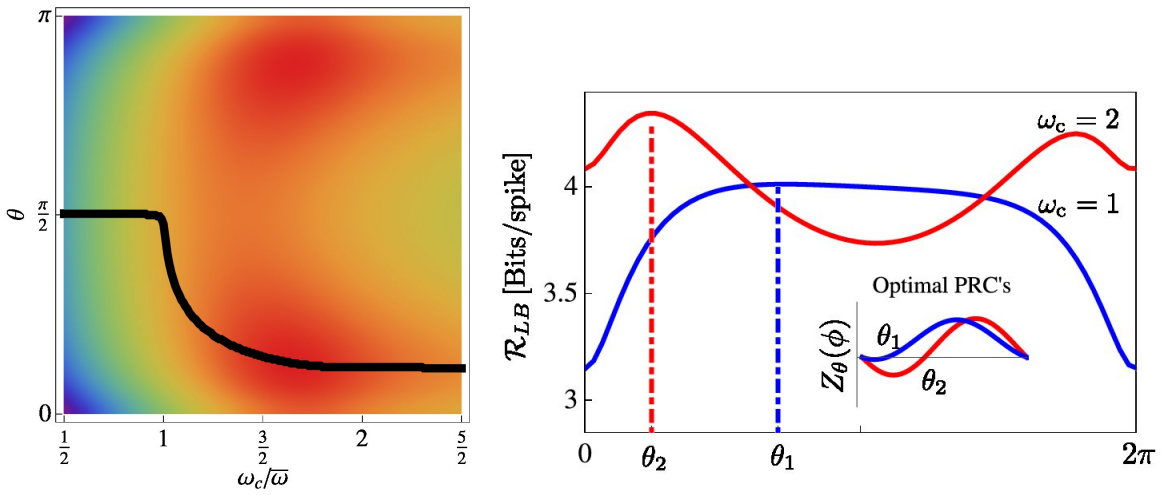

Fig. 7.3: Lower bound to the information transmission rate depending on the systems PRC. Here the information is calculated per spike, *i.e.*, normalised by the firing rate $\mathcal{R}_{\mathrm{LB}} = \mathcal{M}/r_0$. Left: Shows the information rate as a function of the transition parameter of the PRC and the stimulus cutoff frequency. The Black line indicates the highest information rates. When changing ω_c the total variance of the stimulus was keep constant. Right: Cross section of the density plot on the left for at different cutoff frequencies. The PRC's parameter θ interpolates between the canonical PRCs of the Hopf bifurcation, $\theta = 0$ (type II excitability) and the saddle-node node on limit cycle bifurcation (type I excitability), $\theta = \pi$. Other parameters were $\bar{\omega} = 1$, $\bar{\sigma} = 0.04$ and the standard deviation of the stimulus was 0.15.

§7.3 Information optimal PRCs

How information efficient a dynamical system is depends on the stimulus it has to encode. For example one may vary the upper cutoff frequency of the stimulus and this will affect what type of neuron will be better suited encode it. In order to investigate the information optimality we chose a simplified parametric PRC used in Ref. [1]

$$Z_\theta(\phi) = \frac{\bar{\omega}(\sin\theta - \sin(\phi + \theta))}{\sqrt{\pi + 2\pi \sin^2\theta}}. \tag{7.18}$$

By letting θ vary from 0 to π one can transition from the PRC of a Hopf bifurcation (type II) to the PRC of a saddle-node on limit cycle bifurcation (type I), while keeping the PRC norm constant. The resulting information rates as a function of θ and the ratio of cutoff frequency *vs.* intrinsic firing rate are shown in Fig. 7.3. If the cutoff frequencies is below the mean firing rate, the PRC of the saddle-node on LC bifurcation is optimal. For higher cutoff frequencies, the optimum is shifted towards biphasic PRCs characteristic of Hopf bifurcations. These observations parallel the canonical filtering properties observed in Fig. 6.6: near a Hopf bifurcation, frequency components below the mean firing rate are suppressed, while neurons with type I PRCs, and hence significant DC components in the PRC, transmit low frequencies.

§7.4 Summary

In this chapter, we calculate the information carried by the spike train about a time-varying stimulus from the phase response curves. To be more precise, we compute a lower bound on the mutual information rate based on linear reconstruction. For this purpose, we needed to estimate spike train spectra in the presence and absence of a stimulus. We therefore showed in this chapter how to use the renewal theory of point processes to calculate the spike spectrum in the absence of stimulation. In the phase only equation, there will be no serial correlation such that the theory gives accurate results. If amplitude dynamics plays a strong role or long time adaptation currents are present in the neuron, this approximation can fail. For the simple phase oscillator, the spike-spectrum in the absence of stimulation was calculated from the inverse-Gaussian ISI distribution, see Eq. (7.14). This is valid if the original dynamics stays within the attraction of the limit cycle. Some neurons exhibit regimes with bistability, *e.g.*, the Hodgkin-Huxley model near spike onset has an additional unstable limit cycle separating the spiking state from an equilibrium. For particular noise strength such systems show stochastic bursting and have multimodal ISI distributions that are not inverse Gaussian [76].
We show that if the spectral addition rule is valid, the linear reconstruction bound can be calculated from the filter spectrum $|G(\mathrm{i}\omega)|^2$ which depends on the PRC and average phase noise $\bar{\sigma}$, alone. Our approach relies on the linear response filter obtained from the Fokker-Planck equation of the phase in the previous chapter.
Conversely, as the information rate is a functional of the linear response filter and thus the PRC, one can ask what kind of PRCs are information optimal for a particular stimulus. The optimal PRC transitions from type I to type II with increasing ration of stimulus cutoff to intrinsic firing rate.

8 Discussion

The goal of the thesis was to establish analytical relations between the biophysical properties of nerve membranes and the neuronal computations they perform in the presence of noise. To this end, we followed two major lines of investigation. On the one hand, we related microscopic noise caused by the stochastic opening and closing of ion channels to the macroscopic spike jitter that affects neural coding. On the other hand, we derived the suprathreshold filtering properties of neurons based on the phase response curves (PRCs) by perturbing the associated Fokker-Planck equations.

PRCs are based on systematic reductions of the full biophysics, but can also be measured directly in experiments. At special points, known as bifurcations, the shape of the PRC can be predicted analytically. Beyond these points, analytical formulae are not generally available. But, in this thesis, we showed how the framework of numerical continuation can be used to study the relationship between biophysical parameters, such as the number of channels in the membrane, and the phase response curve. Indeed, we can begin to ask what single neuron dynamics would be optimal for neuronal computation.

If the translation of microscopic channel noise to spike jitter is based on the first order phase equation, simple expressions for the phase dependent noise (Eq. (5.3)) can be evaluated, even for high-dimensional models involving multiple channel states described by Markov dynamics. As long as the noise is not too strong, the amount of spike jitter can be accurately captured. Numerical evaluation of the PRC requires only an additional linear system to be solved, *cf.* App. C. This method is suitable to evaluate the magnitude of spike jitter if the noise is not too strong.

Noise can also lead to a change in a neuron's average firing frequency. For this purpose, we showed how to include the radial dynamics along the Floquet modes. To fully identify the second order phase-amplitude model all Floquet modes need to be evaluated. In principal a d-dimensional system would require d^2 additional linear equations. This becomes challenging for high dimensional models. Therefore, the SL model and the low dimensional Na^+/K^+ neuron, were used as examples in Cpt. 5.

Using a secular perturbation approach, Ermentrout *et al.* had related the PRC to the spike-triggered average in systems without intrinsic noise [37]. In §6.2 of this thesis, we extended this result beyond just time-varying stimuli to include intrinsic noise. The usefulness of the approach in §6.2 comes from the fact that it results in a stable filter, which shows the decay in the time domain that is observed in experiments and numerical studies with intrinsic noise (*cf.* the damping of spectral peaks at higher frequencies in Fig. 6.2). The filter can be convolved with the stimulus to obtain firing rate estimates, as in Fig. 6.4.

The relevant measures can all be estimated from experiments. Many methods exist to estimate the PRC [59, 134, 86, 180]. Presenting a constant stimulus would already be sufficient to estimate the overall phase noise from the ISI distribution, *e.g.*, by fitting an inverse Gaussian to the histograms. Hence the first order phase oscillator can be completely identified. Is our theoretical linear response filter in such biological system able to predict the results of a white noise analysis in experiments? This awaits further investigation and

would require to independently estimate the PRC and perform white noise stimulation on a neuron.
The affects of amplitude dynamics on the spike-triggered covariance has been demonstrated in §6.5, but was only numerically evaluated for the Stuart-Landau model. It remains to be clarified if these effects are of real consequence in a more complicated biophysical model. One approach would be to analyse how the eigenfunctions of the STC are changed. To find an analytic expression for the eigenfunctions of our ΔC as a function of the PRC is still an open question.

§8.1 Assumptions

The main assumption used was that of small noise or stimulus, so that perturbation theory could be applied to analyse the nonlinear equations of neuronal dynamics. In fact, in order to establish the link between channel noise and spike jitter or rate filter the small noise assumption was invoked on several levels. Firstly, in order to approximate the Markov channel scheme with the stochastic differential equation in §3.5, the membrane patch was assumed to be sufficiently large to contain many channels and reduce the amplitude of the fluctuations. Secondly, the principled phase reduction in §4.4 requires the perturbation, which we identified with the fluctuation terms in the SDE, to be small. Thirdly, in order to obtain the filtering properties we averaged the intrinsic noise sources. This averaging process again assumed that noise is weak, *cf.* §6.1. Note that all these weakness assumptions are consistent with one another.
By applying the phase reduction one treats neurons as perturbed oscillators. This confines us to the suprathreshold regime of tonically spiking neurons. The statistics of the resulting spike trains can be thought of as the other extreme of the Poisson limit, as one typically has low CVs and the spiking is fairly regular.
In calculating the linear response filter in §6.2 and assuming it is valid for a broad range of stimuli, one assumes that the system does not adapt its intrinsic properties to the stimulus. In reality, the filter itself could be a function of some aspect of the stimulus. This would be comparable to a Kalman filter, where the filter's behaviour adapts to changes in the stimulus statistics.
The gating variables, which describe the fraction of open channels, are restricted to the unit interval $1 \geqslant n(t) \geqslant 0$. As the noise in the biophysical equations is Gaussian we implicitly allowed this restriction to be violated. Again, in our small noise regime this rarely happens. Including the appropriate reflecting boundaries at 0 and 1 would have rendered the analysis difficult.

§8.2 Phase-dependent phase noise

The stochastic opening and closing of voltage-dependent channels in the membrane results in noise that is phase-dependent (§5.1). However, in §6.1 we averaged over the state dependent noise to obtain a constant intrinsic noise strength $\bar{\sigma}$. For the calculation of the kernels, or the STA and STC, one deals with two distinct sources of perturbations, intrinsic and stimulus related. As the goal is to understand the susceptibility to the stimulus, the intrinsic noise was only treated as a simple parameter, *i.e.*, the overall intrinsic noise strength. This was done in order to obtain a simple expression for the response filter, mapping time varying stimuli into instantaneous firing rate. While not necessary for numerical calculations of the ISI variance,

given that AUTO can solve the equations for the moments with phase dependent variance, the averaging step brings with it several advantages.
First, the eigenfunctions of the zeroth order operator $\mathcal{F}^{(0)}$ from the Fokker-Planck system are the trigonometric eigenbase which yields a simple representation of the Volterra kernels. Second, a global noise strength eases the identification of the relevant parameters from experimental data. In many experiments where white noise analysis is applied, a detailed description of the collection of membrane channels is lacking, and thus $\sigma(\phi)$ is not known. Yet, the average noise strength can be estimated from the ISI variance in response to constant stimulation or by using the minimum mean squared to adapt $\bar{\sigma}$ to fit the experimental spike-triggered average.
It would require a more refined experimental setup to estimate the phase dependent function $\sigma(\phi)$. In fact, it is not possible to deduce $\sigma(\phi)$ only from knowledge of the ISI distribution. This is due to a theorem found in Ref. [11, Thm 2.1], stating that the same ISI distribution, *e.g.*, an inverse Gaussian, can be generated from various homogeneous diffusion processes with different state-dependent noise variance, $\sigma^2(\phi)$, *i.e.*, multiplicative noise. Therefore, identifying the phase dependence of the noise strength is not possible only from the spike times; further information is needed.

§8.3 Correlation structure of the noise

In the course of reducing from Markov models of ion channels to stochastic differential equations, one realises that the noise across channels states is correlated. The resulting noise in the gating variable is no longer white, as highlighted in Ref. [115].
In the phase/amplitude coordinates the correlation time scales are given by the Floquet exponents; therefore, by analysing the Floquet spectrum of the complete system, one can assess whether all radial dimensions can be adiabatically eliminated or some radial dimensions have to be retained. In this thesis, we have analysed the first case in detail. A full analysis of the second case awaits further investigation.
Some effects are not captured the stochastic differential equations. For example, it was shown that populations of ion channels in an axon can retain a memory of previous activity [41]. In recent years, researchers have renewed the claim that ion channel opening is cooperative and the functional implications were analysed [189]. In the linear noise approximation ion channels are treated as statistically independent. Further analysis is necessary to link cooperativity at the microscopic level to cooperativity models that operate at a macroscopic level.

§8.4 Future directions

§8.4.1 Population heterogeneity

Throughout this document we have analysed the response properties of single neurons. The instantaneous firing rate in Cpt. 6 was interpreted as a trial averaged quantity. The alternative interpretation is that it is the population activity of an ensemble of identical cells. Then the phase density $p(\phi, t)$ describes the phases of the population of neurons. It is known, however, that neural populations are not homogeneous. For instance, even in small populations of neurons, such as the 80 or so primary auditory receptors of grasshoppers, have varying thresholds. Mitral cells in the olfactory system are rather heterogeneous in their

expression of rebound depolarization (sag) at hyperpolarised potentials. These are mediated by ZD7288-sensitive currents with properties typical of hyperpolarisation-activated cyclic nucleotide gated (HCN) channels [4]. In our simplified phase oscillator model this induces a heterogeneity in the PRCs of the oscillators and will affect the phase distribution of the population. This awaits further studies. An approach to this would be to split the PRC in the population into an average population PRC, $\bar{Z}(\phi)$ and a random perturbation, $\eta(\phi)$, modeling the heterogeneity in the dynamics of the individual neurons, so that $Z(\phi) = \bar{Z}(\phi) + \eta(\phi)$. Here $\eta(\phi)$ is a periodic stochastic process, *i.e.*, with a periodic correlation function.

§8.4.2 Optimal control for channels

Ref. [160] proposes a stochastic control paradigm on the basis of Fokker-Planck operators. Therein, the Fokker-Planck operator, for example of the phase evolution $\mathcal{F}(\phi, t; \alpha_i)$, depends on additional control inputs α_i, which should be chosen to optimise a certain objective. The objective could be formulated as an expectation over the phase distribution $C(\alpha_i, t) = \int_0^{2\pi} \mathrm{d}\phi\, c(\phi) p(\phi, t)$. Objectives could be a measure of the concentration of the distribution of phases quantifying synchronisation, *e.g.*, $c(\phi) = e^{\mathrm{i}\phi}$; or if the adjoint operator $\mathcal{F}^\dagger$ is used, the control the moments of the ISI distribution to achieve an optimal level of spike jitter, $C(\alpha_i) = \int_0^{2\pi} \mathrm{d}\phi\, \delta(\phi) T_n(\phi)$. If the Fokker-Planck operator is a weighted superposition, $\mathcal{F}(\phi, t) = \sum_i \alpha_i \mathcal{F}_i(\phi, t)$ methods of linear control can be applied to dynamically choose the α_i's. From Eq. (5.5) we know that phase variance splits additively in the channels. Therefore, a system parameter yields a linear combination of the individual phase noise contributions if it scales the diffusion matrices $\boldsymbol{D}^{\mathrm{Na}}$ and $\boldsymbol{D}^{\mathrm{K}}$ but does not affect the systems PRCs. Such a parameter would be the unitary conductance, γ_{Na} and γ_{K}, of the channels, given that the maximal conductance, $g_{\mathrm{Na}}^{\max}$, are kept fixed. Then, the sodium channel diffusion matrix scales with $\frac{\gamma_{\mathrm{Na}}}{A g_{\mathrm{Na}}^{\max}}$.
Indeed, on a molecular level unitary conductances are influenced by subunits of the ion channels, *e.g.*, the β4 subunit in calcium channels [161]. On a functional level, unitary conductances change with synaptic activity [122] during learning. Perhaps in the future this frame work can shed light on cellular regulatory control mechanism.

§8.4.3 Inter-spike interval correlations

Many of the spike trains emitted by nerve cells show serial correlations between consecutive inter-spike intervals [45]. It has been shown that serial correlations can play an important role in optimising information transmission in a spike encoder [117]. This behaviour can be studied in models. For example, it is well known that integrate-and-fire models driven with correlated noise exhibit inter-spike interval correlations [130, 116]. A biophysical source of serial correlations are slow, noisy adaptation currents [168]. The interpretation is that the adaptation process filters the noise and induces longer correlations, which then cause the inter spike intervals to be correlated. It is less clear if noise in the fast spike generating process alone can lead to significant serial correlations. One way of addressing this issue is in the framework of phase amplitude models. The amplitude dynamics in Eqs. (4.24b) is like an Ornstein-Uhlenbeck process with a periodically modulated noise amplitude. This process has low-pass characteristics inducing temporal correlations. Yet, due to the typical Floquet spectra of non-adapting neurons these temporal correlations are weak. Note, however that the feedback effect of all the amplitude dimension in Eqs. (4.24a) is additive. One can speculate that the effect of a larger state space (neuron with many different fast channels)

may be such that the sum of all correlation times will cause a significant memory to induce relevant serial correlations. This clearly awaits further study.

§8.4.4 Network dynamics

In this thesis we have used the PRC to deduce single neuron coding properties. Classically, PRC are used to study network phenomena such as synchronisation in the globally coupled Kuramoto model [106, Cpt. 5]. The network interactions are modelled with an coupling function depending only on the phase of the interacting oscillators. The coupling function is given by a convolution of the PRC and a synaptic kernel. Being embedded into an interacting network changes the response properties of the individual neurons. For example, coupling a noisy oscillator to a population of even noisier oscillators regularises its dynamics [121]. Also the linear response filter of the neuron will change through coupling. One approach to calculate this change in response filter is to use formula Eq. (6.6) with the network-PRC derived in Ref. [103]. If in this scenario the resulting linear response filter yields the correct system response still needs to be corroborated.

§8.4.5 Neurons sensitive to multiple features

In §6.5.2 we discussed how the spike-triggered covariance can be obtained from the PRC and possibly additional Floquet modes. An eigenvalue decomposition of the difference of spike-triggered covariance and the *a priori* stimulus covariance function, ΔC, yields additional features to which the neuron is sensitive, *cf.* [6, 169, 148]. We have not yet managed to find a closed expression of these eigenfunction in terms of the PRC and the Floquet exponents. Nonetheless, if the attraction to the limit cycle is not too strong, the higher frequency pattern that emerges on the diagonal of the matrix ΔC (*cf.* Fig. 6.8) will almost surely affect the eigenmodes as can be shown by numerical analysis. We have decided not to present these results here. But as the radial components of the dynamics shape the eigenmodes, these will contribute to the different stimulus features that can cause the neuron to spike. A future study will be devoted to investigating this effects in the STC of a conductance-based model.

A Mathematical appendix

To render the exposure more self-contained, the following paragraphs rederive some known results from the literature, that are used, hinted at or implemented in the main part of the document.

A.1 Novikov-Furutsu-Donsker formula

A relation between Gaussian noise sources and functions of the state variables in stochastic systems is given by the Novikov-Furutsu-Donsker (NFD) formula. It examines the correlation of a stochastic process ξ_t at a fixed instance in time, t, and a function f of $x(t)$, which is an stochastic process that depends on ξ_t [53, 32, 142]. One of the advantages of the NFD formula is that it is applicable to systems with multiplicative noise, as they arise in several applications involving phase response curves. The result is the following

$$\langle f[\xi]\xi(t)\rangle = \tfrac{1}{2}\int_{-\infty}^{\infty}\langle \xi_t\xi_{t_1}\rangle \left\langle \frac{\delta f[\eta+\xi]}{\delta\eta_{t_1}}\Big|_{\eta=0}\right\rangle \mathrm{d}t_1 \tag{A.1}$$

As it is used several times in this document we give a formal and very compact derivation [101]. In many physical examples only the values in the past $t_1 \leqslant t$, influence the functional f and the integration range can be adjusted accordingly.
One may, therefore, treat the function f as a functional of the path $\xi_{t_1} : \forall t_1 \leqslant t$. The first step is to write this functional as a Taylor series around the deterministic function $\eta_t = 0$ (omitting the integral domain take it to be understood from $-\infty$ to t)

$$\begin{aligned} f[\eta+\xi] &= f[\eta]|_{\eta=0} + \sum_{k=1}^{\infty}\frac{1}{k!}\int\cdots\int \mathrm{d}t_1\cdots\mathrm{d}t_k\ \xi_{t_1}\cdots\xi_{t_k}\left(\frac{\delta^k f[\eta]}{\delta\eta_{t_1}\cdots\delta\eta_{t_k}}\right)\Big|_{\eta=0} \\ &= \left(\exp\int \mathrm{d}t'\,\xi_{t'}\frac{\delta}{\delta\eta_{t'}}\right) f[\eta]\big|_{\eta=0}. \end{aligned}$$

The second line is just a formal, compressed way of writing it using the definition of the exponential displacement operator. As $f[\eta]$ is deterministic it can be yanked from any averaging over the noise ensemble, *e.g.*,

$$\langle f[\eta+\xi]\rangle = \left\langle \left(\exp\int \mathrm{d}t'\,\xi_{t'}\frac{\delta}{\delta\eta_{t'}}\right)\right\rangle f[\eta]\big|_{\eta=0}.$$

Hence, we can formally write

$$\langle \xi_t f[\xi]\rangle = \left\langle \xi_t \exp\int \mathrm{d}t'\,\xi_{t'}\frac{\delta}{\delta\eta_{t'}}\right\rangle f[\eta]\big|_{\eta=0} = \frac{\left\langle \xi_t \exp\int \mathrm{d}t'\,\xi_{t'}\frac{\delta}{\delta\eta_{t'}}\right\rangle}{\left\langle \exp\int \mathrm{d}t'\,\xi_{t'}\frac{\delta}{\delta\eta_{t'}}\right\rangle}\langle f[\eta+\xi]\rangle\big|_{\eta=0}. \tag{A.2}$$

Next, one may introduce the infinite dimensional Fourier transform of a stochastic process called the characteristic functional

$$\Phi[\lambda] = \left\langle \exp\left(\mathrm{i}\int \mathrm{d}t'\,\lambda_{t'}\xi_{t'}\right)\right\rangle.$$

For the, by assumption, Gaussian process ξ_t it is known to be the exponential of a quadratic form

$$\Phi[\lambda] = \exp\left(-\frac{1}{2}\int \mathrm{d}t_1\mathrm{d}t_2\ \lambda(t_1)C(t_1,t_2)\lambda(t_2)\right),$$

which must be real, $\Phi[\lambda] \in \mathbb{R}$, because the density is symmetric around $\eta_t = 0$.
With the help of the following ind entity

$$\frac{\langle \xi_t \exp \mathrm{i} \int \mathrm{d}t' \xi_{t'} \lambda_{t'} \rangle}{\langle \exp \mathrm{i} \int \mathrm{d}t' \xi_{t'} \lambda_{t'} \rangle} = \frac{\delta}{\mathrm{i}\delta\lambda} \ln \left\langle \exp \ \mathrm{i} \int \mathrm{d}t' \xi_{t'} \lambda_{t'} \right\rangle = \frac{\delta}{\mathrm{i}\delta\lambda} \ln \Phi[\lambda],$$

and a formal substitution $\delta/\delta\eta_t \to \mathrm{i}\lambda(t)$ we may simplify Eq. (A.2) to

$$\langle \xi_t f[\xi] \rangle = \frac{\delta}{\mathrm{i}\delta\lambda} \ln \Phi[\lambda] \langle f[\eta + \xi] \rangle \big|_{\eta=0} = \frac{\mathrm{i}}{2} \int \mathrm{d}t_1 C(t, t_1) \lambda(t_1) \langle f[\eta + \xi] \rangle \big|_{\eta=0}.$$

Back substituting $\mathrm{i}\lambda(t) \to \delta/\delta\eta_t$ we obtain Eq. (A.1).

A.2 Fokker-Planck equation

There are two common views on Markov processes, one emphasises individual realisations or paths of the process (Langevin equation), the other the evolution of densities, *e.g.*, by a Fokker-Planck equation (FPE). There several ways to arrive at the FPE, but since the NFD formula was already introduced in the preceding paragraph A.1, one can use it to establish an evolution equation for the density starting from the following Langevin equation

$$\dot{x} = F(x, t) = a(x, t) + b(x, t)\xi_t. \tag{A.3}$$

Here $a(x)$ is the deterministic drift part and $b(x)\xi_t$ is the diffusion part. The Gaussian random noise is uncorrelated $C(\tau) = \langle \xi_t \xi_{t+\tau} \rangle = \delta(\tau)$. Nonetheless, for the first steps in the derivation we assume that the noise is „frozen", *i.e.*, a fixed part of the r.h.s. of Eq. (A.3). One can formally introduce the time dependent indicator function or state density of the stochastic process $x(t)$ as

$$\varrho(x, t) = \delta(x(t) - x).$$

The inclined reader needs to be careful here, due to a near clash of symbols: The difference between variational derivative and Dirac's delta is only made by the subtle difference of italic *vs.* upright delta.
By the chain rule one finds

$$\partial_t \varrho(x, t) = (\partial_x \delta(x(t) - x))\, F(x(t)).$$

Solving this equation requires integration and under this operation the indicator function carries the adjoint of its derivative to $F(x, t)$ [102]. We can, therefore, write

$$(\partial_t + \partial_x F)\, \varrho(x, t) = 0, \tag{A.4}$$

which is Liouville's formula for the evolution of the state space density.
This holds for any particular „frozen" path ξ_t involved in F. In the next step we can average over the ensemble of such paths to convert the phase space density to a probability density $p(x, t) = \langle \varrho(x, t) \rangle = \langle \delta(x(t) - x) \rangle$. Averaging Eq. (A.4) the evolution equation becomes

$$\dot{p}(x, t) = \partial_t \langle \varrho(x, t) \rangle = -\partial_x \left(a(x, t) \langle \varrho(x, t) \rangle + b(x, t) \langle \xi_t \varrho(x, t) \rangle \right). \tag{A.5}$$

The last term involves the correlation between noise and the phase space density. This can be evaluated with the help of the NFD formula from Eq. (A.1) and the assumption that ξ is uncorrelated

$$\langle \xi_t \varrho(x, t) \rangle = \tfrac{1}{2} \left\langle \frac{\delta \varrho(x, t)}{\delta \xi_t} \right\rangle = -\tfrac{1}{2} \partial_x \, b(x, t) \langle \varrho(x, t) \rangle$$

where the second inequality follows from Liouville's equation. Inserting this identity back into Eq. (A.5), one obtains a partial differential equation for $p(x, t)$ known as the Fokker-Planck equation

$$\dot{p}(x,t) = \tfrac{1}{2}\partial_x b(x,t)\partial_x b(x,t)p(x,t) - \partial_x a(x,t)p(x,t). \tag{A.6}$$

This derivation leads to the FPE for an SDE in Stratonovich's interpretation, which is the one typically used in this document as it is compatible with the phase reduction mechanism. As the NFD formula has a multidimensional counter part one can also find FPE for multidimensional SDEs.

A.3 Floquet modes of the Stuart-Landau equations

An analytically tractable set of equations showing a limit-cycle oscillator is the Stuart-Landau model [106].
This model introduces a specific parameter η, explicitly controlling the attractiveness of the limit cycle. This parameterisation of the SL model is from (Brown et al., 2004). In this model one may control the Floquet exponent and hence the attractiveness of the limit cycle explicitly. It can be written in complex, Cartesian or polar coordinates

$$\dot{z} = (a + \mathrm{i}\, b)z + (c + \mathrm{i}\, d)|z|^2 z \tag{A.7}$$

$$\dot{x} = \left(ax - by + (cx - dy)\left(x^2 + y^2\right)\right), \tag{A.8}$$

$$\dot{y} = \left(ay + bx + (cy + dx)\left(x^2 + y^2\right)\right), \tag{A.9}$$

$$\text{or} \quad \dot{R} = (a + cR^2)R, \tag{A.10}$$

$$\dot{\theta} = b + dR^2. \tag{A.11}$$

The limit cycle has amplitude $A = \sqrt{-a/c}$, angular frequency $\omega = b + dA^2 = b - ad/c$, and PRCs $Z_x(\phi) = (d\cos\phi + c\sin\phi)/\sqrt{|ac|}$, $Z_y(\phi) = (d\sin\phi - c\cos\phi)/\sqrt{|ac|}$. Denote the r.h.s of the amplitude dynamics as $f(R) = (a + cR^2)R$. Then as we should have $f(A) = 0$, $f'(A) = a - 3a = -2a$, gives the linear amplitude relaxation is

$$R(t) = \sqrt{-a/c} + e^{-2a\,t}.$$

The Floquet exponent is $\lambda = -2a$. It is not affected by a change in frequency - the monodromy matrix and characteristic multipliers however are.
The solution for the dynamics in polar coordinates on the whole plane for initial conditions given by $(R(0), \phi(0)) = (R_0, \phi_0)$ is

$$R(t) = \sqrt{\frac{-a}{c - \left(\frac{a}{R_0^2} + c\right)e^{-2at}}} \tag{A.12}$$

$$\theta(t) = \phi_0 + bt - \frac{d}{2c}\ln\left(1 + \frac{cR_0^2}{a}(1 - e^{2at})\right) \tag{A.13}$$

The phase variable is obtained by letting the angular variable θ evolve for a long time

$$\lim_{t\to\infty}\theta(t) = (b - ad/c)t - \frac{d}{2c}\ln\left(-\frac{cR_0^2}{a}\right).$$

The first term is the monotonically increasing frequency times time term like the relaxed system on the limit cycle would have. The second term compensates for amplitude excursions. In accordance with these two term we can calculate this instantaneous phase on the whole plane as

$$\phi(t) = \arctan 2(y, x) - \frac{d}{2c}\ln\left(-\frac{c(x^2 + y^2)}{a}\right).$$

Note that the second term is equal to zero if the amplitude ratio of instantaneous amplitude to relaxed amplitude is one, or $x^2(t) + y^2(t) = A^2$.

With $c = -1$, $a = 1$, $b = 2$ and $d = -1$ we obtain our previous model.
There are several ways of changing the Floquet exponent. The naive way would be to speed up time $t' \mapsto t/\eta$. In polar coordinates we would have

$$\dot{R} = \eta(a + cR^2)R, \qquad \dot{\theta} = \eta(b + dR^2) \tag{A.14}$$

The radial dynamics linearised around the limit cycle radius 1 is $\approx \sqrt{-a/c} + \delta R\, e^{-2\eta t}$. So the Floquet exponent is -2η. I was previously stating that because the period is also affected by η the Floquet multiplier would not change. That is completely wrong (it is true for the characteristic multiplier of the monodromy matrix I suppose). Obviously this does not change the isochron shape $\theta - b \ln R$ and hence also the PRC will be the same, but scaled. The period on the limit cycle $R = 1$ is scaled $\omega = \eta(b - dc/a)$.
An other possibility to change the Floquet exponents is to change isochron and PRC, e.g., with

$$\dot{x} = \big(\eta x - by - (\eta x + dy)(x^2 + y^2)\big) \tag{A.15}$$
$$\dot{y} = \big(\eta y + bx - (\eta y - dx)(x^2 + y^2)\big) \tag{A.16}$$

With $R = \sqrt{x^2 + y^2}$ and $\theta = \arctan(y/x)$ one easily retrieves the polar coordinate form

$$\dot{R} = \frac{(x\dot{x} + y\dot{y})}{\sqrt{x^2 + y^2}} = \eta\left(\frac{x^2 + y^2 - (x^2 + y^2)^2}{\sqrt{x^2 + y^2}}\right) = \eta(R - R^3) \tag{A.17}$$
$$\dot{\theta} = \frac{x\dot{y} - y\dot{x}}{x^2 + y^2} = \frac{ax^2 + ay^2 - (bx^2 + by^2)(x^2 + y^2)}{x^2 + y^2} = a - bR^2. \tag{A.18}$$

The limit cycle is the unit cycle, the Floquet exponent is again -2η, the period is unharmed $\omega = b - d\eta/\eta = b - d$. The amplitude is still 1. But now the PRCs are changing (not only scaling) as $c = -\eta$.
The third option is to let the Amplitude of the limit cycle change ($A = \sqrt{\eta}$) keeping frequency ω and PRC shape fixed. Their will be a scaling of the PRC though ($\sim 1/\sqrt{\eta}$), which could be compensated by changing σ and ε accordingly. This can be obtained e.g. by $a = \eta$, $b = (\omega + \eta)$, $c = -1$, $d = -1$

$$\dot{x} = \big(\eta x - (\omega + \eta)y - (x - y)\,(x^2 + y^2)\big) \tag{A.19}$$
$$\dot{y} = \big(\eta y + (\omega + \eta)x - (y + x)\,(x^2 + y^2)\big) \tag{A.20}$$

The Floquet exponent is again -2η. The phase is obtained by

$$\phi(t) = \arctan 2\,(y(t), x(t)) - \frac{1}{2}\ln\left(\frac{x^2(t) + y^2(t)}{\eta}\right).$$

This might be the nicest parametrisation for a comparison. However we have to again change $\sigma, \varepsilon \propto \sqrt{\eta}$ in order to obtain the same phase noise!

A.3.1 Isochrons

The isochrons $I(\phi)$ of the SL model are given by the log spiral. The parametric curve for $-\infty < t < \infty$ in $\mathbb{R}^2$ is

$$I(\phi) = -\frac{a}{c} e^{\frac{c}{d}t} \begin{pmatrix} \cos(t + \phi) \\ \sin(t + \phi) \end{pmatrix}. \tag{A.21}$$

A.3.2 Floquet modes

First we repeat the Floquet analysis, which we saw long time back. We shall be switching between complex and real representation of the SL model for brevity. It is also best to stick with the most general parametrisation, as we may want to leave us the possibility to control radius, Floquet multiplier

and frequency.

$$\dot{z} = (a + \mathrm{i}\, b)z + (c + \mathrm{i}\, d)|z|^2 z$$

The limit cycle solution is

$$z_0(t) = x_0(t) + \mathrm{i}\, y_0(t) = A_0\, e^{\mathrm{i}\omega_0\, t}$$

with $\omega_0 = b - ad/c$ and $A_0 = \sqrt{-a/c}$ The Jacobian is

$$J(x,y) = \begin{pmatrix} 2x(cx-dy) + c(x^2+y^2) & 2y(cx-dy) - d(x^2+y^2) \\ b + 2x(dx+cy) + d(x^2+y^2) & a + 2y(dx+cy) + c(x^2+y^2) \end{pmatrix}$$

And on the limit cycle

$$\begin{aligned} J_0 &= \begin{pmatrix} a - 2a\cos^2\omega_0 t + \frac{ad}{c}\cos\omega_0 t \sin\omega_0 t - a & -2a\cos\omega_0 t\sin\omega_0 t + \frac{ad}{c}\sin^2\omega_0 t + \frac{ad}{c} - b \\ b - 2\frac{ad}{c}\cos^2\omega_0 t - a\cos\omega_0 t\sin\omega_0 t - \frac{ad}{c} & -2\frac{ad}{c}\cos\omega_0 t\sin\omega_0 t - a\sin^2\omega_0 t \end{pmatrix} \\ &= \begin{pmatrix} -2a\cos^2\omega_0 t + \frac{ad}{c}\cos\omega_0 t\sin\omega_0 t & -2a\cos\omega_0 t\sin\omega_0 t + \frac{ad}{c}\sin^2\omega_0 t - \omega_0 \\ -2\frac{ad}{c}\cos^2\omega_0 t - a\cos\omega_0 t\sin\omega_0 t + \omega_0 & -2\frac{ad}{c}\cos\omega_0 t\sin\omega_0 t - a\sin^2\omega_0 t \end{pmatrix} \end{aligned}$$

Though slightly more general this SL model is still radially symmetric and the following coordinate change should do the trick.

$$\boldsymbol{S}(t) = \begin{pmatrix} \cos(\omega_0 t) & -\sin(\omega_0 t) \\ \sin(\omega_0 t) & \cos(\omega_0 t) \end{pmatrix}$$

Say

$$\begin{pmatrix} p \\ q \end{pmatrix} = \boldsymbol{S}^{-1} \begin{pmatrix} x \\ y \end{pmatrix}$$

Then

$$\begin{pmatrix} \dot{x} \\ \dot{y} \end{pmatrix} = \dot{\boldsymbol{S}} \begin{pmatrix} p \\ q \end{pmatrix} + \boldsymbol{S} \begin{pmatrix} \dot{p} \\ \dot{q} \end{pmatrix} = \boldsymbol{J}_0 \boldsymbol{S} \begin{pmatrix} p \\ q \end{pmatrix}$$

or

$$\begin{pmatrix} \dot{p} \\ \dot{q} \end{pmatrix} = \boldsymbol{S}^{-1}(\boldsymbol{J}_0 \boldsymbol{S} - \dot{\boldsymbol{S}}) \begin{pmatrix} p \\ q \end{pmatrix}$$

Floquet theory wants

$$\boldsymbol{S}^{-1}(\boldsymbol{J}_0 \boldsymbol{S} - \dot{\boldsymbol{S}}) = \boldsymbol{\Lambda}$$

to be a constant matrix so that the system of (p, q) is easily solved by a matrix exponential.

First of all the time derivative of the transformation matrix is

$$\dot{\boldsymbol{S}} = -\omega_0 \begin{pmatrix} \sin\omega_0 t & \cos\omega_0 t \\ -\cos\omega_0 t & \sin\omega_0 t \end{pmatrix}$$

which is still a rotation matrix shifted by $\pi/4$. Then premultiplying with a rotation in the other direction leaves

$$\boldsymbol{S}^{-1}\dot{\boldsymbol{S}} = \begin{pmatrix} 0 & -\omega_0 \\ \omega_0 & 0 \end{pmatrix}$$

and with some trigonometric identities

$$\boldsymbol{S}^{-1}\boldsymbol{J}_0\boldsymbol{S} = \begin{pmatrix} -2a & -\omega_0 \\ \omega_0 - 2ad/c & 0 \end{pmatrix}$$

From which we get the constant matrix

$$\boldsymbol{\Lambda} = -2 \begin{pmatrix} a & 0 \\ -ad/c & 0 \end{pmatrix}$$

We read the eigenvalues to be $-2a$ and 0. The right eigenvectors $\boldsymbol{\Lambda}\boldsymbol{u}_k = \lambda_k \boldsymbol{u}_k$ are

$$\boldsymbol{u}_0 = \begin{pmatrix} 0 \\ 1 \end{pmatrix}, \qquad \boldsymbol{u}_1 = \begin{pmatrix} \sqrt{\frac{c}{d}} \\ \sqrt{\frac{d}{c}} \end{pmatrix}$$

The left eigenvectors $\boldsymbol{v}_k\boldsymbol{\Lambda} = \lambda_k \boldsymbol{v}_k$ are

$$\boldsymbol{v}_0 = \begin{pmatrix} -\frac{d}{c} \\ 1 \end{pmatrix}, \qquad \boldsymbol{v}_1 = \begin{pmatrix} \sqrt{\frac{d}{c}} \\ 0 \end{pmatrix}$$

All were normalised as $\boldsymbol{v}_j \cdot \boldsymbol{u}_k = \delta jk$.
We may check the PRCs again, which we obtain as

$$\boldsymbol{V}_0(\phi) = \frac{1}{A_0}\boldsymbol{v}_0\boldsymbol{S}^{-1} = \frac{1}{\sqrt{-ac}} \begin{pmatrix} d\cos\phi + c\sin\phi \\ d\sin\phi - c\cos\phi \end{pmatrix}$$

The scaling factor $1/A_0$ was included to fulfil $\boldsymbol{V}_0(0) \cdot \boldsymbol{F}(0) = \omega_0$.
The radial PRCs which we need are

$$\boldsymbol{V}_1(\phi) = \boldsymbol{v}_1\boldsymbol{S}^{-1} = \sqrt{\frac{c}{d}} \begin{pmatrix} \cos\phi \\ \sin\phi \end{pmatrix}$$

and the conjugate

$$\boldsymbol{U}_1(\phi) = \boldsymbol{S}\boldsymbol{u}_1 = \frac{1}{\sqrt{cd}} \begin{pmatrix} c\cos\phi - d\sin\phi \\ c\sin\phi + d\cos\phi \end{pmatrix}$$

A.4 Radial contribution to the second Volterra kernel

For simplicity consider just one radial dimension. Then

$$\begin{aligned} &\int_{}^{t} \mathrm{d}t' e^{t-t')\mathcal{F}^{(0)}} \mathcal{F}^{(2)} \rho^{(0)} \\ &= \frac{1}{2\pi} \iiint \mathrm{d}t' \mathrm{d}r \mathrm{d}s\, \Theta(t-t')\Theta(r)\Theta(s) e^{t-t')\mathcal{F}^{(0)}} \partial_\phi h(\phi) Z_1^2(\phi) e^{\lambda(t-r)} x(r) e^{\lambda(t-r)} x(s) \end{aligned}$$

Substituting $x(t' - \tilde{r}) = \int \delta(t' - q)x(q - \tilde{r})dq$ we obtain

$$\begin{aligned} = \frac{1}{2\pi} \int\!\!\int\!\!\int\!\!\int_{-\infty}^{\infty} &\Theta(p)\Theta(r-v)\Theta(s-p) e^{p\mathcal{F}^{(0)}} e^{\lambda(r-v)} \partial_\phi h(\phi) Z_1^2(\phi) \\ &e^{\lambda(s-p)} \delta(v-p) x(t-r) x(t-s)\, \mathrm{d}r\mathrm{d}s\mathrm{d}v\mathrm{d}p. \end{aligned}$$

From this one can read the kernel as

$$\begin{aligned} &\frac{1}{2\pi} \int\!\!\int_{-\infty}^{\infty} \Theta(p)\Theta(r-v)\Theta(s-p) e^{p\mathcal{F}^{(0)}} \partial_\phi h(\phi) Z_1^2(\phi) e^{\lambda(r-v)} e^{\lambda(s-p)} \delta(v-p)\, dvdp \\ =&\frac{1}{2\pi} \int_{-\infty}^{\infty} \Theta(p)\Theta(r-p)\Theta(s-p) e^{p\mathcal{F}^{(0)}} \partial_\phi h(\phi) Z_1^2(\phi) e^{\lambda(r-p)} e^{\lambda(s-p)}\, dp \end{aligned}$$

In order to obtain the radial contribution to the second order kernel for a particular neuron model one needs to evaluate $\partial_\phi h(\phi) Z_1^2(\phi)$ numerically and fit to it a Fourier series, which are the eigenfunctions of $e^{t\mathcal{F}^{(0)}}$.

B Model definitions

These are the parameters for the original equations describing the squid giant axon, established in a series of articles in the early 1950's by Hodgkin and Huxley and the Traub and Miles model.

	HH	TM	
g_{L}	0.3	0.1	mS/cm^2
E_{Na}	115	48	mV
E_{K}	-12	-82	mV
E_{L}	10.6	- 67	mV
ϱ_{Na}	$30 \cdot 10^8$	$250 \cdot 10^8$	cm^{-2}
ϱ_{K}	$3 \cdot 10^8$	$167 \cdot 10^8$	cm^{-2}
γ_{Na}	$4 \cdot 10^{-9}$	$4 \cdot 10^{-9}$	mS
γ_{K}	$12 \cdot 10^{-9}$	$12 \cdot 10^{-9}$	mS

The reaction rates for the HH model are

$$
\begin{aligned}
a_m(V) &= 0.1(25.0 - V)/(\exp((25.0 - V)/10.0) - 1) \\
b_m(V) &= 4.0 \exp(-V/18.0) \\
a_h(V) &= 0.07 \exp(-V/20.0) \\
b_h(V) &= 1.0/(\exp((30.0 - V)/10.0) + 1) \\
a_n(V) &= 0.01(10.0 - V)/(\exp((10.0 - V)/10.0) - 1) \\
b_n(V) &= 0.125 \exp(-V/80.0)
\end{aligned}
$$

The reaction rates for the TM model are

$$
\begin{aligned}
a_m(V) &= 0.32(V + 54)/(1 - \exp(-(V + 54)/4)) \\
b_m(V) &= 0.28(V + 27)/(\exp((V + 27)/5) - 1) \\
a_h(V) &= 0.128 \exp(-(V + 50)/18) \\
b_h(V) &= 4/(1 + \exp(-(V + 27)/5)) \\
a_n(V) &= 0.032(V + 52)/(1 - \exp(-(V + 52)/5)) \\
b_n(V) &= 0.5 \exp(-(V + 57)/40)
\end{aligned}
$$

$$
\boldsymbol{D}^{\mathrm{K}} = \frac{1}{\varrho_{\mathrm{K}} A}
\begin{bmatrix}
d_1 & -(3a_n n_1 + 2b_n n_2) & 0 & 0 \\
-(3a_n n_1 + 2b_n n_2) & d_2 & -(2a_n n_2 + 3b_n n_3) & 0 \\
0 & -(2a_n n_2 + 3b_n n_3) & d_3 & -(a_n n_3 + 4b_n n_4) \\
0 & 0 & -(a_n n_3 + 4b_n n_4) & d_4
\end{bmatrix}
$$

with diagonal terms

$$
\begin{aligned}
d_1 &= 4a_n n_0 + (3b_n + b_n) n_1 + 2b_n n_2, \\
d_2 &= 3a_n n_1 + 2(a_n + b_n) n_2 + 3b_n n_3, \\
d_3 &= 2a_n n_2 + (a_n + 3b_n) n_3 + 4b_n n_4, \\
d_4 &= a_n n_3 + 4b_n n_4.
\end{aligned}
$$

B Model definitions

The diffusion matrix for the Na^+ channel reads

$$\begin{bmatrix} d_1 & -2a_m m_{10} - b_m m_{20} & 0 & 0 & -a_h m_{10} - b_h m_{11} & 0 & 0 \\ -2(a_m m_{10} + b_m m_{20}) & d_2 & -a_m m_{20} - 3b_m m_{30} & 0 & 0 & -a_h m_{20} - b_h m_{21} & 0 \\ 0 & -(a_m m_{20} + 3b_m m_{30}) & d_3 & 0 & 0 & 0 & -a_h m_{30} - b_n m_{31} \\ 0 & 0 & 0 & d_4 & -(3a_m m_{01} + b_m y_{11}) & 0 & 0 \\ -a_h m_{10} - b_h m_{41} & 0 & 0 & -3a_m m_{01} - b_m m_{11} & d_5 & -2(a_m m_{11} + b_m m_{21}) & 0 \\ 0 & -(a_h m_{20} + b_h m_{21} & 0 & 0 & -2(a_m m_{11} + b_m m_{21}) & d_6 & -(a_m m_{21} + 3b_m m_{31}) \\ 0 & 0 & -a_h m_{30} - b_h m_{31} & 0 & 0 & -a_m m_{21} - 3b_m m_{31} & d_7 \end{bmatrix}$$

with the prefactor $\frac{1}{\varrho_{\mathrm{Na}} A}$.

C The numerical framework of continuation

The goal of this document is to relate quantities that describe the coding properties of neurons to their biophysics via the reduction to phase equations and PRCs. As for all but some canonical models near bifurcations and other low dimensional neural models the PRCs need to be evaluated numerically one requires an efficient numerical recipe. In this thesis we use the well developed framework of numerical continuation of boundary value problems (BVPs) [99]. In the following we will give a brief overview of concepts. The topic of continuation is however a very broad field in numerical analysis.

C.1 Continuation of boundary value problems

In §4.3 it was shown that the PRC is the solution of Eq. (4.13), the adjoint of the first variational equation of the limit cycle ODE. In order to study the encoding properties of for changing parameters, such as different input bias currents, channel densities or temperatures, one requires an efficient method to solve the adjoint equation for a whole range of system parameters. Time integration for each parameter in the set is an option, but it is also possible to predict solution based on known solution for small changes in the parameters of the underlying ODE. This has the strong benefit that solutions can be obtained also for unstable equations. The reason is that there is no time necessary. This is important because the equations for the Floquet modes Eq. (4.11) are unstable in forward and backward time for all $\lambda \neq 0$. The reason is that they have non-empty stable and unstable manifolds, so $t \mapsto -t$ just exchanges stable and unstable manifold. The adjoint equation for the PRC ($\lambda = 0$) itself is unstable in forward time, but time reversal allows stable integration.
Solving for the Floquet modes equires a solution of the limit cycle. So one has a problem with periodic boundary conditions of the following structure

$$\dot{\boldsymbol{x}} = \boldsymbol{f}(\boldsymbol{x}, \theta), \quad \boldsymbol{x}(t) = \boldsymbol{x}(t + T_\mathrm{p}).$$

Here θ denotes a generic system parameter. It is convenient to map the problem onto the unit interval with $t \mapsto tT_\mathrm{p}$, where the period is treated as an other system parameter

$$\dot{\boldsymbol{x}} = T_\mathrm{p}\, \boldsymbol{f}(\boldsymbol{x}, \theta), \quad \boldsymbol{x}(t) = \boldsymbol{x}(t + 1).$$

The general idea of continuation is as follows. Solutions of the BVP are implicitly defined by

$$\boldsymbol{g}(\boldsymbol{x}(\theta), \theta) = \dot{\boldsymbol{x}} - T_\mathrm{p}\boldsymbol{f}(\boldsymbol{x}, \theta) = \boldsymbol{0}. \tag{C.1}$$

Solutions are guaranteed under the conditions of the implicit function theorem. The idea is to start at a given solution $\boldsymbol{x}(t, \theta)$ at a specific parameter θ and then using first order Taylor expansion

$$\boldsymbol{x}(t, \theta + \Delta\theta) \approx \boldsymbol{x}(t, \theta) + \Delta\theta\, \partial_\theta \boldsymbol{x}(t, \theta). \tag{C.2}$$

In order to update the solution in the direction of parameter change one requires $\partial_\theta \boldsymbol{x}(t, \theta)$. This can be calculated in the following way. The total derivative w.r.t. the system parameter θ is

$$\nabla_{\boldsymbol{x}} \boldsymbol{g} \cdot \partial_\theta \boldsymbol{x} + \partial_\theta \boldsymbol{g} = \boldsymbol{0}.$$

As long as the Jacobian, $\boldsymbol{J} = \nabla_{\boldsymbol{x}} \boldsymbol{g}$, can be inverted this linear matrix equation can be solved for $\partial_\theta \boldsymbol{x}(t, \theta)$. Eq. (C.2) is of course only an approximate solution to the implicit function $\boldsymbol{g}(\boldsymbol{x}, \theta + \Delta\theta) = \boldsymbol{0}$

in Eq. (C.1). But it suffices as an initial guess which can be improved by Newton iterations

$$\boldsymbol{x}^{k+1} = \boldsymbol{x}^k - (\nabla_{\boldsymbol{x}} \boldsymbol{g}(\boldsymbol{x}^k, \theta + \Delta\theta))^{-1} \boldsymbol{g}(\boldsymbol{x}^k, \theta + \Delta\theta). \tag{C.3}$$

This type of algorithm is called predictor (Eq. (C.2)) - corrector (Eq. (C.3)) method. In practice, the equations above including time derivatives have to be represented as discretised vectors. In the software package AUTO, which was used for this thesis, the discretisation is controlled and adapted by the orthogonal collocation method [31].

C.2 The extended nonlinear-linear system

In addition to the limit cycle solution one may include in $\boldsymbol{g}(\boldsymbol{x}, \theta)$ the linear equations form the Floquet modes, Eqs. (4.11), or the equations for the ISI moments, Eqs. (5.4). The extended system reads

$$\left.\begin{aligned}
\frac{\mathrm{d}\boldsymbol{x}}{\mathrm{d}t} - T_\mathrm{p}\boldsymbol{f}(\boldsymbol{x}) &= \boldsymbol{0} \\
\left(\frac{\mathrm{d}}{dt} + T_\mathrm{p}\boldsymbol{J}^\dagger\right)\boldsymbol{Z}_k - \lambda_k \boldsymbol{Z}_k &= \boldsymbol{0} \\
\left(\frac{\mathrm{d}}{dt} - T_\mathrm{p}\boldsymbol{J}\right)\boldsymbol{W}_k - \tilde{\lambda}_k \boldsymbol{W}_k &= \boldsymbol{0} \\
\dot{T}_1 - S_1 &= 0 \\
\dot{S}_1 + 2\,\frac{1 + \left[1 + \bar{h}(t) + \frac{1}{2}\sigma'(t)\sigma(t)\right] S_1}{\sigma^2(\phi)} &= 0 \\
\dot{T}_2 - S_2 &= 0 \\
\dot{S}_2 + 2\,\frac{2T_1 + \left[1 + \bar{h}(t) + \frac{1}{2}\sigma'(t)\sigma(t)\right] S_2}{\sigma^2(\phi)} &= 0
\end{aligned}\right\} \tag{C.4}$$

with periodic boundary conditions for $\boldsymbol{x}(0) = \boldsymbol{x}(1)$, $\boldsymbol{Z}_k(0) = \boldsymbol{Z}_k(1)$, $\boldsymbol{W}_k(0) = \boldsymbol{W}_k(1)$ and $S_1(0) = 0$, $S_2(0) = 0$, $T_1(1) = 0$, $T_2(1) = 0$. The term $\bar{h}(t)$ and $\sigma(t)$ themselves dependt on $\boldsymbol{x}(t)$, $\boldsymbol{Z}_k(t)$ and $\boldsymbol{W}_k(t)$.

C.3 Computation of isochrons as BVP

Ref. [144] has cast the computation of isochrons into a BVP, where the initial condition is a free parameter that determines points on the isochron. The method is most straightforwardly implemented for planar systems. By varying the end point of the solution isochron is sampled as the starting points of solution bundles that end on a linear approximation of the isochron.

C.4 Homotopy parameter for potentials with poles

As mentioned above the continuation method requires an initial guess for the solution. Often time integration can be used to compute the first solution as a specific parameter. However, as some of the equations are impervious to time integration a different approach is called for. One way is to use homotopy parameters to switch of some part of the nonlinear equation so that the solution is possible. For example by introducing the parameters o_1 and o_2 the equation

$$\dot{S} = -2\frac{1 + o_1 h(\phi)}{(1 - o_2) + o_2\sigma^2(\phi)},$$

can be converted to $\dot{S} = -2$ if we set $o_1 = o_2 = 0$. From the simple solution one can then continue in the parameters o_i one by one until they reach 1.

Bibliography

[1] A. Abouzeid, B. Ermentrout. Type-ii phase resetting curve is optimal for stochastic synchrony. *Phys. Rev. E*, 80:011911, 2009.

[2] E. D. Adrian. *The Basis of Sensation*. Christophers, London, 1928.

[3] T. Akam, I. Oren, L. Mantoan, E. Ferenczi, D. Kullmann. Oscillatory dynamics in the hippocampus support dentate gyrus-CA3 coupling. *Nat Neurosci*, 15(5):763–768, 2012.

[4] K. Angelo, T. W. Margrie. Population diversity and function of hyperpolarization-activated current in olfactory bulb mitral cells. *Sci. Rep.*, 1, 2011.

[5] V. Anishchenko, V. Astakhov, A. Neiman, T. Vadivasova, L. Schimansky-Geier. *Nonlinear Dynamics of Chaotic and Stochastic Systems: Tutorial and Modern Developments*. No. Bd. 10 in Springer Complexity. Springer, 2007.

[6] B. A. y. Arcas, A. L. Fairhall. What causes a neuron to spike? *Neural Comput.*, 15(8):1789–1807, 2003.

[7] F. Arecchi, A. Politi. Transient fluctuations in the decay of an unstable state. *Phys. Rev. Lett.*, 45(15):1219–1222, 1980.

[8] J. J. Atick. Could information theory provide an ecological theory of sensory processing. *Network: Computation in Neural Systems*, 3:213–251, 1992.

[9] A. Balanov, N. Janson, D. Postnov, O. Sosnovtseva. *Synchronization: From Simple to Complex*. Springer Series in Synergetics. Springer, 2009.

[10] H. Barlow. Possible principles underlying the transformation of sensory messages. *Sensory Communication*, pp. 217–234, 1961.

[11] O. Barndorff-Nielsen, P. Blaesild, C. Halgreen. First hitting time models for the generalized inverse gaussian distribution. *Stoch. Processes Appl.*, 7:49–54, 1978.

[12] J. Benda, H. Schütze, T. Gollisch, A. V. M. Herz. Class I phase-resetting curves in auditory receptor cells in locusts. In *Proceedings of the 28th Göttingen Neurobiology Conference*, vol. I, p. 242. Georg Thieme Verlag, Stuttgart and New York, 2001.

[13] W. Bialek, R. R. de Ruyter van Steveninck. Features and dimensions: Motion estimation in fly vision, 2004. Unpublished manuscript.

[14] W. Bialek, M. Deweese, F. Rieke, D. Warland. Bits and brains: Information flow in the nervous system. *Physica A: Statistical Mechanics and its Applications*, 200(1-4):581–593, 1993.

[15] A. Borst, F. E. Theunissen. Information theory and neural coding. *Nat Neurosci*, 2(11):947–957, 1999.

[16] J. Bradbury, S. Vehrencamp. *Principles of Animal Communication*. Sinauer Associates, 2011.

[17] C. D. Brody, J. Hopfield. Simple networks for spike-timing-based computation, with application to olfactory processing. *Neuron*, 37(5):843 – 852, 2003.

[18] E. Brown, J. Moehlis, P. Holmes. On the phase reduction and response dynamics of neural oscillator populations. *Neural Computation*, 16(4):673–715, 2004.

[19] N. Brunel, V. Hakim. Fast global oscillations in networks of integrate-and-fire neurons with low firing rates. *Neural Computation*, 11:1621–1671, 1998.

[20] F. Byron, R. Fuller. *Mathematics of Classical and Quantum Physics*. Dover Books on Physics. Dover Publications, 1992.

[21] M. J. Chacron. Nonlinear information processing in a model sensory system. *Journal of Neurophysiology*, 95(5):2933–2946, May 2006.

[22] C. Chicone. *Ordinary Differential Equations With Applications*. Texts in Applied Mathematics. Springer, 2006.

[23] T. M. Cover, J. A. Thomas. *Elements of Information Theory*. Wiley Series in Telecommunications and Signal Processing. Wiley-Interscience, 2006.

[24] H. D., M. G., M. C. Synchrony in excitatory neural networks. *Neural Computation*, 7:307–337, 1995.

[25] P. Dayan, L. Abbott. *Theoretical neuroscience: computational and mathematical modeling of neural systems*. Computational neuroscience. MIT Press, 2005.

[26] P. Dayan, L. F. Abbott. *Theoretical Neuroscience: Computational and Mathematical Modeling of Neural Systems*. The MIT Press, 1st edn., 2001.

[27] E. de Boer, H. R. de Jongh. On cochlear encoding: potentialities and limitations of the reverse-correlation technique. *J Acoust Soc Am*, 63:115–135, 1978.

[28] E. De Schutter. *Computational Modeling Methods for Neuroscientists*. Computational Neuroscience. Mit Press, 2009.

[29] L. J. DeFelice. *Introduction to membrane noise*. Plenum Press, 1981.

[30] K. Diba, C. Koch, I. Segev. Spike propagation in dendrites with stochastic ion channels. *Journal of Computational Neuroscience*, 20(1):77–84, 2006.

[31] E. J. Doedel, A. R. Champneys, T. F. Fairgrieve, Y. A. Kuznetsov, B. Sandstede, X. Wang. Auto 97: Continuation and bifurcation software for ordinary differential equations (with homcont), 1997.

[32] M. D. Donsker. *On function space integrals*, pp. 17–30. MIT Press, 1964.

[33] E. du Bois-Reymond. Über die Grenzen des Naturerkennens. In *der zweiten allgemeinen Sitzung der 45. Versammlung Deutscher Naturforscher und Ärzte zu Leipzig am 14. August 1872 gehaltener Vortrag*, vol. 1. Veit & Comp, Leipzig, 2 edn., 1912.

[34] D. Dusenbery. *Sensory Ecology: How Organisms Acquire and Respond to Information*. W.H. Freeman, 1992.

[35] J. J. Eggermont, P. M. Johannesma, A. M. Aertsen. Reverse-correlation methods in auditory research. *Q. Rev. Biophys.*, 16(3):341–414, 1983.

[36] G. B. Ermentrout. Type I Membranes, Phase Resetting Curves, and Synchrony. *Neural Comput*, 8:979–1001, 1995.

[37] G. B. Ermentrout, R. F. Galán, N. N. Urban. Relating neural dynamics to neural coding. *Phys. Rev. Lett.*, 99:248103, 2007.

[38] G. B. Ermentrout, B. B. II, T. Troyer, T. I. Netoff. The variance of phase-resetting curves. *Journal of Computational Neuroscience*, 31(2):185–197, 2011.

[39] G. B. Ermentrout, N. Kopell. Oscillator death in systems of coupled neural oscillators. *SIAM J. Appl. Math.*, 50(1):125–146, 1990.

[40] G. B. Ermentrout, D. H. Terman. *Mathematical Foundations of Neuroscience*. Interdisciplinary Applied Mathematics. Springer, 2010.

[41] A. A. Faisal, S. B. Laughlin. Stochastic simulations on the reliability of action potential propagation in thin axons. *PLoS Comput Biol*, 3(5):e79, 2007.

[42] A. A. Faisal, J. E. Niven. A simple method to simultaneously track the numbers of expressed channel proteins in a neuron. In *Proceedings of the Second international conference on Computational Life Sciences*, CompLife'06, pp. 257–267. Springer-Verlag, Berlin, Heidelberg, 2006.

[43] A. A. Faisal, L. P. J. Selen, D. M. Wolpert. Noise in the nervous system. *Nat Rev Neurosci*, 9(4):292–303, 2008.

[44] F. Farkhooi, M. F. Strube-Bloss, M. P. Nawrot. Serial correlation in neural spike trains: Experimental evidence, stochastic modeling, and single neuron variability. *Phys. Rev. E*, 79:021905, 2009.

[45] F. Farkhooi, M. F. Strube-Bloss, M. P. Nawrot. Serial correlation in neural spike trains: experimental evidence, stochastic modeling, and single neuron variability. *Phys Rev E Stat Nonlin Soft Matter Phys*, 79(2 Pt 1):021905, 2009.

[46] N. Fourcaud-Trocmé, D. Hansel, C. van Vreeswijk, N. Brunel. How spike generation mechanisms determine the neuronal response to fluctuating inputs. *J Neurosci*, 23(37):11628–11640, 2003.

[47] J. L. Fox, A. L. Fairhall, T. L. Daniel. Encoding properties of haltere neurons enable motion feature detection in a biological gyroscope. *Proceedings of the National Academy of Sciences*, 107(8):3840–3845, 2010.

[48] R. F. Fox. *Gaussian Stochastic Processes in Physics*. Physics reports. North-Holland Publishing Company, 1978.

[49] R. F. Fox. Stochastic versions of the Hodgkin-Huxley equations. *Biophysical Journal*, 72(5):2068–2074, 1997.

[50] R. F. Fox, Y. Lu. Emergent collective behavior in large numbers of globally coupled independently stochastic ion channels. *Phys. Rev. E*, 49(4):3421–3431, 1994.

[51] J. Franklin, W. Bair. The effect of a refractory period on the power spectrum of neuronal discharge. *Siam J Appl Math*, 55:1074–1093, 1995.

[52] K. Friston. The free-energy principle: a unified brain theory? *Nat Rev Neurosci*, 11(2):127–138, 2010.

[53] K. Furutsu. On the statistical theory of electromagnetic waves in a fluctuating medium. *Journal of the Research of the National Bureau of Standards*, D67:303, 1963.

[54] F. Gabbiani. Coding of time-varying signals in spike trains of linear and half-wave rectifying neurons. *Network-Computation In Neural Systems*, 7:61–85, 1996.

[55] F. Gabbiani, S. Cox. *Mathematics for Neuroscientists*. Academic Press. Elsevier Academic Press, 2010.

[56] F. Gabbiani, C. Koch. Principles of spike train analysis. In C. Koch, I. Segev, eds., *Methods in Neuronal Modeling: From ions to networks*, pp. 313–360. MIT Press, Cambridge, MA, 1998.

[57] R. Galan, G. Bardermentrout, N. Urban. Reliability and stochastic synchronization in type I vs. type II neural oscillators. *Neurocomputing*, 70(10-12):2102–2106, 2007.

[58] R. F. Galán. Analytical calculation of the frequency shift in phase oscillators driven by colored noise: Implications for electrical engineering and neuroscience. *Phys. Rev. E*, 80:036113, 2009.

[59] R. F. Galán, G. B. Ermentrout, N. N. Urban. Efficient estimation of phase-resetting curves in real neurons and its significance for neural-network modeling. *Phys. Rev. Lett.*, 94:158101, 2005.

[60] R. F. Galán, G. B. Ermentrout, N. N. Urban. Predicting synchronized neural assemblies from experimentally estimated phase-resetting curves. *Neurocomputing*, 69(10–12):1112–1115, 2006.

[61] C. Gardiner. *Stochastic Methods: A Handbook for the Natural and Social Sciences*. Springer Series in Synergetics Series. Springer, 2010.

[62] W. Gerstner, W. Kistler. *Spiking Neuron Models*. Cambridge University Press, 2002.

[63] D. T. Gillespie. *Markov Processes: An Introduction for Physical Scientists*. Academic Press, 1992.

[64] D. T. Gillespie. A rigorous derivation of the chemical master equation. *Physica A*, 188:404–425, 1992.

[65] D. T. Gillespie. The chemical langevin equation. *J. Chem. Phys.*, 113(1):297–306, 2000.

[66] D. T. Gillespie. Stochastic Simulation of Chemical Kinetics. *Annual Review of Physical Chemistry*, 58(1):35–55, 2007.

[67] D. S. Goldobin, A. S. Pikovsky. Synchronization of self-sustained oscillators by common white noise. *Physica A: Statistical Mechanics and its Applications*, 351(1):126–132, 2005.

[68] J. Goldwyn, N. Imennov, M. Famulare, E. Shea-Brown. Stochastic differential equation models for ion channel noise in Hodgkin-Huxley neurons. *Phys. Rev. E*, 83:041908, 2011.

[69] J. Goldwyn, E. Shea-Brown. The what and where of adding channel noise to the Hodgkin-Huxley equations. *PLoS Comput Biol*, 7(11):e1002247, 2011.

[70] J. Grasman, O. Van Herwaarden. *Asymptotic Methods for the Fokker-Planck Equation and the Exit Problem in Applications*. Springer Series in Synergetics. Springer, 2010.

[71] C. M. Gray, W. Singer. Stimulus-specific neuronal oscillations in orientation columns of cat visual cortex. *Proceedings of the National Academy of Sciences*, 86(5):1698–1702, 1989.

[72] R. J. Greenspan. *An Introduction To Nervous Systems*. Cold Spring Harbor Laboratory Press, 2007.

[73] S. Grillner. The motor infrastructure: from ion channels to neuronal networks. *Nat Rev Neurosci*, 4(7):573–586, 2003.

[74] S. Grossberg. Adaptive pattern classification and universal recoding, II: Feedback, expectations, olfaction, and illusions. *Biol. Cybernetics*, pp. 187–202, 1976.

[75] J. Guckenheimer, P. Holmes. *Nonlinear Oscillations, Dynamical Systems, and Bifurcations of Vector Fields*. No. Bd. 42 in Applied Mathematical Sciences. Springer, 1983.

[76] B. Gutkin, J. Jost, H. C. Tuckwell. Inhibition of rhythmic neural spiking by noise: the occurrence of a minimum in activity with increasing noise. *Naturwissenschaften*, 96(9):1091–1097, 2009.

[77] J. Hale. *Ordinary differential equations*. Pure and applied mathematics. Wiley-Interscience, 1969.

[78] A. Hawkes. *Stochastic Modelling of Single Ion Channels*, chap. 5, pp. 131–157. Mathematical & Computational Biology. Chapman and Hall/CRC, 2003.

[79] M. Hayes. *Statistical digital signal processing and modeling*. John Wiley & Sons, 1996.

[80] J. Hemmen, T. Sejnowski. *23 problems in systems neuroscience*. Computational neuroscience. Oxford University Press, 2006.

[81] D. J. Higham. Modeling and simulating chemical reactions. *SIAM Review*, 2007.

[82] A. Hilfinger, J. Paulsson. Separating intrinsic from extrinsic fluctuations in dynamic biological systems. *Proceedings of the National Academy of Sciences*, 108(29):12167–12172, 2011.

[83] B. Hille. *Ion channels of excitable membranes*. Sinauer, 2001.

[84] A. L. Hodgkin, A. F. Huxley. A quantitative description of membrane current and its application to conduction and excitation in nerve. *The Journal of Physiology*, 117(4):500–544, 1952.

[85] A. V. Holden. *Models of the Stochastic Activity of Neurones*, vol. 12 of *Lecture Notes in Biomathematics*. Springer-Verlag, 1976.

[86] S. Hong, E. De Schutter. Efficient estimation of phase response curves via compressive sensing. *BMC Neuroscience*, 12:1–2, 2011.

[87] J. J. Hopfield. Pattern recognition computation using action potential timing for stimulus representation. *Nature*, 376(6535):33–36, 1995.

[88] F. C. Hoppensteadt, E. M. Izhikevich. *Weakly connected neural networks*. Springer-Verlag New York, Inc., Secaucus, NJ, USA, 1997.

[89] D. H. Hubel, T. N. Wiesel. Receptive fields of single neurones in the cat's striate cortex. *J. Physiol.*, 148:574–591, 1959.

[90] A. Hyvärinen, J. Hurri, P. Hoyer. *Natural Image Statistics*. Computational Imaging and Vision. Springer London, 2009.

[91] P. Hänggi. Stochastic resonance in biology how noise can enhance detection of weak signals and help improve biological information processing. *ChemPhysChem*, 3(3), 2002.

[92] E. Izhikevich. *Dynamical Systems in Neuroscience: The Geometry of Excitability and Bursting*. Computational Neuroscience. The MIT Press, 2007.

[93] M. Jensen, V. Jogini, D. W. Borhani, A. E. Leffler, R. O. Dror, D. E. Shaw. Mechanism of voltage gating in potassium channels. *Science*, 336(6078):229–233, 2012.

[94] D. H. Johnson, C. M. Gruner, K. Baggerly, C. Seshagiri, R. Seshagiri. Information-theoretic analysis of neural coding. *J. Comp. Neuroscience*, 10:47–69, 2000.

[95] D. Johnston, S. Wu. *Foundations of cellular neurophysiology*. Bradford Books. MIT Press, 1995.

[96] M. Juusola, A. S. French. *Neuron*, vol. 18, chap. The Efficiency of Sensory Information Coding by Mechanoreceptor Neurons, pp. 959–968. Cell Press,, 1997.

[97] P. E. Kaissling K E. Olfactory threshold of silk moths. *Naturwissenschaften*, 57:23–28, 1970.

[98] E. Kandel, J. Schwartz, T. Jessell. *Principles of Neural Science, Fourth Edition*. McGraw-Hill Companies, Incorporated, 2000.

[99] H. Kielhöfer. *Bifurcation Theory: An Introduction With Applications to PDEs*. Applied Mathematical Sciences. Springer, 2004.

[100] A. J. Kim, A. A. Lazar. Recovery of stimuli encoded with a Hodgkin-Huxley neuron using conditional PRCs. *Phase Response Curves in Neuroscience, N.W. Schultheiss, A. Prinz, and R. Butera, eds., Springer*, 2011.

[101] V. Klyatskin. *Dynamics of stochastic systems*. Elsevier, 2005.

[102] V. Klyatskin. *Stochastic equastions through the eye of the physicist*. Elsevier, 2005.

[103] T.-W. Ko, G. B. Ermentrout. Phase-response curves of coupled oscillators. *Phys. Rev. E*, 79:016211, 2009.

[104] C. Koch. *Biophysics of Computation: Information Processing in Single Neurons (Computational Neuroscience)*. Oxford University Press, 1 edn., 1998.

[105] Y. Kuramoto. *Chemical oscillations, waves, and turbulence*. Springer, 1984.

[106] Y. Kuramoto. *Chemical oscillations, waves, and turbulence*. Chemistry Series. Dover Publications, 2003.

[107] L. Lapicque. Recherches quantitatives sur l'excitation électrique des nerfs traitée comme une polarisation. *J. Physiol. Pathol. Gen.*, 9:620–635, 1907.

[108] S. Laughlin. A simple coding procedure enhances a neuron's information capacity. *Zeitschrift für Naturforschung. Section C: Biosciences*, 36(9-10):910–912, 1981.

[109] S. B. Laughlin. Energy as a constraint on the coding and processing of sensory information. *Current opinion in neurobiology*, 11(4):475–480, 2001. Review,Research Support, Non-U.S. Gov't,.

[110] A. A. Lazar. Information representation with an ensemble of Hodgkin-Huxley neurons. *Neurocomputing*, 70:1764–1771, 2007.

[111] A. A. Lazar. Population encoding with Hodgkin-Huxley neurons. *IEEE Transactions on Information Theory*, 56(2):821–837, 2010. Special Issue on Molecular Biology and Neuroscience.

[112] M. S. Lewicki. Efficient coding of natural sounds. *Nature Neuroscience*, 5(4):356–363, 2002.

[113] Y. Li, B. Lence. Applicability of rice's formula in stochastic hydrological modeling. *Journal of Hydrologic Engineering*, 13(9):776–780, 2008.

[114] K. K. Lin, K. C. A. Wedgwood, S. Coombes, L.-S. Young. Limitations of perturbative techniques in the analysis of rhythms and oscillations. *Journal of Mathematical Biology*, 2012.

[115] D. Linaro, M. Storace, M. Giugliano. Accurate and fast simulation of channel noise in conductance-based model neurons by diffusion approximation. *PLoS Comput Biol*, 7(3):e1001102, 2011.

[116] B. Lindner. Interspike interval statistics of neurons driven by colored noise. *Phys. Rev. E*, 69:022901, 2004.

[117] B. Lindner, M. J. Chacron, A. Longtin. Integrate-and-fire neurons with threshold noise: A tractable model of how interspike invertal correlations affect neuronal signal transmission. *Phys. Rev. E*, 72(2):021911, 2005.

[118] B. Lindner, L. Schimansky-Geier. Transmission of noise coded versus additive signals through a neuronal ensemble. *Phys. Rev. Lett.*, 86:2934–2937, 2001.

[119] M. London, A. Roth, L. Beeren, M. Hausser, P. E. Latham. Sensitivity to perturbations in vivo implies high noise and suggests rate coding in cortex. *Nature*, 466(7302):123–127, 2010.

[120] B. Lundstrom, S. Hong, M. Higgs, A. Fairhall. Two computational regimes of a single-compartment neuron separated by a planar boundary in conductance space. *Neural Computation*, 20(5):1239–1260, 2008.

[121] C. Ly, G. B. Ermentrout. Coupling regularizes individual units in noisy populations. *Phys. Rev. E*, 81:011911, 2010.

[122] A. Lüthi, M. A. Wikström, M. J. Palmer, P. Matthews, T. A. Benke, J. T. Isaac, G. L. Collingridge. Bi-directional modulation of ampa receptor unitary conductance by synaptic activity. *BMC Neuroscience*, 5, 2004.

[123] C. K. Machens, M. B. Stemmler, P. Prinz, R. Krahe, B. Ronacher, A. V. M. Herz. Representation of acoustic communication signals by insect auditory receptor neurons. *J. Neurosci*, 21:3215–3227, 2001.

[124] R. MacKinnon, S. L. Cohen, A. Kuo, A. Lee, B. T. Chait. Structural conservation in prokaryotic and eukaryotic potassium channels. *Science*, 280(5360):106–109, 1998.

[125] A. Manning, M. Dawkins. *An Introduction to Animal Behaviour*. Cambridge University Press, 1998.

[126] A. Manwani, C. Koch. Detecting and estimating signals in noisy cable structure, i: neuronal noise sources. *Neural Comput*, 11(8):1797–1829, 1999.

[127] A. Manwani, P. N. Steinmetz, C. Koch. Channel noise in excitable neuronal membranes. In *Advances in Neural Information Processing Systems*, vol. 12, pp. 143–149. 2000.

[128] U. M. B. Marconi, A. Puglisi, L. Rondoni, A. Vulpiani. Fluctuation-dissipation: Response theory in statistical physics. *Physics Reports*, 461(4–6):111–195, 2008.

[129] M. D. McDonnell, D. Abbott. What is stochastic resonance? definitions, misconceptions, debates, and its relevance to biology. *PLoS Comput Biol*, 5(5):e1000348, 2009.

[130] J. W. Middleton, M. J. Chacron, B. Lindner, A. Longtin. Firing statistics of a neuron model driven by long-range correlated noise. *Phys. Rev. E*, 68:021920, 2003.

[131] H. Mino, J. T. Rubinstein, J. A. White. Comparison of Algorithms for the Simulation of Action Potentials with Stochastic Sodium Channels. *Annals of Biomedical Engineering*, 30(4):578–587–587, 2002.

[132] H. Mori, T. Morita, K. T. Mashiyama. Contraction of state variables in non-equilibrium open systems. I. *Progress of Theoretical Physics*, 63(6):1865–1884, 1980.

[133] Z. Nadasdy. Information encoding and reconstruction from the phase of action potentials. *Frontiers in Systems Neuroscience*, 3(00006), 2009.

[134] K. Nakae, Y. Iba, Y. Tsubo, T. Fukai, T. o Aoyagi. Bayesian estimation of phase response curves. *Neural Networks*, 23(6):752 – 763, 2010. <ce:title>Analysis and Modeling of Massively Parallel Neural Signals</ce :title>.

[135] H. Nakao, K. Arai, Y. Kawamura. Noise-induced synchronization and clustering in ensembles of uncoupled limit-cycle oscillators. *Phys. Rev. Lett.*, 98:184101, 2007.

[136] G. Nalbach. The halteres of the blowfly Calliphora. *Journal of Comparative Physiology A: Neuroethology, Sensory, Neural, and Behavioral Physiology*, 173(3):293–300, 1993.

[137] B. Naundorf, T. Geisel, F. Wolf. Dynamical response properties of a canonical model for type-I membranes. *Neurocomputing*, 65-66:421–428, 2005.

[138] E. Neher, B. Sakmann. Single-channel currents recorded from membrane of denervated frog muscle fibres. *Nature*, 260(5554):799–802, 1976.

[139] E. Neher, C. F. Stevens. Conductance Fluctuations and Ionic Pores in Membranes. *Annual Review of Biophysics and Bioengineering*, 6(1):345–381, 1977.

[140] A. Neiman, D. Russell. Sensory coding in oscillatory electroreceptors of paddlefish. *Chaos*, 21(4):047505, 2011.

[141] R. Northrop. *Introduction to Dynamic Modeling of Neuro-Sensory Systems*. Biomedical Engineering Series. CRC Press, 2001.

[142] E. A. Novikov. Functionals and the random-force method in turbulence theory. *Soviet Physics – JETP Letters*, 20:1290–1294, 1965.

[143] B. Øksendal. *Stochastic differential equations: an introduction with applications*. Universitext (1979). Springer, 1998.

[144] H. Osinga, J. Moehlis. Continuation-based computation of global isochrons. *SIAM Journal on Applied Dynamical Systems*, 9(4):1201–1228, 2010.

[145] L. Paninski. The spike-triggered average of the integrate-and-fire cell driven by gaussian white noise. *Neural Comput.*, 18(11):2592–2616, 2006.

[146] A. Patel, B. Kosko. Stochastic resonance in continuous and spiking neuron models with levy noise. *IEEE Transactions on Neural Networks*, 2008.

[147] J. Paulsson. Summing up the noise in gene networks. *Nature*, 427(6973):415–418, 2004.

[148] J. W. Pillow, E. P. Simoncelli. Dimensionality reduction in neural models: An information-theoretic generalization of spike-triggered average and covariance analysis. *Journal of Vision*, 6(4), 2006.

[149] S. Redner. *A Guide to First-Passage Processes*. Cambridge University Press, 2001.

[150] M. W. H. Remme, M. Lengyel, B. S. Gutkin. The role of ongoing dendritic oscillations in single-neuron dynamics. *PLoS Comput Biol*, 5(9):e1000493, 2009.

[151] V. P. Repunte, H. Nakamura, A. Fujita, Y. Horio, I. Findlay, L. Pott, Y. Kurachi. Extracellular links in Kir subunits control the unitary conductance of SUR/Kir6.0 ion channels. *EMBO Journal*, 18(12):3317–3324, 1999.

[152] S. Rice. *Mathematical Analysis of Random Noise*. Bell telephone system technical publications. American Telephone and Telegraph Company, 1944.

[153] S. Rice. *Statistical Properties of a Sine Wave Plus Random Noise*. Technical publications: Monograph. Bell Telephone Laboratories, 1948.

[154] M. J. E. Richardson. Firing-rate response of linear and nonlinear integrate-and-fire neurons to modulated current-based and conductance-based synaptic drive. *Phys. Rev. E*, 76:021919, 2007.

[155] F. Rieke, W. Bialek, D. Warland. *Spikes: exploring the neural code*. Computational neuroscience. MIT Press, 1999.

[156] H. Risken. *The Fokker-Planck equation: methods of solution and applications*. Springer series in synergetics. Springer, 1996.

[157] R. M. Robertson, K. G. Pearson. Neural circuits in the flight system of the locust. *Journal of Neurophysiology*, 53(1):110–128, 1985.

[158] M. H. Rowe, A. B. Neiman. Information analysis of posterior canal afferents in the turtle, trachemys scripta elegans. *Brain Research*, 2011.

[159] C. Rozell, D. H. Johnson, R. M. Glantz. Measuring information transfer in crayfish sustaining fiber spike generators: Methods and analysis. *J. Biol. Cybernetics*, 90:89–97, 2004.

[160] T. D. Sanger. Distributed Control of Uncertain Systems Using Superpositions of Linear Operators. *Neural Computation*, 23(8):1911–1934, 2011.

[161] J. M. Schjött, S.-C. Hsu, M. R. Plummer. The neuronal $\beta 4$ subunit increases the unitary conductance of l-type voltage-gated calcium channels in pc12 cells. *Journal of Biological Chemistry*, 278(36):33936–33942, 2003.

[162] J.-H. Schleimer, M. Stemmler. Coding of information in limit cycle oscillators. *Phys. Rev. Lett.*, 103:248105, 2009.

[163] A. Schmidt, B. Ronacher, R. Hennig. The role of frequency, phase and time for processing of amplitude modulated signals by grasshoppers. *Journal of Comparative Physiology A: Neuroethology, Sensory, Neural, and Behavioral Physiology*, 194:221–233, 2008.

[164] E. Schneidman, B. Freedman, I. Segev. Ion channel stochasticity may be critical in determining the reliability and precision of spike timing. *Neural Computation*, 10:1679–1703, 1998.

[165] S. Schreiber, J.-M. Fellous, P. Tiesinga, T. J. Sejnowski. Sejnowski influence of ionic conductances on spike timing reliability of cortical neurons for suprathreshold rhythmic inputs. *J. Neurophysiol*, p. 205, 2003.

[166] N. Schultheiss, A. Prinz, R. Butera, eds. *Phase Response Curves in Neuroscience*. Springer, 2011.

[167] J. T. C. Schwabedal, A. Pikovsky. Effective phase dynamics of noise-induced oscillations in excitable systems. *Phys. Rev. E*, 81:046218, 2010.

[168] T. Schwalger, K. Fisch, J. Benda, B. Lindner. How noisy adaptation of neurons shapes interspike interval histograms and correlations. *PLoS Comput Biol*, 6(12):e1001026, 2010.

[169] O. Schwartz, J. W. Pillow, N. C. Rust, E. P. Simoncelli. Spike-triggered neural characterization. *Journal of Vision*, 6(4), 2006.

[170] T. Shibata, K. Fujimoto. Noisy signal amplification in ultrasensitive signal transduction. *Proceedings of the National Academy of Sciences of the United States of America*, 102(2):331–336, 2005.

[171] S. Sinanović, D. H. Johnson. Toward a theory of information processing. In *IEEE Trans. Signal Processing*. 2002.

[172] R. B. Stein, A. S. French, A. V. Holden. The frequency response, coherence, and information capacity of two neuronal models. *Biophysical Journal*, 12(3):295–322, 1972.

[173] K. M. Stiefel, B. S. Gutkin, T. J. Sejnowski. Cholinergic neuromodulation changes phase response curve shape and type in cortical pyramidal neurons. *PLoS ONE*, 3(12):e3947, 2008.

[174] R. Stratonovich. *Topics In The Theory Of Random Noise*. No. Bd. 2 in Mathematics and Its Applications. Gordon and Breach, 1967.

[175] S. P. Strong, R. Koberle, R. R. de Ruyter van Steveninck, W. Bialek. Entropy and information in neural spike trains. *Phys. Rev. Lett.*, 80:197–200, 1998.

[176] J. Teramae, H. Nakao, G. B. Ermentrout. Stochastic phase reduction for a general class of noisy limit cycle oscillators. *Phys. Rev. Lett.*, 102(19):194102, 2009.

[177] J.-n. Teramae, H. Nakao, G. B. Ermentrout. Stochastic phase reduction for a general class of noisy limit cycle oscillators. *Phys. Rev. Lett.*, 102(19):194102, 2009.

[178] W. Theiss, U. M. Titulaer. The systematic adiabatic elimination of fast variables from a many-dimensional Fokker-Planck equation. *Physica A: Statistical and Theoretical Physics*, 130:123–142, 1985.

[179] U. M. Titulaer. The Chapman-Enskog procedure as a form of degenerate perturbation theory. *Physica A: Statistical Mechanics and its Applications*, 100:234–250, 1980.

[180] B. Torben-Nielsen, M. Uusisaari, K. Stiefel. A comparison of methods to determine neuronal phase-response curves. *Frontiers in Neuroinformatics*, 4(00006), 2010.

[181] A. Treves, S. Panzeri, E. T. Rolls, M. Booth, E. A. Wakeman. Firing rate distributions and efficiency of information transmission of inferior temporal cortex neurons to natural visual stimuli. *Neural Computation*, 11:601–631, 1999.

[182] S. Tănase-Nicola, P. Warren, P. ten Wolde. Signal detection, modularity, and the correlation between extrinsic and intrinsic noise in biochemical networks. *Phys. Rev. Lett.*, 97:068102, 2006.

[183] H. Tuckwell. *Introduction to Theoretical Neurobiology: Nonlinear and stochastic theories*. Cambridge studies in mathematical biology. Cambridge University Press, 1988.

[184] H. Tuckwell. *Stochastic Processes in the Neurosciences*. CBMS-NSF Regional Conference Series in Applied Mathematics. Society for Industrial and Applied Mathematics, 1989.

[185] N. van Kampen. *Stochastic Differential Equations*. Physics reports. North-Holland Publishing Company, 1976.

[186] N. van Kampen. *Stochastic processes in physics and chemistry*. North-Holland personal library. North-Holland, 1981.

[187] A. T. Winfree. *Geometry of Biological Time*. Springer-Verlag, Heidelberg, Germany, 2nd edn., 2001.

[188] K. Yoshimura, K. Arai. Phase reduction of stochastic limit cycle oscillators. *Phys. Rev. Lett.*, 101(15):154101, 2008.

[189] D. Zarubin, E. Zhuchkova, S. Schreiber. Effects of cooperative ion-channel interactions on the dynamics of excitable membranes. *Phys. Rev. E*, 85:061904, 2012.

Acknowledgements

Foremost, I would like to thank my supervisor Martin Stemmler for his great enthusiasm and the invaluable guidance and advice. He was never tiered of getting his hands dirty to corroborate results, sparking new ideas in the process. I have learned so much during this time!
I fervently thank Bernd Ronacher and his group for re-waking my interest in animal behaviour and natural history in general. I particularly enjoied the discussions with Mathias Hennig,Jannis Hildebrandt, Jan Clements and Ulrike Ziehm. The later two were also companions in the structured PhD program.
I am very grateful to Susanne Schreiber for both her advice and the financial support at the end of the PhD. Also Richard Kempter has provided funding for this project and I had quite a lot of fun tutoring in some of his lectures.
I am also thankful to Grisha Bordyugov for putting me in front of a black board with only chalk to defend myself against inquisitive students. He was incredibly valuable as a source of help with the theory of numerical continuation analysis as well as practical advice. He is also an early years computer enthusiast indulging in vi, gnuplot, perl and all those fun things.
I would like to thank Frederic Römschied for the exciting and fruitful collaboration. I enjoyed the nice conference trips and am grateful that you took care of all of the organisational issues.
All the inhabitants of room 1309, present and past. These include Agnes for pleasant off topic talks, although restructuring did part us in the end. Also Bartosz Telenczuk for speaking the Python language to me. Yü Hien for his interest in my work and his good natured spirit, Janina for her pancakes, kindness and encouragements. Fabien Santi was a wonderful roommate we went hiking and had a good time, his curiosity about science was an inspiration to me.
Three cheers for the open source community! Particularly Esibelius Doedel and Bart Oldeman for the software package AUTO. This LaTeXdocumenet contains python/matplotlib figures, and AUTO-07p simulations and was written on a Linux box. And of course our ingenious duo of admins Andreas Hanschmann and Titiano Zito for their 24 hour system support.
I am particularly grateful to my parents for the much appreciated help of fending of that notorious dragon, bureaucracy, and any real life threat it poses as well as the winter holidays.
My sister for welcoming me in Eberswalde (no I never actually lived in Berlin for any extended period) and giving me a very cosy home there.
Also I would like to thank Schlieres for walking me every morning providing daily exercise and fresh air and first hand insights into animal misbehaviour. The mice I spared as a theoretical biologist, he more than equalled out, may they R.I.P.
Finally and most specially I would like to thank Ulrike Scharfenberger, there would not be a thesis without her. She kept me going whenever I needed reasons and slowed me down whenever I was pushing to hard.

Selbständigkeitserklärung

Ich erkläre hiermit, dass ich die vorliegende Arbeit selbständig und nur unter Verwendung der angegebenen Literatur und Hilfsmittel angefertigt habe.

Berlin, den 18.09.2012 Jan-Hendrik Schleimer